AD-A043 184 PRINCETON UNIV N J DEPT OF AEROSPACE AND MECHANICAL--ETC F/G 20/5
ANHARMONIC OSCILLATOR LASERS.(U)
JUL 77 J A SMITH, S H LAM, G K BIENKOWSKI F44620-73-C-0059
UNCLASSIFIED AFOSR-TR-77-0956 NL

1 OF 2
AD A043184

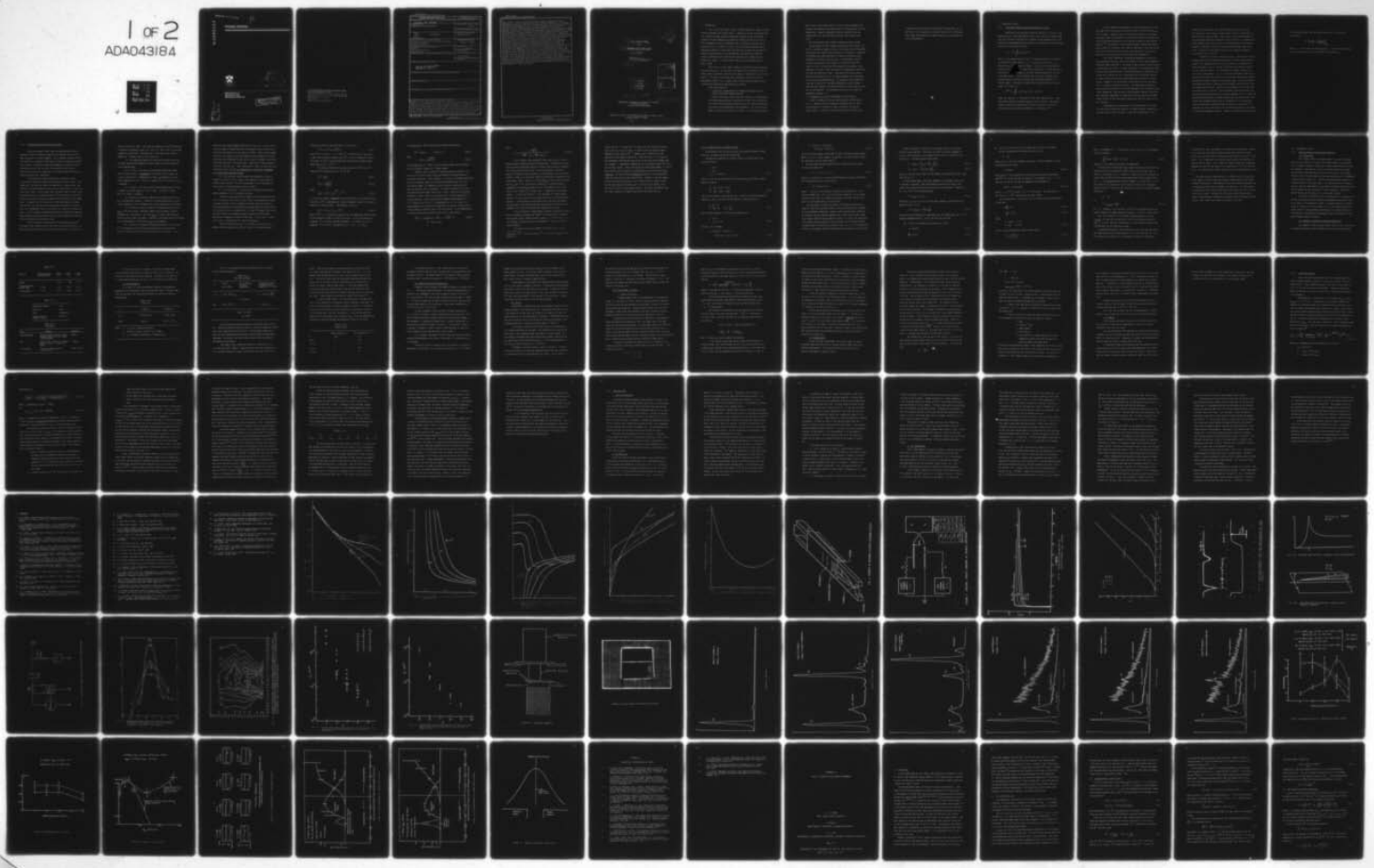

Princeton University

Department of Aerospace and Mechanical Sciences

AIR FORCE OFFICE OF SCIENTIFIC RESEARCH (AFSC)
NOTICE OF TRANSMITTAL TO DDC
This technical report has been reviewed and is
approved for public release IAW AFR 190-12 (7b).
Distribution is unlimited.
A. D. BLOSE
Technical Information Officer

UNCLASSIFIED

SECURITY CLASSIFICATION OF THIS PAGE (When Data Entered)

REPORT DOCUMENTATION PAGE		READ INSTRUCTIONS BEFORE COMPLETING FORM
1. REPORT NUMBER AFOSR-TR- 77-0956	2. GOVT ACCESSION NO.	3. RECIPIENT'S CATALOG NUMBER
4. TITLE (and Subtitle) ANHARMONIC OSCILLATOR LASERS		5. TYPE OF REPORT & PERIOD COVERED Final
		6. PERFORMING ORG. REPORT NUMBER
7. AUTHOR(s) A Smith R B Miles H Lam G K Bienkowski		8. CONTRACT OR GRANT NUMBER(s) F44620-73-C-0059
9. PERFORMING ORGANIZATION NAME AND ADDRESS Department of Aerospace and Mechanical Sciences Princeton University Princeton NJ 08540		10. PROGRAM ELEMENT, PROJECT, TASK AREA & WORK UNIT NUMBERS 2301-A1 61102F
11. CONTROLLING OFFICE NAME AND ADDRESS AFOSR/NP Bolling AFB, Bldg.410 Wash DC 20332		12. REPORT DATE Jul 1977 13. NUMBER OF PAGES 125
14. MONITORING AGENCY NAME & ADDRESS (if different from Controlling Office)		15. SECURITY CLASS. (of this report) Unclassified 15a. DECLASSIFICATION/DOWNGRADING SCHEDULE

16. DISTRIBUTION STATEMENT (of this Report)

Approved for public release;
distribution unlimited.

17. DISTRIBUTION STATEMENT (of the abstract entered in Block 20, if different from Report)

18. SUPPLEMENTARY NOTES

19. KEY WORDS (Continue on reverse side if necessary and identify by block number)

20. ABSTRACT (Continue on reverse side if necessary and identify by block number)

Emphasis of the work performed uner this contract has been placed on fundamental theoretical and experimental studies of various phenomena associated with diatomic molecular gas flows in which anharmonicity plays an important role in producing or maintaining an inversion which is suitable for lasing. Most of the work concerned carbon monoxide gas dynamic or electrically excited flows because these systems were capable of being studied in our laboratories, had considerable potential practical importance, and displayed many characteristics common to other diatomic gas lasers. In several cases the results may be generalized to

DD FORM 1 JAN 73 1473 EDITION OF 1 NOV 65 IS OBSOLETE

UNCLASSIFIED

SECURITY CLASSIFICATION OF THIS PAGE (When Data Entered)

other systems. Study of the master kinetic equations demonstrated that approximate analytical solutions exist under certain conditions. It is shown that quantitative prediction of the vibrational population distribution can be determined from knowledge of just a few key parameters in many cases of practical interest. The experimental measurement of small signal gains in highly expanded CO-N2 mixtures confirmed the anticipated large gains achievable at very low temperatures. However, unexpected rotational nonequilibrium was observed which can limit the power available from P branch laser lines. A summary of efforts to provide a simplified method of computing vibrational excitation rates in a discharge is presented. A modified E/N parameter was established which is shown to correlate results determined in a variety of gas mixtures. An experimental study of a double discharge excitation scheme in a supersonic CO-N2 flow disclosed that the secondary pin discharge is not capable of providing a stable discharge with independently controlled E/N under the conditions tested. Considerable effort was made to measure the characteristics of the plasma obtained and to characterize the arcing phenoma observed. An outgrowth of the experimental study was an analysis of the double discharge ionization scheme with particular emphasis on those characteristics which lead to arcing such as that observed. A small CO waveguide laser was constructed and tested. Although lasing was observed, performance was far below that estimated in a theoretical study (discussed in an earlier annual report). An analysis of the electrodes after several hours of operation and other operating conditions indicated that iron impurities in the CO probably was the major cause of poor performance. Small signal gain measurements showed unanticipated nonuniformities in the lasing medium.

(9) FINAL PROGRESS REPORT

ON

(6) ANHARMONIC OSCILLATOR LASERS

(11) JULY 1977

Approved for public release;
distribution unlimited.

(12) 129p.

(10) J. A. Smith
S. H. Lam
G. K. Bienkowski
R. B. Miles

(16) 2301 (17) A1 (18) AFOSR (19) TR-77-0956

Department of Aerospace and Mechanical Sciences
Princeton University
Princeton, New Jersey 08540

Prepared for the Air Force Office of Scientific Research under
Contract (15) F44620-73-C-0059

I. INTRODUCTION

This is the final report on work for AFOSR contract AF 44620-73-C-0059 entitled "Anharmonic Oscillator Lasers". Emphasis of the work performed under this contract has been placed on fundamental theoretical and experimental studies of various phenomena associated with diatomic molecular gas flows in which anharmonicity plays an important role in producing or maintaining an inversion which is suitable for lasing. Most of the work concerned carbon monoxide gas dynamic or electrically excited flows because these systems were capable of being studied in our laboratories, had considerable potential practical importance, and displayed many characteristics common to other diatomic gas lasers. In several cases the results may be generalized to other systems.

While this is a final report, emphasis is placed on results obtained during the past year. In many cases the reader will be referred to earlier annual reports, published literature, and theses for additional discussion and details. The report is organized into a theoretical section (II) and an experimental section (III); however, each of the three broad areas studied involved bothe experimental and theoretical portions.

These three areas are:

1. Calculation and Measurement of Vibrational Population Distributions Under Quasi-Steady Conditions

   Study of the master kinetic equations (Section II-B) demonstrated that approximate analytical solutions exist under certain conditions. It is shown that quantitative prediction of the vibrational population distribution can be determined from knowledge of just a few key parameters in many cases of practical interest. The experimental measure-

ment of small signal gains (Section III-B) in highly expanded CO-N_2 mixtures confirmed the anticipated large gains achievable at very low temperatures. However, unexpected rotational nonequilibrium was observed which can limit the power available from P branch laser lines.

2. Electron Excitation and a Double Discharge Excitation Scheme

Various aspects of this important problem area were studied. Section II.A presents a summary of efforts to provide a simplified method of computing vibrational excitation rates in a discharge. A modified E/N parameter was established which is shown to correlate results determined in a variety of gas mixtures. An experimental study of a double discharge excitation scheme in a supersonic CO-N_2 flow (Section III.A) disclosed that the secondary pin discharge is not capable of providing a stable discharge with independently controlled E/N under the conditions tested. Considerable effort was made to measure the characteristics of the plasma obtained and to characterize the arcing phenomena observed. An outgrowth of the experimental study was an analysis of the double discharge ionization scheme with particular emphasis on those characteristics which lead to arcing such as that observed. The preliminary results of this study are presented in Section II.C.

3. CO Waveguide Laser and Time Dependent Electron Pumping

A Small CO waveguide laser was constructed and tested (Section III.C). Although lasing was observed, performance was far below that estimated in a theoretical study (discussed in an earlier annual report). An analysis of the electrodes after several hours

of operation and other operating conditions indicated that iron impurities in the CO probably was the major cause of poor performance. Small signal gain measurements showed unanticipated nonuniformities in the lasing medium.

II. THEORETICAL STUDIES

II.A. Vibrational Pumping by Electron-Molecule Collisions

Knowledge of the electron distribution function is critical to the determination of vibrational pumping rates in any electrically pumped laser. When the vibrational distribution is computed in the standard way, by integrating the time dependent master equations, the distribution function enters directly into the rates as follows:

$$k_{i\to j} = N_i n_e \int_0^\infty S_{ij}(\varepsilon) f_e(\varepsilon) \varepsilon d\varepsilon$$

Here N_i is the number density of the i^{th} vibrational state of the molecule n_e the electron number density, $S_{ij}(\varepsilon)$ the cross section of the i to j transition by electron impact at energy, ε and $f_e(\varepsilon)$ is the electron distribution funct[illegible] For the quasi-steady calculation, the determination of the specific [illegible]n depends on the total quantum pumping rate into the vibrational states. This net pumping rate is similarly related to the electron energy distribution function when the pumping mechanism is by electron impact. The external pumping rate representing the net input of quanta into vibration is:

$$p^{ext} = \alpha_e \int_0^\infty \sum_i \delta_i \sum_j S_{ij}(\varepsilon)(j-i) \; f_e(\varepsilon) \varepsilon d\varepsilon$$

where $\alpha_e = n_e N$ and $\delta_i = N_i/N$ and N is the total number density. Since the electron energy distribution generally varies rapidly in the energy range of interest, the approximation of the distribution function by a Boltzmann one at some electron temperature is inaccurate.[1,2,3]

The most commonly used procedure in laser applications is to compute numerically the electron distribution function for each mixture and E/N of interest. Generally only collisions with molecules in the ground vibrational state are considered in the electron distribution function calculation even when superelastic collisions are included in the vibration kinetics.[4,5] The objective of this research effort, started three years ago, has been to a) ascertain the effect of superelastic collisions on the electron distribution function and thus the rates and b) to explore alternatives to the conventional strictly numerical computations.

The initial formulation including the superelastic collisions, some approximate solutions, and initial numerical results were presented in the Annual Report 1974-1975.[6] The stress at that time was on the inclusion of superelastic collisions. The main conclusion is that below about 1500°K effective low-vibrational-level vibrational temperature, superelastic collisions play virtually no role in determining the distribution function. At higher effective vibrational temperatures the distribution function slope is changed in the vibrationally active region and the high energy "tail" is raised as reported previously. As expected,the fraction of power going into vibration at a fixed E/N decreases with increasing vibrational temperature. Because even in highly pumped situations the zero to one vibrational temperature is seldom very high, the exclusion of superelastic effects on the distribution function are therefore generally not very important.

Subsequent effort was devoted to the development of a scaling law that would eliminate the necessity of lengthy numerical computations for each specific mixture and E/N. A modified E/N parameter arising

naturally from the analysis was found to scale the results of He, CO, N_2 mixtures over a wide range of mixture ratios as long as electronic excitation was not very important. Some initial results were presented at the 28th Gaseous Electronic Conference in Rolla, Missouri, in October 1975. A more complete report was published in the Proceedings of the Princeton University Conference on Partially Ionized Uranium Plasmas (NASA, Sept. 1976). A preprint of the latter publication was attached as appendix A to the Annual Report 1975-76.[7]

The main conclusions of that work follow. A modified E/N scaling parameter which can be interpreted as the ratio of energy gained from the electric field between typical inelastic collisions to a characteristic energy exchanged in such an inelastic collision arises naturally and explicitly from the analysis. The correlation is, however, essentially a local one in energy space, i.e., it is the local logarithmic slope of the distribution function that scales with the modified E/N parameter based on the dominant inelastic process in that energy range. For the cases where vibrational excitation is dominant the distribution function and its relevant moments were shown to correlate to within about 10% for a wide range of mixtures of CO, N_2 and He.[7] For sufficiently high E/N, electronic excitation contributes significantly to energy exchange, and it is clear that the distribution function at higher energies does not correlate well with respect to a parameter based solely on vibrational collision processes. Local correlation on a parameter based on electronic cross-sections is possible, but clearly the value of the correlation decreases as the number of correlation parametersincreases. However, vibrational excitation rates

(the important results for laser applications) are still very well correlated by

$$\alpha^* = \frac{E}{N} \frac{1}{\sqrt{\varepsilon_o \delta}} \left(\frac{1}{\sqrt{(Q_m S_v)}} \right)_{max}$$

where ε_o is the vibrational energy spacing, δ the half width in energy space of the prcduct of total vibrational cross section Q_m.

III. EXPERIMENTAL STUDIES

II.B. Vibrational Kinetics of CO Laser Systems

Given the relevant kinetic rates the complete master kinetic equation for the CO vibrational population distribution can be written down and solved on a digital computer. Such a computer code was written at Princeton by J. Boulnois,[8] applicable to electric-discharge excited CO laser systems. In addition to making performance calculations for the CO wave-guide laser, this code was used to generate "exact" quasi-equilibrium solutions for comparison to other approximate solutions obtained using analytical techniques.[9]

The rationale for pursuing analytical solutions for quasi-equilibrium CO vibrational population distributions are as follows. Even though exact solutions can readily be generated by a computer code, such numerical solutions inherently require explicit specifications of the relevant kinetic rates. At the present time, reliable VV and VT kinetic rates are available only at low quantum numbers,[10] and the required qualitative features of the exact solutions are known to be insensitive to the assumed rates. In general, the first few levels follow approximately a Treanor distribution, the very high levels tend toward a Boltzmann distribution, and in the intermediate levels a relatively flat Plateau distribution prevails. It is of interest to understand the physical mechanisms underlying these observed qualitative behaviors and to relate quantiatively the population distributions to the kinetic rates.

Using a differential approximation first introduced by Brau,[12] the master kinetic equation can be simplified and solved analytically, expressing the quasi-equilibrium CO population distribution n_i explicitly in

terms of the kinetic rates. This work[9] was presented in the 5th Conference of Chemical and Molecular Lasers (St. Louis, Mo., April, 1977) and has been accepted for publication. The manuscript is included in this report as Appendix B. The major results of this work are:

(i) The approximate analytical solutions are simple and are surprisingly accurate when compared to "exact" numerical solutions obtained by the computer code.

(ii) At given T, the locus of the boundary between the Treanor and the Plateau region is <u>independent</u> of the kinetic rates assumed, but is only a function of T, α(anharmonicity) and θ_{vib}(characteristic vibrational temperature of CO). An explicit formula for this locus N_i^* (T,α,θ_{vib}) is obtained.

(iii) At given T, the locus of the Plateau-Boltzmann knee is found to depend on a certain <u>ratio</u> of VT to VV rates. An explicit formula N_i^{**} (VT,VV rates) is obtained.

(iv) An explicit analytical formula for the Plateau distribution $\overline{N}_i$ is derived which contains, in addition to N_i^{**} described above, an integration constant $\overline{N}_o$ which represents the nominal magnitude of the Plateau.

(v) An explicit analytical formula is obtained relating $\overline{N}_o$ with Q_{total}, the rate of total vibrational quanta input by external (electric discharge, etc.) excitation. Thus, once Q_{total} is known, the Plateau distribution can be simply calculated. Conversely, given the Plateau distribution (e.d., experimentally(, the value of Q_{total} can be deduced.

(vi) The rate of vibrational quanta deactivation by VT collisions, D^{VT}, is obtained explicitly, identifying separately the contributions from local low level VT collisions and high level VT collisions. It is

shown that under weakly pumped conditions, the local low level VT collisions are capable of deactivating the input quanta, and the resulting CO population distribution will not exhibit a Plateau. Under strongly pumped conditions, the "excess" input quanta which can not adequately be locally deactivated are transported to high levels by nearly resonant VV collisions to be deactivated by VT collisions there. Under most CO laser operating conditions, the local low level contribution is small, giving rise to the interesting result that D^{VT} is independent of VT rates but is dependent only on the nearly resonant VV rates.

(vii) The analytical solution shows that the details of the VV adiabaticity factor in the VV rates is not important so long as the off-resonant rates are small. Only the second moment of the VV adiabaticity factor enters in the approximate solution (via N_i^{**}).

(viii) The function N_i^{**} is sensitive to the magnitude and quantum number dependence of the VT adiabaticity factor.

Since the quasi-equilibrium CO population distribution can be explicitly related to the VV and VT kinetic rates via the analytical theory, it becomes possible to infer information on these rates particularly at high quantum numbers from experimentally measured population distributions. In collaboration with A. Lightman and E. R. Fisher[13] of Wayne State University and H. Rabitz of Princeton, we have successfully inferred some quantitative information on CO-He VT rates near $i \cong 25$ at 150°K. A draft of this work is included with this report as Appendix C.

Before discussing this work, it is useful to review briefly a common estimation procedure for CO-He VT rates at high quantum numbers.[11]

Motivated by the well known SSH theory,[14] we can write

$$k^{VT}(i\downarrow) = k^{VT}(0\downarrow)\ \ell_i^{VT} A_i^{VT}(T) \qquad \text{(IIB.1)}$$

where $k^{VT}(i\downarrow)$ is the $i+1 \rightarrow i$ VT rate, ℓ_i^{VT} is proportional to the square of the transition matrix element, and $A_i^{VT}(T)$ is the VT adiabaticity factor. The values of $k^{VT}(0\downarrow)$ can be obtained from the relatively abundant experimental data ($\ell_o{}^{VT} = 1$, $A_o{}^{VT} = 1$).

Following the earlier work of Keck and Carrier,[15] Rich et al[11] suggested the following forms for ℓ_i^{VT} and A_i^{VT}:

$$\ell_i^{VT} = \frac{1+i}{1-i\alpha} \qquad \text{(IIB.2)}$$

$$A_i^{VT}(T) = \frac{F_{KC}(y_i)}{F_{KC}(y_o)} \qquad \text{(IIB.3a)}$$

where

$$F_{KC}(y) = \frac{3}{2}\left(1 - \frac{1}{3} e^{-\frac{2}{3}y}\right) e^{-\frac{2}{3}y} \qquad \text{(IIB.3b)}$$

is a curve-fit formula recommended by Keck and Carrier as a convenient representation of $A_i^{VT}(T)$ computed using a simple exponential repulsive interaction potential via the SSH theory. The parameter is given by

$$y_i(T) \equiv (1-2\ \alpha_i)\ \theta_{vib}\ \theta^{VT}/\delta T. \qquad \text{(IIB.3c)}$$

where $\theta^{VT}(^\circ K^{-1})$ is a constant proportional to the reduced mass and the square of the interaction length L of the VT collision. In this rate estimation procedure, θ^{VT} is the only adjustable parameter. For CO-He, Rich et al[11] suggested $\theta^{VT} = 0.114^\circ K^{-1}$, corresponding to $L \cong 0.2$ Å. For large y_i

(low temperatures), $A_i^{VT}(T)$ simplifies and becomes approximately

$$A_i^{VT} \cong \exp(\beta_i) \qquad \text{(Rich et. al)} \tag{IIB.4}$$

where

$$\beta = \frac{4}{3} \alpha \theta_{vib} \sqrt{\theta^{VT}/8T} \tag{IIB.5}$$

At low temperatures ($T < 300°K$), the high quantum number rates estimated by this procedure increase with i rather steeply.

Recently, Verter and Rabitz[16] performed extensive numerical calculations for CO-He VT rates using three-dimensional quantum mechanical close-coupling methods. Their computed $1 \rightarrow 0$ rates at low temperatures agree within an acceptable factor with available experimental data, but their high quantum number, low temperature rates disagree substantially with those estimated by the Rich procedure. As reported previously,[17] we have correlated the Verter-Rabitz rates by Eq. (IIB.1), obtaining an equivalent adiabaticity factor $A_i^{VT}(y_i,T)$ by curve-fitting. At high temperatures, it is found that Eqs. (IIB.3) correlated the computed rates adequately if θ^{VT} is chosen to be $0.271\ °K^{-1}$, corresponding to $L \cong 0.3$ Å which is in good agreement to the interaction length near the strongly repulsive part of the interaction potential used in the calculations. At low temperatures, a distinctly different correlation results and is given below:

$$A_i^{VT}(T) = a_i \exp\left\{\left[0.525\left(1+\frac{16}{T}\right)\beta - \frac{\alpha \theta_{vib}}{T}\right] i\right\} \tag{IIB.6a}$$

($T < 300\ °K$ only)

where

$$a_i = \frac{1 + \left(\frac{280}{T}\right)^2}{1 + \left(\frac{280}{T}\right)^2 \exp\left[\frac{150}{T}(y_i - y_o)\right]} \qquad \text{(II.B.6b)}$$

In Eq. (IIB.6a), the exponential factor $\exp(-\alpha\theta_{vib}/T)i$ was included because of detailed balance considerations. The theoretical rates could have been correlated without this factor (thus yielding a different set of curve-fitting coefficients), but we have chosen to include it because it formally should be present in the SSH theory. This simple correlation allows us to succinctly identify the distinctive features of the Verter-Rabitz rates. These are (1) the presence of the exponential factor $\exp(-\alpha\theta_{vib}/T)i$ in Eq. (IIB.6a) which renders A_i^{VT} a much more gradual i dependence at high quantum numbers* and (2) the presence of the coefficient a_i which renders A_i^{VT} a rather rapid i dependence at low quantum numbers. Of particular interest is the unexpected low quantum number behavior of a_i which has so far not been satisfactorily interpreted theoretically. In the absence of experimental data, the above qualitative features remain to be substantiated and the substantial quantitative disagreement with the Rich estimated rates remains to be resolved.

From a collection of experimentally measured CO population distributions obtained by Lightman and Fisher[13] in a CO-He electric discharge laser system, we have inferred CO-He VT rates for $i \cong 25$ at 150°K. To our knowledge, these are the first experimental VT rates at such high quantum numbers.

Our results as given in Appendix B indicate that (1) the in-

*Note that β ($\theta^{VT} = 0.114$) and $0.525\beta(\theta^{VT} = 0.271)$ are reasonably close numerically.

ferred rates for $i \cong 25$ and 150 °K is larger than the theoretical Verter-Rabitz rates by a factor of about 7-8, and (2) the high quantum number i dependence of the inferred A_i^{VT} is gradual and is consistent with the theoretical Verter-Rabitz predictions. Since the CO-He $1 \rightarrow 0$ VT rates are well-documented, the observed large values of the high quantum number rates (with gradual i dependence) suggests that at low quantum numbers A_i^{VT} (or a_i) must increase rapidly. Hence, even though the high quantum number, T = 150 °K Verter-Rabitz rates substantially underestimates the inferred rates quantitatively, the two distinctive qualitative features of the Verter-Rabitz rates are consistent with the inferred rates. Because of the small amount of data available, the accuracy of our inferred rates is rather limited. But the data reduction technique used is interesting and appears to be particularly useful at high quantum numbers. Additional experimental data are clearly needed to collaborate and refine the present results.

II.(C) Further Studies on Double-Discharge

At the present time, no self-consistent and complete theoretical model exists for the double-discharge configuration.

The governing equations for a weakly ionized, continuum plasma flow are the following

$$\begin{aligned} \nabla \cdot \underline{j}_e &= S \\ \nabla \cdot \underline{j}_i &= S \\ \varepsilon_o \nabla \cdot \underline{E} &= e(n_i - n_e) \end{aligned} \tag{IIC.1}$$

where S is the net volume ionization rate and $\underline{j}_i$ and $\underline{j}_e$ are number current densities given by

$$\begin{aligned} \underline{j}_i &= n_i \underline{u} - D_i \nabla n_i + n_i \mu_i \underline{E} \\ \underline{j}_e &= n_e \underline{u} - D_e \nabla n_e - n_e \mu_e \underline{E} \end{aligned} \tag{IIC.2}$$

and $\underline{u}$ is the velocity of the neutral flow. D_i and D_e are diffusion coefficients and μ_i and μ_e are mobility coefficients. Defining $\underline{j}$ and $\hat{\underline{j}}$ by

$$\begin{aligned} \underline{j} &\equiv \underline{j}_e - \underline{j}_i \\ \hat{\underline{j}} &\equiv \mu \underline{j}_e + \underline{j}_i \qquad \left(\mu \equiv \frac{\mu_i}{\mu_e} \right) \end{aligned} \tag{IIC.3}$$

the first two equations in (IIC.1) can be rewritten as

$$\begin{aligned} \nabla \cdot \underline{j} &= 0 \\ \nabla \cdot \hat{\underline{j}} &= (1 + \mu) S \end{aligned} \tag{IIC.4}$$

and Eqs. (IIC.2) become

$$\begin{aligned} \underline{j} = (n_e - n_i)\underline{u} &- D_i \nabla (n_e - n_i) \\ &- (D_e - D_i) \nabla n_e - (n_e \mu_e + n_i \mu_i) \underline{E} \end{aligned} \tag{IIC.5}$$

$$\hat{\underline{j}} = (\mu n_e + n_i)\underline{u} - (D_i + \mu D_e)\nabla n_i + (n_i - n_e)\mu_i \underline{E} + \mu D_e \nabla(n_i - n_e) \qquad \text{(IIC.6)}$$

If the local Debye length of the plasma is small, the quasi-neutral approximation $n_i \cong n_e = n$ can be invoked . An analysis of the quasi-neutral theory was reported in the last Annual Report.[7]

The quasi-neutral approximation yields a convection-diffusion model for the plasma density n:

$$\underline{u} \cdot \nabla n = D_a \nabla^2 n + S - n\nabla \cdot \underline{u} \qquad \text{(IIC.7)}$$

where $D_a = (D_i + \mu D_e)/(1+\mu)$ is the so-called ambi-polar diffusion coefficient. The irrotational electric field satisfies

$$\nabla \cdot \sigma \underline{E} + (D_e - D_i)\nabla^2 n = 0 \qquad \text{(IIC.8)}$$

where $\sigma = (\mu_i + \mu_e)n$ is the electrical conductivity (divided by e). The coupling between Eqs. (IIC.7) and (IIC.8) occurs through S, the net volume ionization rate, which is a sensitive function of the local value of E/N where N is the number density of the neutrals.

The quasi-neutral formulation accounts for convective effects and is capable of describing upstream effects (such as the upstream pin discharge) on the developments downstream. However, under the operational conditions of interest, the quasi-neutral approximation is only valid in some limited local regions where the plasma density is high; it is clearly not applicable in the sheath regions adjacent to the electrodes and in the region beyond the outer edge of the ambi-polar diffusion layer. Because of its non-uniform validity, the boundary conditions appropriate for the model are not yet clear.

We shall confine our attention to the cathode sheath and the sheath-diffusion layer interface. Physically, we expect the normal components of $\underline{j}$ and $\hat{\underline{j}}$ to be continuous at the interface (which shall be identified by the subscript ∞). The quasi-neutral model yields:

$$j_\infty \equiv (\underline{j}\cdot\underline{y})_\infty = \left[-(D_e-D_i)\,\frac{\partial n}{\partial y} + \sigma\frac{\partial V}{\partial y}\right]_\infty , \tag{IIC.9}$$

$$\hat{j}_\infty \equiv (\hat{\underline{j}}\cdot\underline{y})_\infty = -\left[(D_i+\mu D_e)\,\frac{\partial n}{\partial y}\right]_\infty , \tag{IIC.10}$$

where $\underline{y}$ is the unit vector normal to the cathode (and therefore the thin interface) and $\underline{E} = -\nabla V$.

In the cathode sheath, the normal component of $\underline{E}$ (denoted simply by E) is expected to dominate. Near the cathode and away from the edge of the sheath, both convective and diffusive effects may be neglected. Denoting $\underline{j}\cdot\underline{y}$ by j, Eq. (IIC.5) in the sheath becomes

$$j \tilde{=} -(n_e\mu_e + n_i\mu_i)E . \tag{IIC.11}$$

Denoting $\hat{\underline{j}}\cdot\underline{y}$ by $\hat{j}$, Eq. (IIC.6) in the sheath becomes, using the Poisson's equation in Eqs. (IIC.1):

$$\hat{j} \tilde{=} (n_i-n_e)\mu_i E = \frac{\varepsilon_o\mu_i}{e}\,E\,\frac{\partial E}{\partial y} . \tag{IIC.12}$$

Note that as quasi-neutrality is approached near the sheath edge, Eq. (IIC.12) becomes untenable while Eq. (IIC.11) can still be justified.

Eqs. (IIC.4) in the sheath can be written as follows

$$j = \text{constant} \tag{IIC.13}$$

$$\frac{d\hat{j}}{dy} = (1+\mu)S . \tag{IIC.14}$$

Eqs. (IIC.12), (IIC.13), and (IIC.14) govern the structure of the sheath.

We shall represent the net volume ionization rate by

$$S = \alpha j_e$$

where $\alpha(cm^{-1})$ is the first Townsend coefficient. We shall represent α by the following empirical formula

$$\alpha = N\beta(N/E) \tag{IIC.15a}$$

where $\beta(N/E)$ is to be determined by correlating the available experimental data[18-22] for N_2 which has been collected and is presented in Fig. 1. It is seen that for low N/E the data can adequately be represented by

$$\beta(N/E) = a \exp\left(-b \frac{N}{E}\right) \tag{IIC.15b}$$

where $a = 3 \times 10^{-16}$ cm^2 and $b = 8.3 \times 10^{-15}$ volts-cm^2. For high values of N/E ($N/E \gtrsim 0.7 \times 10^{15}$), the data has very wide scatter.

We can rewrite Eqs. (IIC.12) and (IIC.14) in the following non-dimensionalized form:

$$E \frac{dE}{d\eta} = B \hat{J} \tag{IIC.16}$$

$$\frac{d\hat{J}}{d\eta} = (1+\hat{J})\beta \tag{IIC.17}$$

where

$$E = -E/bN, \quad \hat{J} = \hat{j}/j ,$$
$$\eta = aNy, \quad \beta = \beta(E) \tag{IIC.18}$$

and B is the non-dimensional normal current density

$$B = \frac{ej}{ab^2 \varepsilon_o \mu_i N^3} \tag{IIC.19}$$

which is independent of η. Dividing Eqs. (IIC.16) by (IIC.17) and integrating once, we obtain

$$\int_{E_\infty}^{E} \xi\beta(\xi)d\xi = B\left\{\hat{J} - \ell n\ (1+\hat{J})\right\} \qquad \text{(IIC.20)}$$

where E_∞ is an integration constant to be determined.

The above mobility-dominated theory cannot be matched directly with the convective-diffusive quasi-neutral theory because the two models have no region of overlapped validity. However, it appears physically reasonable to require that the sheath solution should become quasi-neutral asymptotically as $\eta \to \infty$. This ad hoc boundary condition imposes $E_\infty = 0$ and $\hat{J}(\eta=\infty) = 0$. At the surface of the cathode, we shall assume that the electron (secondary) emission current is related to the incoming ion current by the second Townsend coefficient γ:

$$j_e = -\gamma j_i$$

or

$$\hat{J} = \hat{J}_{cathode} \equiv \frac{\mu\gamma-1}{\gamma+1} \qquad \text{(IIC.21)}$$

at $\eta = 0$. Although γ can be as small as $O(10^{-4})$ for molecularly clean conductor surfaces, for common engineering surfaces $\gamma = O(10^{-1})$ is more typical.

Eqs. (IIC.16) and (IIC.17) have been integrated numerically using $\hat{J}_{cathode} = 0.1$ and $\beta(E)$ as given by Eq. (IIC.15) for various values of B. Figs. 2, 3, and 4 show the distributions of E, the normalized electron and ion densities, and the normalized voltage.

As mentioned previously, these solutions are not valid near the edge of the sheath away from the cathode because, first of all, the data for $\beta(E)$ is not reliable at low values of E, and secondly the effects of convection

(particularly of ions) and perhaps of diffusion are not negligible. However, Fig. 3 shows that the sheath solutions approach quasi-neutrality rather rapidly, and the nearly neutral normalized plasma density varies with η very slowly. Fig. 4 shows that in the nearly neutral region the normalized voltage also varies slowly. Fig. 5 shows the "sheath voltage drop" between the cathode and a point at the "edge" of the sheath with $\hat{J} = 10^{-3}$ as a function of B. It is seen that this sheath voltage drop varies non-monotonically with B.

The sheath analysis presented here is intended as one of the building blocks toward a self-consistent and complete plasma theory for the double-discharge configuration. The sheath-diffusion layer matching procedure used is an ad hoc one and further refinements are necessary. The region beyond the upper edge of the diffusion layer where quasi-neutrality also fails has not yet been treated. The modeling of the net volume ionization rate is rather simple-minded and recombination and other kinetic processes have been ignored. Much further work remains to be done in this area.

III. EXPERIMENTAL STUDIES

III.A. Double Discharge, Experiments and Modelling

(1) Introduction

The Princeton electric discharge channel is a double discharge scheme for the production of stable, distributed plasmas in a supersonic ($M \sim 4$) stream of diatomic nitrogen and nitrogen-carbon monoxide mixtures. This research is motivated by a desire to produce electrically pumped, near infrared, carbon monoxide lasing action from stable, large volume plasmas in which electron number density and average energy are independently and externally manipulated. The envisioned devices would operate continuously and be of high output power. Our research efforts are aimed at gaining a physical understanding of the double discharge stabilization technique introduced by Blom and Hanson,[23] while attempting to determine if present devices can be scaled up in size and power loading.

Following a brief description of the apparatus (2), summaries will be made of work done, results obtained and hypotheses entertained in each of five topics: fluid mechanics studies (3), general electrical characteristics (4), analysis of arcing instability (5), preliminary model of the plasma stream (6) and experimental determination of plasma properties (7). This report will concentrate on developments since the completion of the Annual Progress Report of 1975-76.[7]

(2) Apparatus: Dimensions, Design and Description

The schematic of the discharge channel (Figure 6) plus the following tables and comments should adequately describe the discharge channel.

TABLE III A.1

Position	Reference Length (From Throat)	Height cm	Width cm	X-area cm^2
Throat	0	2.54	.635	1.61
Discharge Volume Leading Edge	21.90	2.55	6.40	16.31
Trailing Edge	72.71	2.93	6.40	18.76

TABLE III A.2

Nominal Mach Number	3.93
Area Ratio	10.08
Type	Contoured, 2D
Length, Throat to Parallel Section	19.69 cm

TABLE III A.3

ELECTRODES

Item	Geometry	Materials
Discharge Plates	(50.80 cm) long, span full width, rounded leading & trailing edges (latter exposed)	Copper
Pins	.0635 cm dia. Flush with cathode surface 7 rows of 5 across the width	Tungsten
Pin Insulators	Flush with cathode surface (.2381 cm dia.)	Boron Nitride

The first row of pins is located 1.27 cm from the leading edge of the discharge plates with four successive rows at 2.54 cm spacings. Row five and six are spaced at 7.62 cm intervals. The center pin of each row is on the tunnel centerline, the rest at 1.27 cm intervals on either side.

(3) Fluid Mechanics

It is useful to review our estimates of general flow properties computed with one dimensional isentropic gasdynamic theory. Assuming choked flow, one can derive the following expressions for mass flow in the discharge channel:

TABLE III A.4
MASS FLOW

T_o	$\dot{m}$ (gm/sec)	$\dot{m}$(lbm/sec)
T_o, °K	$44.205\ P_o/\sqrt{T_o}$	$.09740\ P_o/\sqrt{T_o}$
300°K	$2.552\ P_o$	$5.627 \times 10^{-3}\ P_o$

where: 1) P_o in psia, stagnation pressure.
2) (multiply above by 14.696 for P_o in ATMS.)
3) T_o is stagnation temperature in degrees Kelvin

For M = 3.93 the number density and pressure can be calculated from the following formulas:

TABLE III A.5
TEST SECTION DENSITY

T_o	$N\#/cm^3$ (P_o in ATMS)	Cavity Pressure at cavity temperature	Equivalent Pressure at density N and temperature T = 300°K
T_o, °K	$2.155 \times 10^{20}\ P_o/T_o$		$P = 22.474\ P_o(\frac{300}{T_o})$
		$P = 5.497\ P_o$	
300	$7.185 \times 10^{17}\ P_o$		$P = 22.474\ P_o$

where P in TORR

P_o in ATM.

Pitot surveys were made and reported in the Annual Report of 1975-76.[7] These data indicated that while there is a region of reasonably uniform flow a very complicated flow field exists in the discharge channel which cannot be fully analyzed without additional sophisticated flow measurement techniques. The value of the results did not warrant such an extensive and expensive investigation.

The boundary layers probed have been thick, ranging from .6 to 1 cm along the tunnel sidewalls. Boundary layers along the electrodes are not of uniform thickness and appear to bulge near the center line of the

tunnel. Pitot profiles exhibit noticeable peaks and valleys which make any simple identification of boundary layer edges difficult. It is also probable that oblique wave patterns exist in both planes along the flow axis. Our nozzle contour could be inaccurately machined creating an expansion fan; or the break from the contoured section to parallel walls might be too sharp, creating shock waves. In the plane perpendicular to the nozzle expansion we might have a shock pattern induced by rapid electrode boundary layer growth or leakage across the throat-top and bottom wall seals; these effects are discussed by Simons[24] and Director.[25]

As the discharge channel is a long duct of small cross-sectional area, viscous effects will be important even at supersonic velocities. The ratio of electrode length to hydraulic diameter is about 13. An estimate of the level and variation of flow variables can be obtained on the basis of a one-dimensional frictional flow analysis. Using the estimated Mach number at the leading edge of the electrode of $M_{LE} = 3.82$, the computed flow properties at the trailing edge are presented in Table III A.6 below.

TABLE III A.6.
VISCOUS EFFECTS

	Leading Edge (L.E.)	Trailing Edge (T.E.)
M	3.83	2.77
$P/P_{L.E.}$	1	1.72
$\rho/\rho_{L.E.}$	1	1.11
$T/T_{L.E.}$	1	1.55
$P_o/P_{oL.E.}$	1	0.37

This estimate of M(T.E.) is not inconsistent with one that can be deduced from pitot and wall static pressure data in conjunction with this estimate of P_o(T.E.). We predict about an 11% increase in density and an equivalent drop in velocity from about 6.7×10^4 cm/sec to 6×10^4 cm/sec.

(4) General Electrical Characteristics

A general circuit diagram of the double discharge is provided in Figure 7. The desired operating feature in the double discharge design is the ability to independently set plate voltage and current at a given P_o (or cavity density), that this has been accomplished can be seen in Figure 8. It should be noted that the total variability of (E/N) (electric field to total number density) for this device is quite small, ranging within 2×10^{-16} v-cm^2 to 4×10^{-16} v-cm^2.

The major parameters affecting double discharge operation are P_o, I_o (total pin current), cathode current density and arcing rate. The most noticeable effects on discharge operation are exhibited by changes in the parameters P_o (stagnation pressure which is linearly proportional to cavity pressure, density and mass flow) and I_o. At any given P_o there is a minimum I_o necessary in order to have arc free operation (or specified arcing frequency) with a desired level of main current, I.

As I_o increases, the amount of main current that can be delivered without arcing increases; this effect is duplicated if P_o decreases and I_o is maintained.

The onset of arcing is gradual, and arcing frequency increases for decreasing, "insufficient" I_o or increasing "excessive" P_o. An arc formed

between the electrode plates must be swept out of the discharge volume before another can form. Arcs can be visually detected in N_2 as pinkish peachy flames. Frequent arcing manifests itself on main voltage versus main current plots as a region of negative slope.

A measurement of arcing rate versus average anode current was made at one P_0 and fixed pin geometry (Figure 9). The gradual arcing thresholds are clearly visible as is the effect of pin current. A sample error bar is shown on our values of average current in the linear portions of the graph. This error diminishes rapidly in the regions of low arcing rate. Further discussion of arcing is given in the following sections.

(5) Arcing

As mentioned in the previous section, the major instability of the double discharge is the formation of arcs. Experiments were done in which it was shown that solitary arcs are formed and are swept out of the discharge volume at the flow speed before a recurrence. Photomultiplier tubes were used to monitor arcs as they passed one location in the tunnel in an experiment described in the Annual Progress Report of 1975-76.[7]

In an effort to check and refine the results of the photo-tube data another experiment was performed. One photo-multiplier observed two posistions in the discharge channel separated by a known distance. An oscillogram of the photo-tube signal would show two peaks representing an arc passing each of the monitored positions. This direct measurement of arc velocity yields a value of 5.4×10^4 cm/sec.

A schematic of an oscillogram is given in Figure 10. The peaks in the oscillogram are of different magnitude because each was transmitted by a different leg of an uncalibrated optical system. The RC delay of

the photo-tube circuitry was measured and minimized sufficiently that our ultimate detectability of "arc thickness" was .013 μs or 7×10^{-4} cm moving at the flow speed of 5.4×10^{4} cm/sec. The half-width of these signals is about 60 μs, indicating a maximum arc thickness of 3.2 cm. The same data could however be explained by a much thinner sheet inclined with respect to the optical axis.

(6) Plasma Model, A Synopsis

1. Governing Equations

The Debye length likely to be encountered in the double discharge is of the order of 10^{-3} cm., hence a continuum theory of ambipolar diffusion, convection and production of the plasma in the bulk of the test section should be appropriate. Assuming singly charged ions, negligible attachment, steady state, quasi-neutrality and small ionization fraction, governing equations for the plasma flow can be derived as in Ref. 26.

The application of this formalism to modelling of the double-discharge configuration was described in the last annual report[7] and some simplified solutions were presented. For convenience some results from that report for the infinite space and semi-infinite space solutions due to a single source term are shown in Figure 11a and 11b respectively. We expect that the semi-infinite space solution is the more relevant to our configuration and is indicative of the primary spatial variation of number density.

The analytic expression of Equation IV (F.17) in Reference 7 can be used as a guide in anticipating plasma density distribution data. If we consider the case of

$$|x - x_o| \gg |y - y_o|$$

$$|z - z_o|$$

where $(x-x_o)$ is the streamwise distance and $(y-y_o)$ and $(z-z_o)$ are the transverse distances from the source, we can find an approximate expression for the variations of the number density n with z and y with a given cross section:

$$n \propto \exp\left[-\frac{1}{2|x-x_o|}\sqrt{\frac{k^2}{4} - \tilde{\alpha}}\left((y-y_o)^2 + (z-z_o)^2\right)\right]$$

where $k = u/D_a$, the flow velocity u divided by the ambipolar diffusion coefficient D_a, and $\tilde{\alpha} = \alpha/D_a$ where α is the ionization rate.

From this expression we would anticipate data at a given cross section when plotted semi-logarithmically versus the coordinate $(y-y_o)^2 + (z - z_o)^2$ to be linear with negative slope, and when plotted versus y or z to be parabolic.

An estimate of the ambipolar diffusion coefficient can be made from the slope of the lines just described. If $\frac{k^2}{4} >> \tilde{\alpha}$ as appears to be true at least in certain locations in the discharge volume slopes of $\ln(n)$ versus

$$(y-y_o)^2 + (z-z_o)^2 \quad \text{should be proportional to}$$

$$-\frac{1}{|x-x_o|}\quad\frac{k}{4} = -\frac{u}{4|x-x_o|D_a}$$

With u known, D_a can be estimated from the data.

If all data at a given cross section cannot be correlated by a single straight line, then the model may still be valid but require a distributed source instead of the single concentrated one. As the model equation is linear, one can experiment with source distributions in order to

analytically duplicate experimental results. Electron and ion distributions between the electrodes at $x = x_o$ are not known because of low plasma density and resulting non quasi-neutrality. There is, therefore, a certain amount of freedom in the initial conditions which can account for some discrepancy between the model and the data. If the resulting values of D_a are, however, reasonable and the model predicts distributions at several cross section locations it is most likely that the major assumptions are correct.

A test can be made to determine if volume ionization does or does not play a role in the bulk of our discharge volume. It is well known that the dependence of ionization rate (α) on the electric field E is extremely rapid, being much stronger than that of D_a, hence $k^2/4$ is almost independent of E compared to the rapid variation of $\tilde{\alpha}$.

One can measure density distributions at one cross section of the tunnel, first with sustainer plates active to enhance $\tilde{\alpha}$ and then with sustainer plates off, at one value of pin current. Plots of ln(n) versus $(y-y_o)^2 + (z-z_o)^2$ will have slopes proportional to $-\sqrt{\frac{k^2}{4} - \tilde{\alpha}}$, if this drop-off in density is much slower in the active sustainer case than in the passive sustainer case and the level of density is higher at a given location, then volume ionization will have been shown to be a significant effect in producing the plasma cloud.

(7) Plasma Probing

The most desirable measurements that could be made in a double-discharge plasma would be spatially resolved electron number density and potential measurements. This requires the design, construction and successful employment of Langmuir probes.

The probing scheme developed during the past year is shown in Figure 12. As our electrons have an energy of about 1 ev an electric probe in the plasma should saturate when biased by a few volts from floating potential. A measurement of this saturation current can be related to plasma density. Our technique is to send a five volt 200 Hz sine wave through a d.c. blocking capacitor to the probe. Circuit components are sized so that the probe to plasma voltage drop is practically the entire five volts. The current at 200 Hz is monitored on the low voltage side of the capacitor by measuring the differential rms voltage across a precision resistor with a lock-in amplifier. The frequency of 200 Hz was chosen because the plasma is relatively quiet there. This was checked with a spectrum analyzer. In the range of 100-300 Hz we see only white noise at about 1.6 volts; our lock-in amplifier has no trouble monitoring our 200 Hz signal. These readings of saturation current can be plotted versus position to produce a relative plasma density map. Figure 13 is a plot of such signals versus $\frac{z}{z_{total}}$ (.5 = tunnel centerline) at a given y locations from the cathode surface. Figure 14 is a cross plot from Figure 13 which shows contours of constant signal level at a given cross section. The data spans two orders of magnitude in density.

An estimate of D_a from the data is 24.2 cm^2/sec. Using the fact that electrons are much hotter than ions in this type of plasma and from data on ionic mobility coefficients[27] we can estimate D_a. Using the formula:

$$D_a \simeq \frac{kTe}{e} \mu+$$

with $\frac{kTe}{e} \simeq 1$ volt,

$E \simeq 500$ v/cm,

p @ 73 °K $\sim$ 12.2 torr,

$p_{equivalent}$ @ 300 °K $\sim$ 50 torr,

we find $D_a \simeq 26$ to 50 cm^2/sec in nitrogen depending on whether atomic or molecular ions are involved. Though our data is limited we see that the model has some validity. A reasonable D_a also appears to describe the amount of spanwise spreading observed near the cathode.

It appears that some source distribution instead of just a delta function at $x = x_o$ (i.e. upstream), is more likely to be consistent with the present data.

In order to arrive at an absolute number density estimate from our measurements of saturation currents we proceed as follows:

$I = enuA$

$e = 1.602\ 20^{-19}$ coul.

n = number density

u = flow velocity

A = cross section of a stream tube whose bounding streamlines traverse the probe bow shock and graze the edge of the probe sheath.

We say that the quasineutral plasma is swept downstream at the flow velocity flow velocity and that all particles in the stream tube are carried into an electric sheath where they are retrieved by the probe. Our problem is in estimating A. Most relevant theories of plasma probing surveyedseem to

give estimates of probe sheath thickness within a factor of 2 or 3 of each other and with a slow dependence on n. For our experiment we expect the ratio of sheath thickness to probe diameter to be smaller than or nearly equal to 1. Therefore as a first estimate we say that A is approximately equal to the frontal area of the probe wire and is a constant value wherever we make our measurements. In actuality A increases as n decreases reducing spatial resolution in regions of lower plasma density and signal level.

Between the value of noise level and the maximum signal our instrument can assimilate (the range in Figure 13) we estimate an ability to detect densities from $\sim 10^{10}$ to 7×10^{11} cm^{-3}.

As a final note we should say that we have measured a floating potential rise of about 230 volts within 0.1 cm of the cathode surface.

(8) Summary

Brief reviews were made of the results of earlier flow and terminal electrical characteristic measurements, as well as of the arc propagation and plasma flow models.

Data was presented on the dependence of arcing rate on discharge parameters and the arc propagation model was checked with a direct measurement of arc speed and width. Cathode fall voltages have been measured at some locations and found to be about 200 to 230 volts.

A successful plasma probing technique was developed and relative plasma density profiles and contours have been mapped out at the middle window port with one pin and the sustainer plates active. Comparison of data with theory indicates a need to improve our modelling of the source

terms but does not negate as yet the foundations of the theory. More data is needed to further test the soundness of our theoretical model and to elucidate the role of volume ionization in the discharge volume.

III.B. CO-Gain Measurements

Small signal gain measurements, made in a low temperature CO-N_2 mixture expanded through a hypersonic nozzle, were reported in the last annual report.[7] Static temperatures were varied over a narrow range (30, 35, 41 °K) by altering nozzle throat diameter. Stagnation conditions, 2000 psia and 2000 °K, and gas mixtures, CO:N_2 = 15:85, were maintained fixed throughout.

Attention here is focused on the M = 18.5 data (T_{trans} = 30.3°K, $n_{N_2\text{-}CO} = 1.2 \times 10^{16}$ cm^{-3}). Specifically, this discussion concerns the detection of rotational nonequilibrium deduced from the vibrational populations computed from measured small signal gains. Details of the three pass optical system employed to measure gain may be found in Refs. 7 and 28. The measured gains are presented graphically in Ref. 7 and are tabulated in Ref. 28. Vibrational populations corresponding to the values of gain measured for T_{trans} = 30.3 are shown in Figure 15. These populations were derived from the small signal gain equation for a Doppler broadened line using the equation[29]

$$\alpha_{\substack{V\to V-1 \\ J-1\to J}} = \frac{A_{10}}{8\pi \tilde{\nu}_{10}^3} \frac{J}{\sqrt{2\frac{k}{m}T_{trans}}} \left|\frac{R_{V,V-1}}{R_{10}}\right|^2 \frac{1}{Q_{rot}} \left(e^{-\frac{J(J+1)\theta}{T}}\right)\left(n_V e^{\frac{2J\theta}{T}} - n_{V-1}\right) \qquad \text{(III.B.1.)}$$

where A_{10} = spontaneous transition probability = 30.3 sec^{-1}

$\tilde{\nu}_{10}$ = 2143.2 cm^{-1}

K = 1.38×10^{-16} ergs/°K

m = 4.648×10^{-23} grams.

From Reference 29

$$\left|\frac{R_{V,V-1}}{R_{10}}\right|^2 = V\left[\frac{1-2x_e}{1-2x_eV}\right]^2\left\{\frac{(1-2x_eV-x_e)(1-2x_eV+x_e)}{(1-3x_e)(1-x_eV)}\right\}, \qquad \text{(III.B.2)}$$

where x_e = anharmonicity factor - .006126,

and

$$Q_{rot} = \sum_{J=1} (2J+1)\exp\left(-\frac{J(J+1)\theta}{T}\right), \qquad \text{(III.B.3)}$$

where θ = characteristic rotational temperature = 2.78 °K. The symbol T is used to denote the rotational temperature as defined from the relative population of rotational states J-1 and J, in the most general case.

The vibrational populations shown in Figure 15 correspond to solutions of Eq. III.B.1 using $T = T_{trans}$ = 30 °K and pairs of gain values for two P branch transitions on the same vibrational band. The particular pair of P branch gains used to compute n_V are denoted on the figure. The open symbols denote values of n_V computed from gains on the V band, whereas the closed symbols were computed from gains on the V+1 band. Three features are to be noted in Figure 15.

1. There is a surprising amount of scatter in the populations, indicating that the populations predicted are greatly influenced by the particular pair of gain values used in the computation. This is disturbing since according to the theory and associated assumptions these points should lie on top of one another.
2. A general tendency exists that the populations computed from

lower rotational states are lower than those computed from higher rotational transitions.

3. The V=6 populations computed from V=7 band data are approximately a factor of four larger than those derived from V=6 data.

It was postulated in Reference 7 that the major source of the scatter arose from the possibility of rotational nonequilibrium. Initially, values of T greater than T_{trans} were employed in Equation III.B.1, with the result that the scatter reduced somewhat as T increased until T exceeded 35 °K (T_{trans} = 30 °K), at which point the scatter increased as T was raised further. This was not only unsatisfactory as far as collapsing values of n_V to a series of single points, but it is inconsistent, we believe, to assume that if nonequilibrium exists between rotational and translational modes, the rotational populations can be described by a simple Boltzmann distribution. (For $J \geq 6$ the rotational spacing $2J\theta$ exceeds the translational temperature at this low temperature.) The scatter in Figure 15 is greater than can be attributed to errors in gain measurement particularly for the V=7 and 8 bands. Gains were derived from an average of three separate measurements, which for all but the smallest gains varied by less than ± 10%.

There is experimental evidence of another sort that indicates rotational nonequilibrium exists under conditions similar to those studied here. In the 1960's several attempts to determine gas temperature using the electron beam fluorescence technique indicated the possibility of rotational nonequilibrium.[30-34] In these studies rotational temperature was determined from measured rotational fine structure of the emission from the (0-0) band

of the N_2^+ first negative system. They all determined that the rotational temperature deduced from rotational line intensities was higher than the calculated or inferred translational temperature (inferred from auxilliary measurements of pitot pressure and stagnation conditions). Furthermore, the extent of apparent nonequilibrium between the rotational and translational modes (1) increased as static temperature decreased and (2) increased with increasing rotational quantum number, i.e., fairly close agreement between rotational and translational temperature existed down to 20-30 °K if only the first four rotational line intensities were used, but a higher temperature resulted from the first eight line intensities, and an even higher one if additional rotational lines were incorporated. Thus, it appeared that rotational temperature increased with increasing rotational quantum number.

The primary emphasis prevailing at that time was that this anomaly was the result of either (1) inadequacies of the Muntz model[35] in describing the spectra derived from electronic excitation-deexcitation processes[30,31,32] or (2) the presence of secondary electrons which preferentially excited the higher J states,[33,34] or both. While evidence was presented that both causes had validity, the results were not entirely conclusive that some rotational nonequilibrium did not exist, except for Ashkenas[31] whose tests were performed in an essentially static gas. Marrone[34] did suggest the possibility that the apparent rotational nonequilibrium might be real for his free jet flow. Ashkenas was limited to liquid nitrogen temperatures so the degree of nonequilibrium observed was smaller ($\frac{T_{rot}}{T_{trans}} \simeq 1.1$) than that derived in studies performed in free jets or nozzle expansions where translational temperatures down to 4°K[30] were inferred ($\frac{T_{rot}}{T_{trans}} \simeq 1.5$). It is possible then that some fraction of the apparent discrepancy between the rotational and translational temperatures arose from the electron beam excitation-deexcitation model and

the rest, particularly at the lower temperatures, was real.

Vibrational populations were computed from the measured gains using a variety of rotational temperature models which had the general characteristic that T increased gradually as J increased. The variation of T that appeared to produce the least scatter is given in table III.B.1. The convention used here is that J corresponds to the rotational quantum number of the final state, e.g. T(J=5) is the assumed temperature corresponding to the relative populations of rotational states J = 4 and J = 5. It was necessary to assume temperatures T(1) - T(4) in order to compute the rotational partition function (Equation III.B.3). The contributions to Q_{rot} from states $J \geq 11$ are less than .02%, and gains were measured only for $5 \leq J \leq 10$, so no model for higher level temperatures is warranted.

TABLE III.B.1

J	1-4	5	6	7	8	9	10
T(J)°K	30.3	30.7	31.8	33.3	34.7	36.1	37.7

The results using this model are shown in Figure 16. The scatter has been reduced to the extent that all points fall within $\pm$ 10% of the centroid of values computed for a particular n_V with only two exceptions. The data fall so close to one another that the symbol designation of Figure 15 becomes meaningless in Figure 16. The two exceptions are that values of n_6 computed from V=7 band data fall a factor of two (versus a factor of four in Figure 15) below those computed from V = 6 band data. And two of the values of n_8 computed from V = 9 band data fall distinctly below those derived from V = 8 band results. The values of n_V computed from V = 6 and 9 band data may be less reliable than those from V = 7 and 8 bands since the gains are

smaller and thus more subject to statistical error. That is, solution of Equation III.B.1 for a pair of gain values corresponds to seeking a small difference between two large numbers to determine n_v and n_{v-1}. Therefore small variations in measured gains can produce large changes in the computed populations. (Likewise small variations in assumed rotational temperature can produce large variations in computed populations.) The scatter in the measured gains[28] for the smallest gains is sufficient to account for the apparent disagreement in values of n_6 and n_8 noted above.

The high degree of correlation between populations computed using a variety of rotational levels, we believe, justifies the assumption of rotational nonequilibrium. There is no independent method to determine if the values of T in Table III.B.1 are the correct ones from the present data. They do increase gradually from T_{trans}, which one would expect, and they are consistent with electron beam derived results for similar gas temperatures[30,33] in pure nitrogen flows. Thus we conclude that when the rotational spacing becomes of the order of or greater than the translational temperature in supersonic flows, rotational nonequilibrium will be observed even when traditional collision frequency and rotational equilibrium concepts indicates that it is unlikely. In the present case, for example, each CO molecule suffers approximately 10 collisions/cm transiting the test section which is more than 20 cm long. Several measurements in shock structure studies indicate that two to ten collisions are required for rotational equilibrium. However, this result is probably misleading in the present case since in a shock wave the translational temperature exceeds the rotational temperature in contrast to the rapid expansion case. Moreover, on the high temperature side of the shock, detailed measurements have not been performed at high

rotational levels where the rotational spacing $2J\theta$ might be greater than the translational temperature to see whether they are indeed equilibrating as quickly. Further evidence of the difference between shock wave and expansion flow rotational equilibrium has been recently described for hydrogen.[36] The results of the analysis in Reference 36 are consistent qualitatively with the phenomena suggested here.

It is interesting to note that the rotational nonequilibrium observed in highly expanded flows presents a serious limitation on the achievable small signal gain or output power that can be derived. That is, while we certainly observed gains that were large compared to those anticipated at higher temperatures (less expansion from identical plenum conditions), they are not as large as those possible if rotational equilibrium with the translational mode were maintained.

III.C. Waveguide Laser

1. Design and Operation

A transverse discharge waveguide laser sketched in Figure 17 was constructed using a liquid nitrogen cooled copper block as one electrode, a polished aluminum coated glass plate as the other electrode and edge polished glass slides as spacers. The waveguide channel was 2 mm x 2mm square and 10 cm long. Operation was achieved at a nominal gas temperature of 100 °K with gas mixtures of He:CO in the range of 4:1 to 10:1 at total flow rates of about 4 liters/min. Upstream and downstream pressures of 65 Torr and 25 Torr, respectively, were maintained. This corresponds to a gas exchange rate of about 1.5 changes/ sec. The gas discharge was achieved using 500 volt pulses which had a half width of 60 μsec.

The laser output was measured to peak at about 5 - 10 mW with a pulse width of 50 -120 μsec. The electrical efficiency of this system based on an assumed peak current value of 4.6 amps is approximately .001%. It was not possible to optimize the output parameters with respect to gas mixture or discharge conditions because of the deterioration of the strip electrode.

2. Gas Impurities

During the course of the gain measurement it was observed that a visible layer of material was deposited on all of the waveguide walls if the discharge was operated for a half hour or more. For a discharge period of about 30 minutes the deposits appeared as a thin-film, yellow and red in color. As the discharge times became longer the deposited film became thicker, more uniform and brown in color. One of these

deposits is pictures in Figure 18. The deposits did not appear in a pure helium discharge but only when carbon monoxide was present. They also did not appear unless the discharge was switched on; i.e. no deposits were left from the flowing gas alone. The character of deposits was also not affected by the discharge polarity.

These observations suggested that there was some impurity present in the carbon monoxide. Since the same bottle of CO had been used throughout the research period it was conjectured that the metal walls inside of the gas bottle could have been 'flaking' and progessively adding a metal (most likely iron) impurity to the gas. (It should be noted that a dry ice/methanol cold trap was introduced in the gas flow line to facilitate the removal of the impurity. By visual observation the character of the discolorations was unaffected by this step.)

The possible existence of an impurity was investigated by examining two anode plates via x-ray spectrum measurements in a scanning electron microscope (SEM). The first plate (#1) was used in a discharge for a total of about 12 hours. The initial bottle (A) of CO was used to supply this discharge. Thick deposits, brown/black in color were present on the plate when it was removed. The second plate (#2) was used for about 2 hours with a new bottle (B) of CO of nominal purity 99.99%. No colored deposits were present, however a thin whitish film and bright spots along the waveguide path were observable. For an operating time of two hours with the initial bottle of CO, colored films were clearly present. By this observation, then, the purity of bottle B was much improved over that of bottle A.

The SEM data are shown in Figures 19 through 24. Referring to Figure 18 there were three regions that were examined: the anode plate off of the deposited stripe, the background of the stripe and some bright spots which appear along the stripe. For both plates the region off the stripe showed aluminum only (Figures 19 and 22). In the case of plate #1 the stripe background is clearly composed of iron (Figure 20) while the bright spots are predominantly copper with a substantial amount of iron also present (Figure 21). Both regions also shown the presence of aluminum, as expected. The data for plate #1 show that the signal from iron is about as strong as that for aluminum on the stripe region. (The scanning electrons penetrate several hundred Å). For plate #2 the strip background contains a slight amount of iron, approximately .2% of the amount of aluminum (Figure 23). The bright spots on plate #2 do not contain any copper, but do contain an increased fraction of iron, about 6% (Figure 24).

From these data we infer the following:

a) Iron is present as an impurity in both bottles of carbon monoxide perhaps in the form $FE(CO)_5$.[37] The amount of the impurity present in the gas probably increases with time because of 'flaking' of the walls of the gas bottle. Bottle A was in use for one and one-half years, the impurity became noticeable after about 6 to 8 months. In addition, the nominal purity of bottle A was 99.00%. Thus, the reduced fraction of iron in bottle B versus bottle A is most likely a consequence of its higher purity and 'newness'.

b) The presence or absence of copper in the bright spots probably

reflects the length of time the discharge was operating and the severity of arcing in the discharge. Cathode sputtering is a common phenomenon in gas discharges wherein the impact of ions on the cathode surface causes some cathode material to be removed. The high current densities associated with arcing enhance the sputtering effect. (Sputtering at the anode is not likely because electrons are much less massive than the positive ions). Since in this work the copper block serves as cathode, sputtering is the likely source of copper on plate #1.

The absence of copper on plate #2 reflects the different conditions of plates #1 and #2. Plate #1 was used on three or four consectuve occasions for a cumulative discharge time of about 12 hours. During the last occasion, arcing was especially acute as a result of the thick deposits on the anode and cathode. In comparison, plate #2 was used for two hours in a very homogeneous discharge. Arcing was present but greatly reduced.

3. Gain Measurements

Initial measurements of the gain of several vibrational-rotational transitions for a gas temperature of 215 °K exhibited uniformly small values with a peak of .064%/cm $\pm$ .005 on the 8 P(10) line. The measured gains were generally a factor of 10 or 20 less than what was expected. These magnitudes did not vary more than a factor of two (i.e., .032% to .C64%) by optimizing gas mixture or electric discharge properties.

It was, however, possible to verify some of the expected qualitative features of the small-signal gain. In Figure 25 the gain is plotted vs. vibrational level for three sets of measurements. The magnitudes

are normalized with the peak value set equal to one in each case. Two measurements using CO gas with an iron impurity (bottle A) both shown peak gains in the range V = 8 to V = 10 and a clear reduction at V = 11 and V = 12. The higher purity CO (bottle B) exhibited a similar distribution of gain, but with the peak value clearly shifted to V=11. It should be recalled that previous reports of gain vs. vibrational level gave V = 7, 8 and V = 8, 9 as the optimum values of V.

The distribution of gain vs. J-levels is not so clearly defined. Measurements were made on the 8th vibrational level for J = 8, 9, 10, 12. Only these J-levels were used because lower J-levels have transition frequencies which are near those of the upper J-levels of the V = 7 the the line selection mechanism of the probe laser did not allow clear resolution between these transitions. The data are shown as total percentage gain vs. J, in Figure 26. To within experimental error there is no apparent gain variation over J = 8, 9, 10 and there is an apparent decrease at J = 12.

Increasing the O_2 flow rate from zero to about 20% of the CO flow rate was found to enhance the measured gain by approximately a factor of two. This is shown in Figure 27, where total gain (%) is plotted against Q_{O_2} (liters/min). Because other researchers have found laser operation to be sensitive to the O_2 fraction[38] it was expected that there would be an optimum value of Q_{O_2} with gain decreasing on either side of the optimum. This is shown in the figure by a curve extrapolated to zero gain as Q_{O_2} increases. However, the data points at Q_{O_2}/C_{CO} = 1.4 and 2.7 indicate that the expected decrease of the gain as Q_{O_2} increases

does not occur. Thus, the increase of gain with small values of Q_{O_2} agrees with observed enhancement of CO laser performance by addition of O_2. But the fact that the gain does not decrease for large values of Q_{O_2} is contrary to expectations and not well understood.

The gas impurity discussed in the previous section did not significantly affect the gain. The peak total gain using bottle B was .90% whereas using bottle A the peak was .58%. As shown in Figure 25 the gain peak shifted to V = 11, from the region V = 8 to V = 10 by substituting the 'clean' CO.

The small-signal gain profile of the waveguide discharge was found to be spatially non-uniform. The variations occurred only along the line between the anode and cathode (vertical direction) and not in the horizontal directions. The sequence of oscillographs shown in Figure 28 follows the movement of the beam center across the waveguide from anode to cathode. As the beam is moved in the direction of the cathode the gain increases while absorption tends to zero; when the beam moves toward the anode the reverse is true. This was observed to be the case on several transitions and with the discharge polarity reversed.

Plots of measured gain and absorption versus separation between beam center and waveguide center are shown in Figures 29 and 30. The measurements of Figure 29 were made for an average pressure of 44 Torr, those of Figure 30 for 82 Torr. The 10P (10) line was used for both measurements. To draw conclusions from this data it is first necessary to recall that the probe beam exhibits a Gaussian intensity distribution as shown in Figure 31. Thus, when the beam is aligned for maximum transmission, the peak intensity passes through the waveguide center

while at the walls the intensity has dropped by some fraction.

Consideration of Figures 29 and 30 shows that the region of high gain and zero absorption appears when the beam center is just past the cathode edge of the waveguide whereas the high absorption and low gain region peaks near the anode wall (1.0 mm from center) and tends to zero on either side of this point. This indicates: 1) that the region of absorption extends over a larger portion of the discharge than does the gain region; ii) that the gain region is located very near the cathode. This conclusion is drawn because the gaussian intensity distribution drops from one waveguide edge to the other when the beam center is positioned outside of the waveguide. Consequently, the intensity near the cathode wall is sufficient to exhibit the gain region but decreases away from the cathode so that the absorption signal is very small. Furthermore, the gain goes to zero if the beam center is located in the waveguide at position Z =-.75 mm. Then the signal intensity is smaller near the cathcde than in the absorption region.

Two further points should be noted. First of all, increasing the pressure appears to reduce the extent of the gain region. Secondly, there is a region of absorpticn and gain which is observed after the beam center passes the anode edge of the waveguide. This may be the result of grazing reflections on the anode.

The reason for the non-uniformity of the gain is not certain. One possible cause is the input electrical pulse length. The gain measurements were performed using pulse lengths on the order of 1 μsec. Computations by Boulnois[8] show that under ccnstant pumping, steady-state vibrational populations are achieved after about 40 μsec. Furthermore, it should

be recalled that laser oscillation was achieved using 100 μsec wide pulses. It is possible that the short pulses (1 μsec) do not deposit enough energy into the medium for inversion to be obtained. The presence of gain in the cathode fall region may result from the comparatively high electron energies found there. That is, there may be a spatial distribution of available electrical energy such that gain is obtained in the more energetic cathode fall region but not in the less energetic positive column.

On the other hand this hypothesis does not account for two facts. First of all, in the gain region the absorption is zero. The expected mechanism of population inversion involves an initially non-inverted (absorbing) distribution created by electron energy transfer to CO, followed by V-V pumping to achieve the inverted population. Secondly, transverse discharge CO lasers have been reported which operate using voltage pulse widths on the order of 0.5 μsec.[39,40]

IV. REFERENCES

1. W. L. Nighan, "Electron Energy Distributions and Collision Rates in Electrically Excited N_2, CO and CO_2," Physical Review A, Vol. 2, p. 1989 (1970).

2. A. G. Englehardt, A. V. Phelps, and C. G. Rich, "Determination of Momentum Transfer and Inelastic Collision Cross Sections for Electrons in Nitrogen using Transport Coefficients," Physical Review, Vol. 135, p. A1566 (1964).

3. W. L. Nighan, "Electron Kinetic Processes in CO Lasers," Appl Phys. Lett., Vol. 20, p. 96 (1972).

4. T. G. Jones, S. R. Byron, A. L. Hoffman, B. B. O'Brien, and W. B. Lacina, "Electron-Beam-Stabilized C. W. Electric Discharge Laser in Supersonically Cooled $CO/N_2/Ar$ Mixtures," AIAA 7th Fluid and Plasma Dynamics Conference, Paper 74-562 (June 1974).

5. J. A. Lordi, S. J. Falk, and J. W. Rich, "Analytical Studies of the Kinetics of Electrically Excited Continuously Operating CO Flow Lasers," AIAA 7th Fluid and Plasma Dynamics Conference, Paper 74-563 (June 1974).

6. J. A. Smith, S. H. Lam, R. B. Miles and G. K. Bienkowski, Anharmonic Oscillator Lasers, Annual Progress Report, (1975). AFOSR Contract F44620-73-C-0059.

7. J. A. Smith, S. H. Lam, R. B. Miles, and G. K. Bienkowski, "Annual Progress Report on Anharmonic Oscillator Lasers for the Period April 2, 1975 to March 31, 1976," prepared for AFOSR Contract F44620-73-C-0059 (1976).

8. J. Boulnois, "Carbon Monoxide Vibrational Kinetics in a Transverse Electric Discharge Wave Guide Laser," Ph.D. Thesis, AMS Dept., Princeton University (1975).

9. S. H. Lam, to appear in J. Chem. Phys. Sept. 1977. See Appendix B of this report.

10. W. S. Drozdoski, R. M. Young, R. D. Bates Jr. and J. K. Hancock, J. Chem. Phys. 65 1542 (1976).

11. J. W. Rich, J. A. Lordi, R. A. Gibson and S. K. Kang, Calspan Corp. Rept. WG-5164-A-3 (1974).

12. C. A. Brau, Physica. 58 533 (1972). See also B. F. Gordiets and Sh. S. Mamedov, Prik. Mat. Teor. Fiz. 3 13 (1974).

13. A. J. Lightman and E. R. Fisher, "Measurements of CO Vibrational Distributions in MIxtures with N_2, O_2, Ar and He," presented at 5th Conference on Chemical and Molecular Lasers, WAI6, St. Louis, Mo. (1977).

14. R. N. Schwartz, A. I. Slawsky and K. F. Herzfeld, J. Chem. Phys. 20 1591 (1952). Also see R. N. Schwartz and K. F. Herzfeld. J. Chem. Phys. 22 767 (1954).

15. J. Keck and G. Carrier, J. Chem. Phys. 43 2284 (1974).

16. M. Verter and H. Rabitz, J. Chem. Phys. 64 2939 (1976).

17. S. H. Lam and H. Rabitz, "Correlation of Vibration-Translation Rates in CO-He," Annual Progress Report on Anharmonic Oscillator Lasers. AFOSR Contract F44620-73-C-0059, March 1976.

18. T. L. R. Ayers, Phil. Mag. 45 353 (1923).

19. J. Dutton, S. C. Haydon, and F. Llewellyn-Jones, Proc. Roy. Soc. 213A 203 (1952).

20. M. A. Harrison, Phys. Rev., 105 366 (1957).

21. K. Masch, Arch. Electrotech., 26 587 (1932).

22. D. Q. Posin, Phys. Rev., 53 293 (1938).

23. J. H. Blom, R. K. Hanson, Appl. Phys. Lett. 190 (1975).

24. G. A. Simons, AIAA Paper #72-709, Boston, Massachusetts, June 1972.

25. M. Director, AIAA Paper #73-626, Palm Springs, California, June 1973.

26. S. H. Lam, AIAA Paper #65-543, San Francisco, California, July 1965.

27. E. W. McDaniel, Collision Phenomena in Ionized Gases, John Wiley & Sons, Inc., New York, 1964, p. 475.

28. P. J. Susko, "Small Signal Gain Measurements in a Low Temperature CO-N_2 Hypersonic Flow," M.S.E. Thesis, Aerospace and Mechanical Sciences Department, Princeton University 1977.

29. W. B. Lacina, "Kinetic Model and Theoretical Calculations for Steady State Analysis of Electrically Excited CO Laser Amplifier System," Northrup Corporate Laboratories REport NCL 71-32R, August 1971.

30. F. Robben and L. Talbot, "Measurements of Rotational Temperatures in a Low Density Wind Tunnel," Phys. Fluids, 9, p. 644-652, April 1966.

31. H. Ashkenas, "Rotational Temperature Measurements in Electron-Beam Excited Nitrogen," Phys. Fluids, 10, pp. 2509-2519, December 1967.

32. P. J. Harbour, "Absolute Determination of Flow Parameters in a Low Density Hypersonic Tunnel," Rarefied Gas Dynamics, Suppl. 5, Vol. II, L. Trilling and H. V. Wachman, eds., Academic Press, New York, pp. 1713-1722, 1969.

33. S. L. Petrie and A. A. Boiarski, "The Electron Beam Diagnostic Technique for Rarefied Flows at Low Static Temperatures," ibid., pp. 1685-1701.

34. P. V. Marrone, "Temperature and Density Measurements in Free Jets and Shock Waves," Phys. Fluids, 10, pp. 521-538, March 1967.

35. E. P. Muntz, "Static Temperature Measurements in a Flowing Gas", Phys. Fluids, 5, pp. 80-90 (1962).

36. H. Rabitz and S. H. Lam, "Rotational Energy Relaxation in Molecular Hydrogen," J. Chem. Phys., 63, pp. 3532-42, 1975.

37. R. E. Center, "High Pressure Electrical CO Laser," IEEE Journal of Quantum Electronics. Vol. QE-10, pp. 208-213, February 1974.

38. H. Keren, P. Avivi and F. Dothan, "The Influence of Oxygen on CO-Laser Performance," IEEE Journal of Quantum Electronics, Vol. QE-11, pp. 590-594, August 1975.

39. W. Q. Jeffers and C. E. Wiswall, "Excitation and Relaxation in a High Pressure CO Laser," IEEE Journal of Quantum Electronics, Vol. QE-7, pp. 408-412, August 1971.

40. D. B. Cohn, "CO TEA Laser at 77^{o}K," Applied Physics Letters, Vol. 21, pp. 343-345, October 1972.

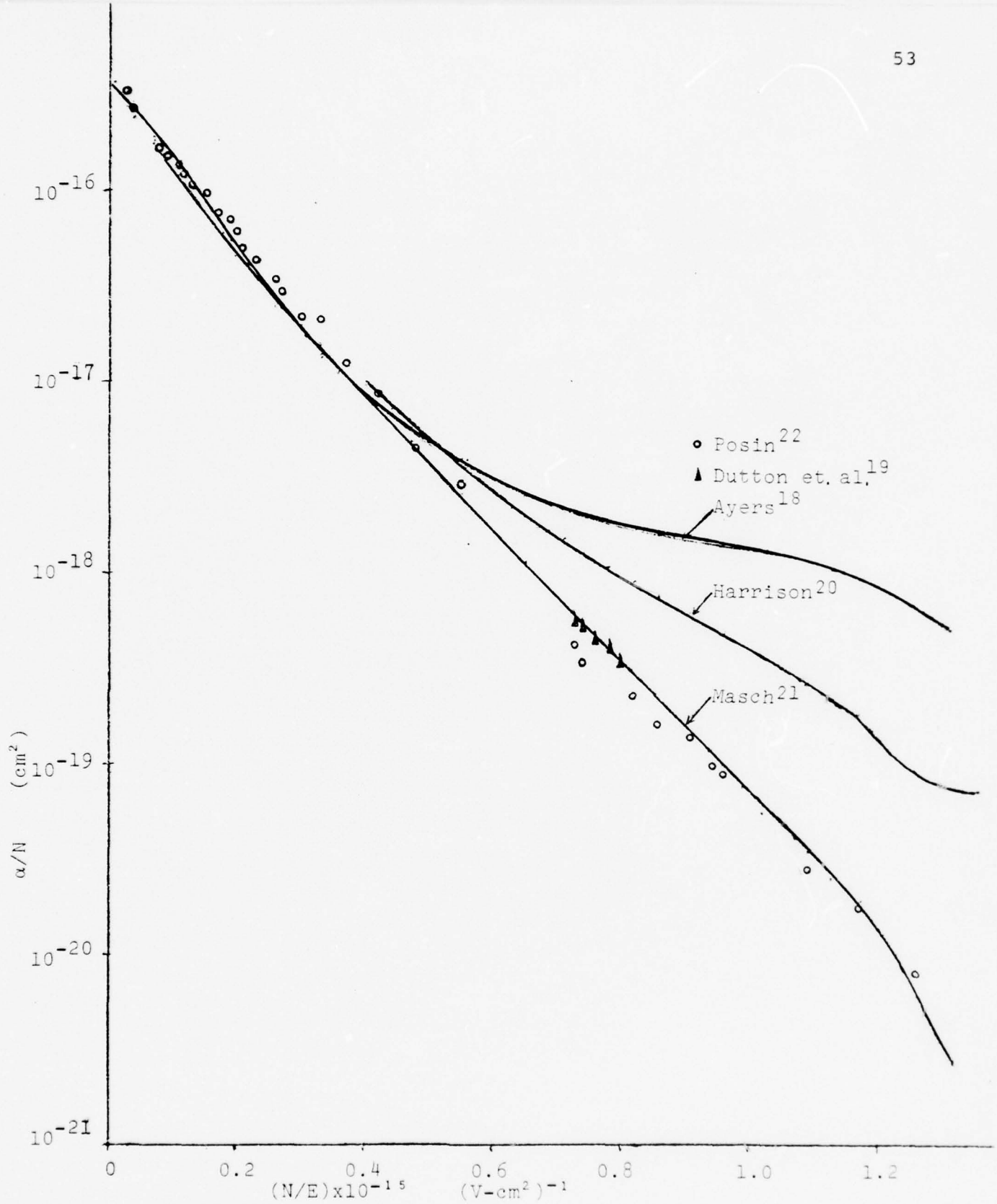

Fig 1: α/N vs. N/E from experiments in N_2

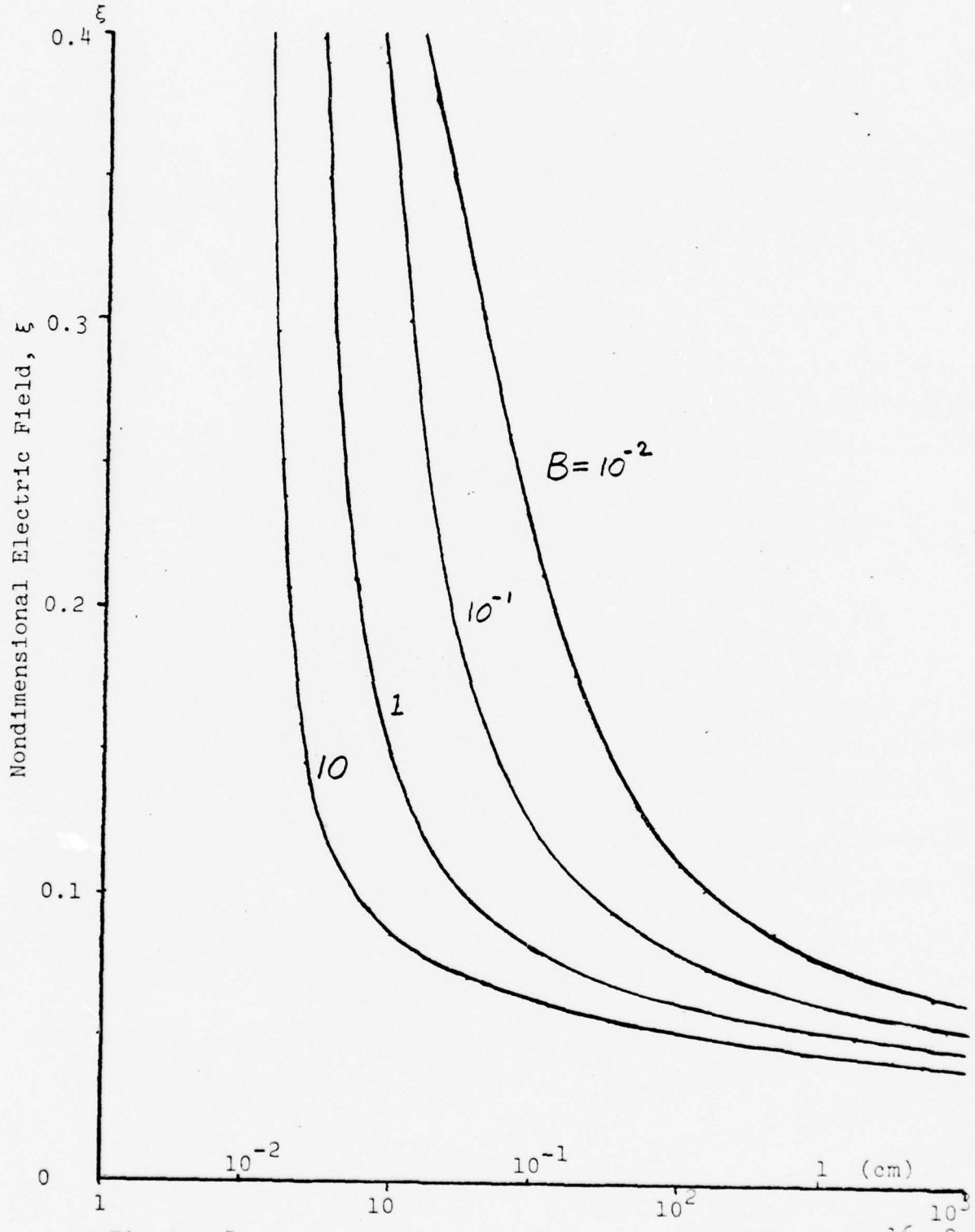

Fig. 2: ξ vs. η and y. y is computed assuming $a=3\times10^{-16}cm^2$ and $N=10^{18}cm^{-3}$

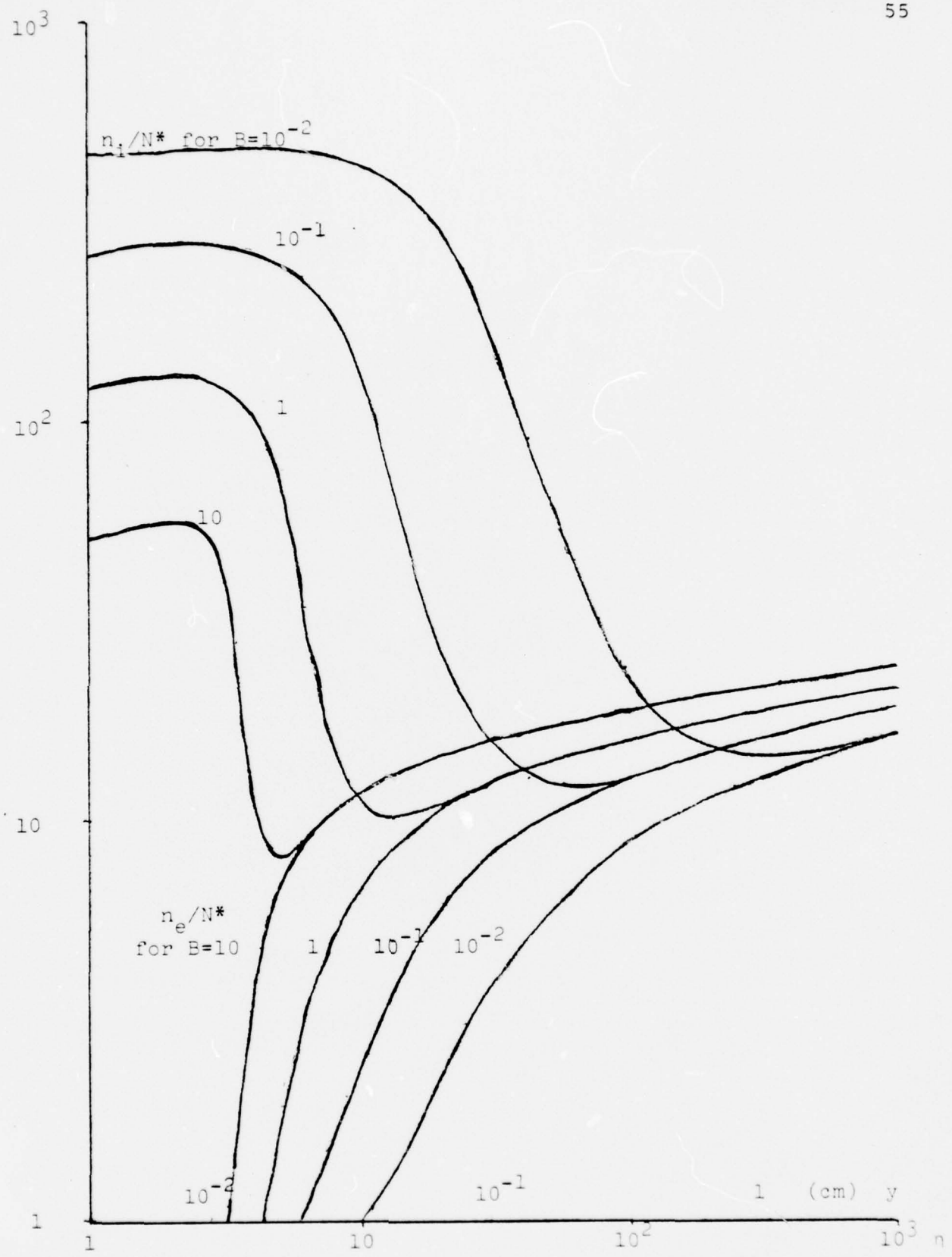

Fig. 3: Normalized densities vs. distance from cathode, η and y. $N^{*-1}=(\mu_e+\mu_i)bN/j$. y is computed assuming $a=3\times10^{-16}$ cm^2 and $N=10^{18}$ cm^{-3}.

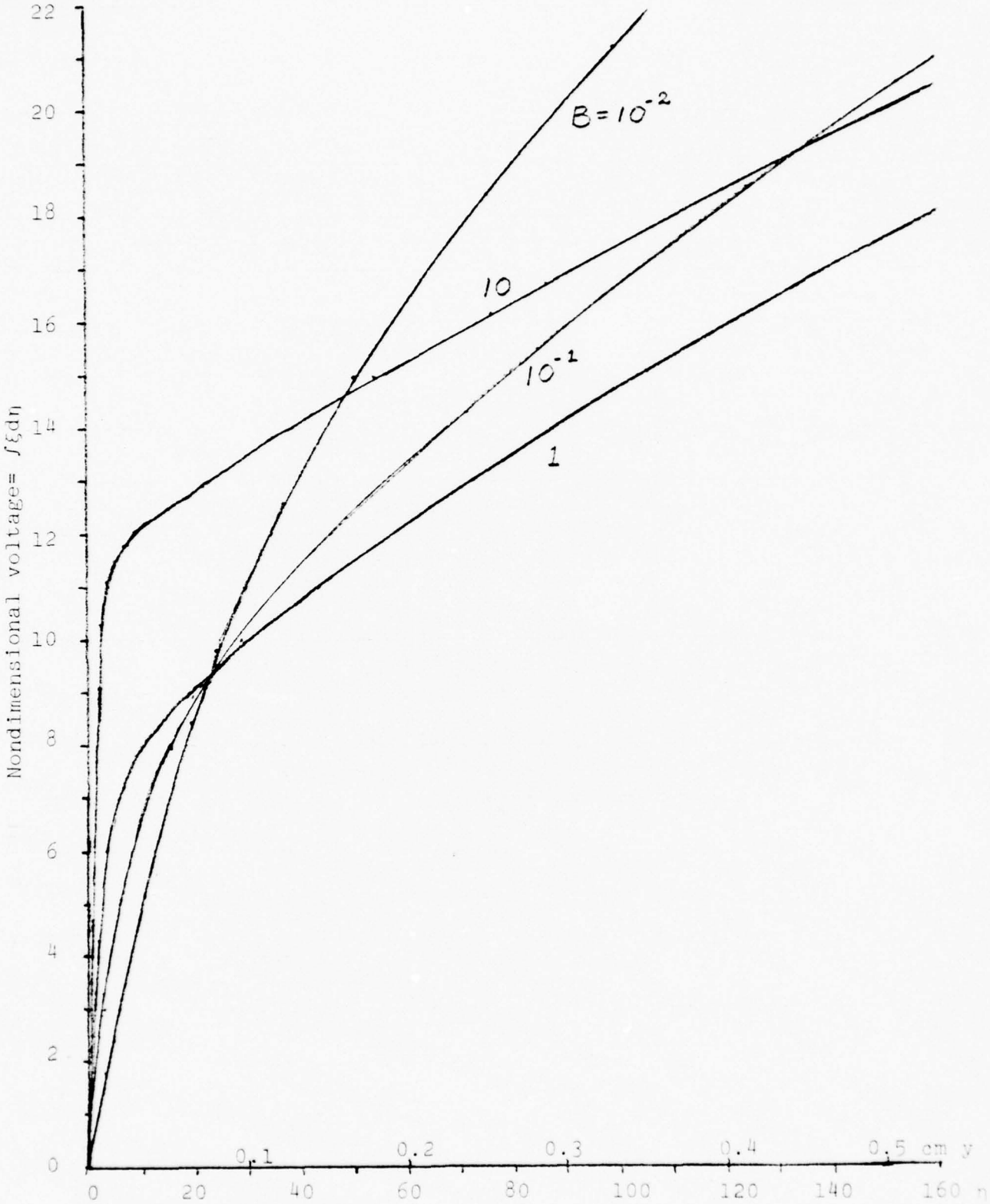

Fig. 4: Nondimensional voltage vs. distance from cathode y is computed assuming $a=3\times10^{-16}$ cm^2 and $N=10^{18}$ cm^{-3}

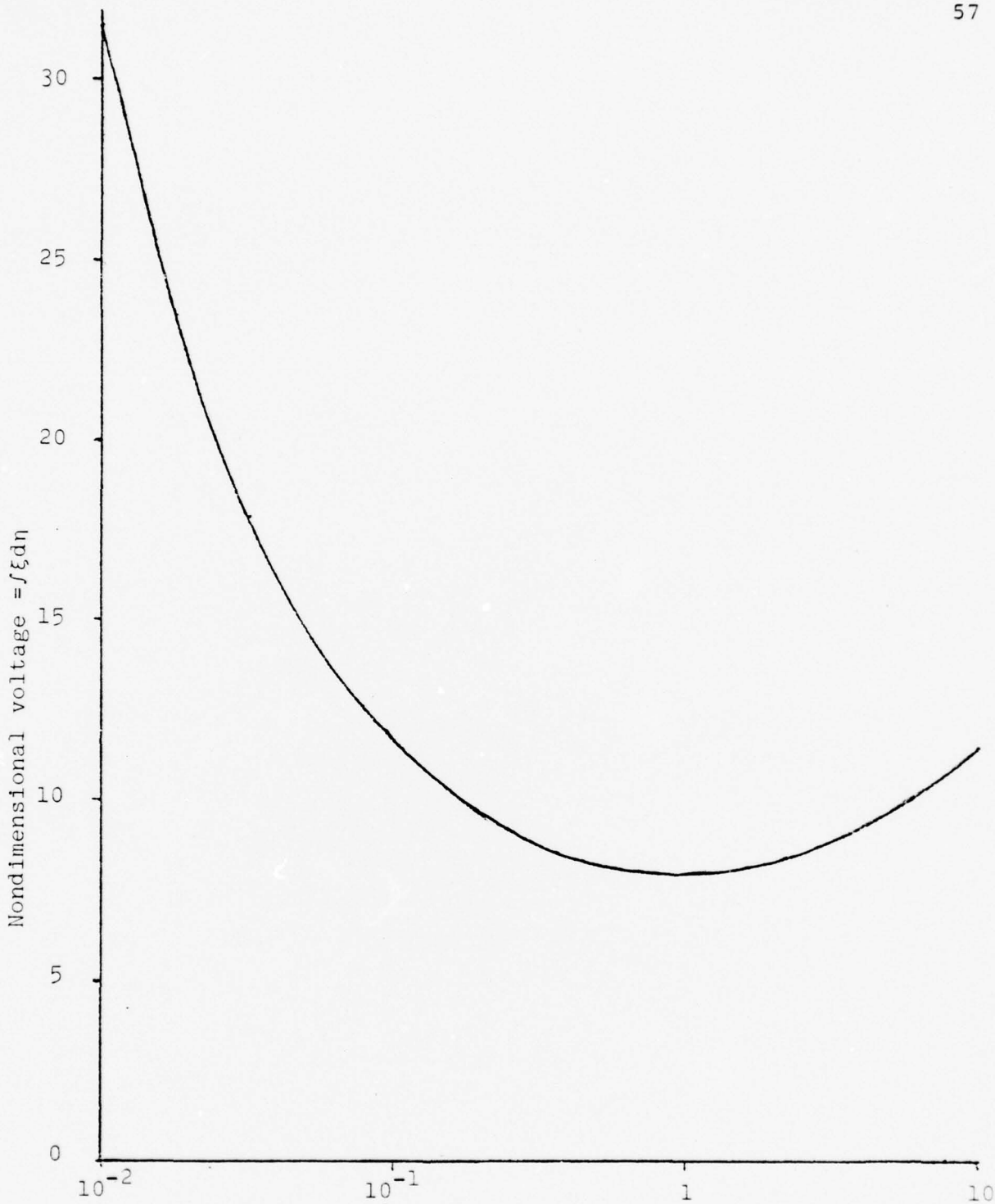

Fig. 5: Voltage at $\hat{J}=10^{-3}$ vs. nondimensional current density, B.

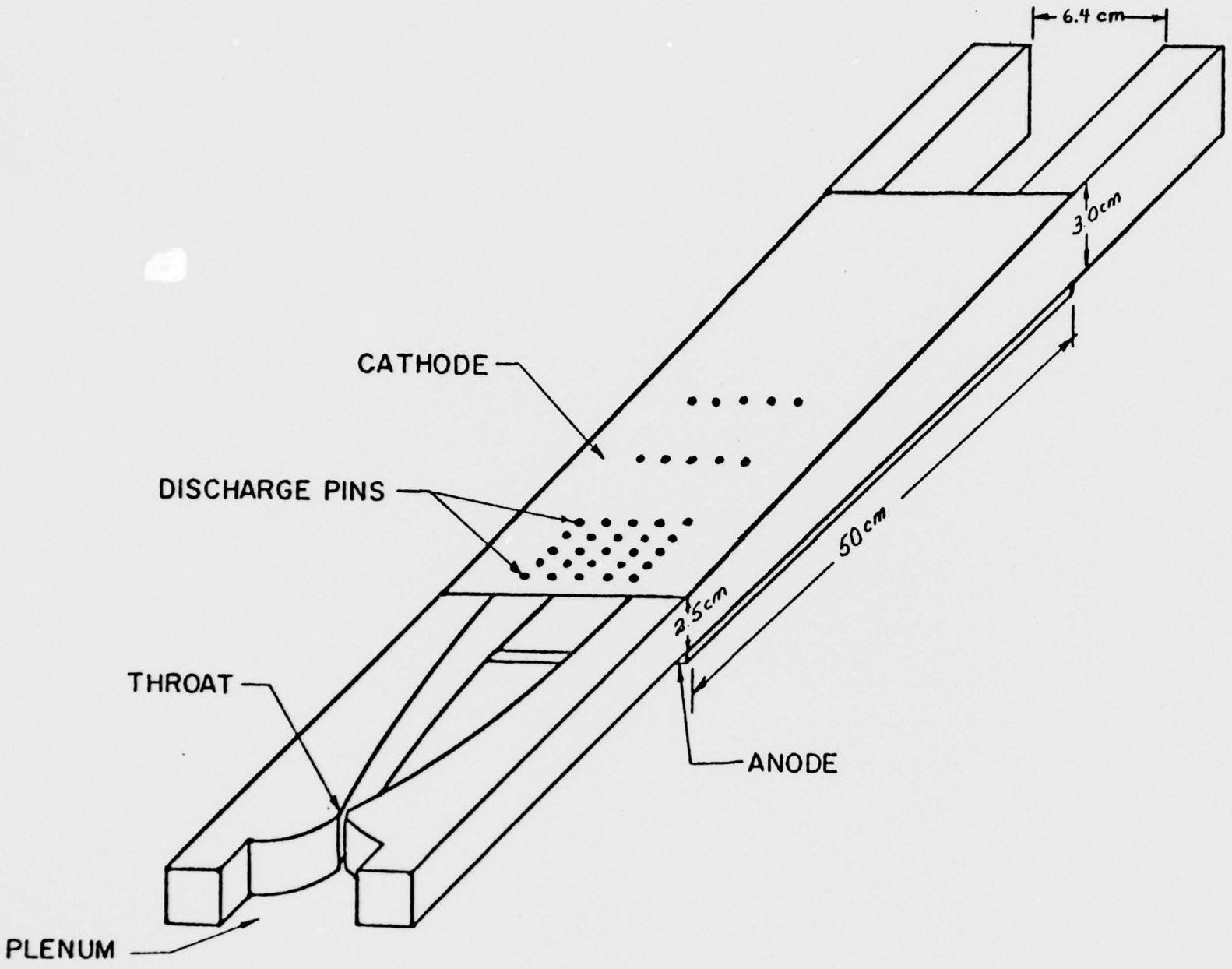

FIG. 6. SCHEMATIC OF SUPERSONIC ELECTRIC DISCHARGE FACILITY

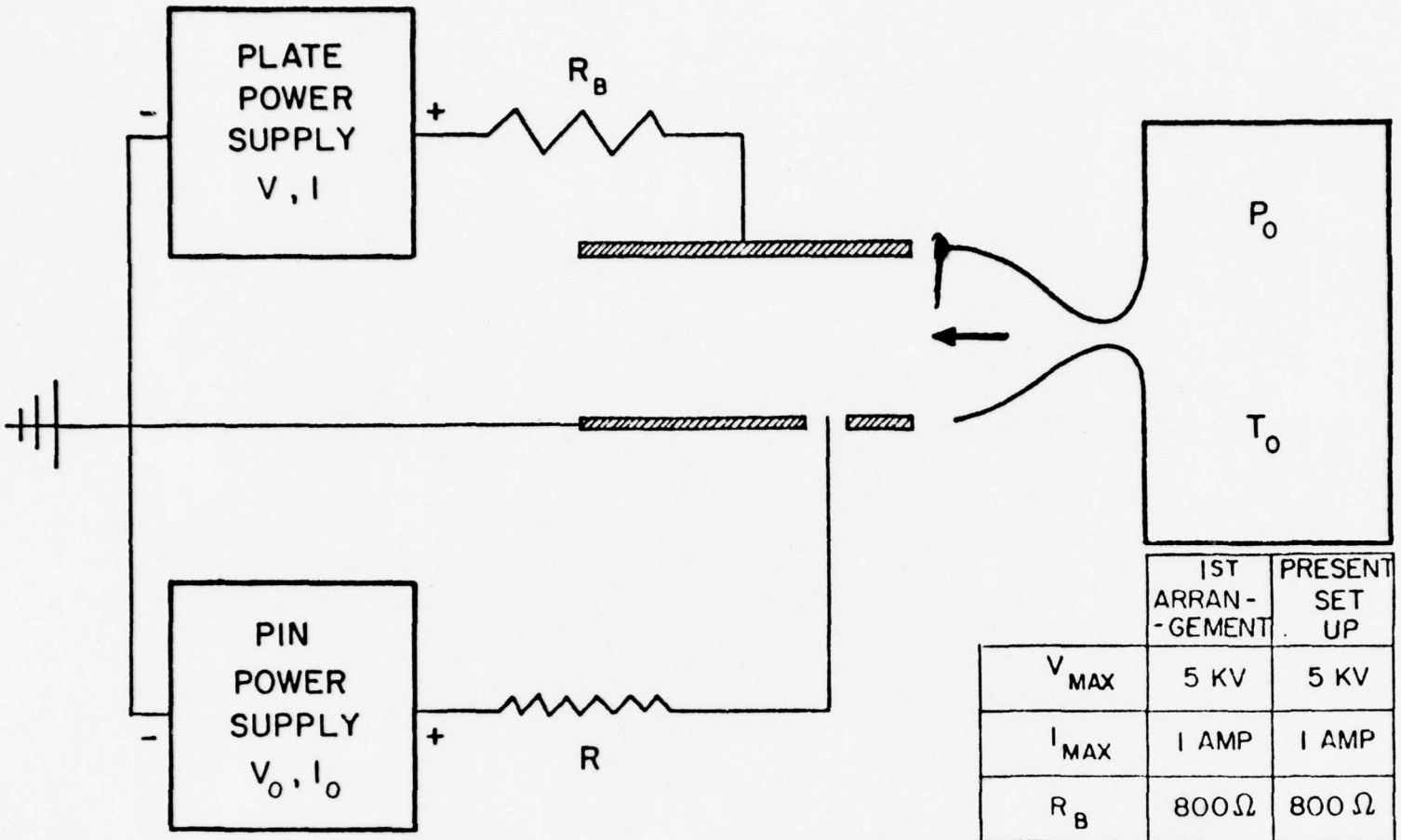

	1ST ARRAN-GEMENT	PRESENT SET UP
V_{MAX}	5 KV	5 KV
I_{MAX}	1 AMP	1 AMP
R_B	800Ω	800 Ω
$V_{O_{MAX}}$	850 V	1.25 KV
$I_{O_{MAX}}$	.150 AMP	2.5 AMP
R; 10 SUCH, PARALLEL	30,000Ω OR VARI-ABLE	3000 Ω

FIGURE 7. GENERAL CIRCUIT DIAGRAM OF DOUBLE DISCHARGE

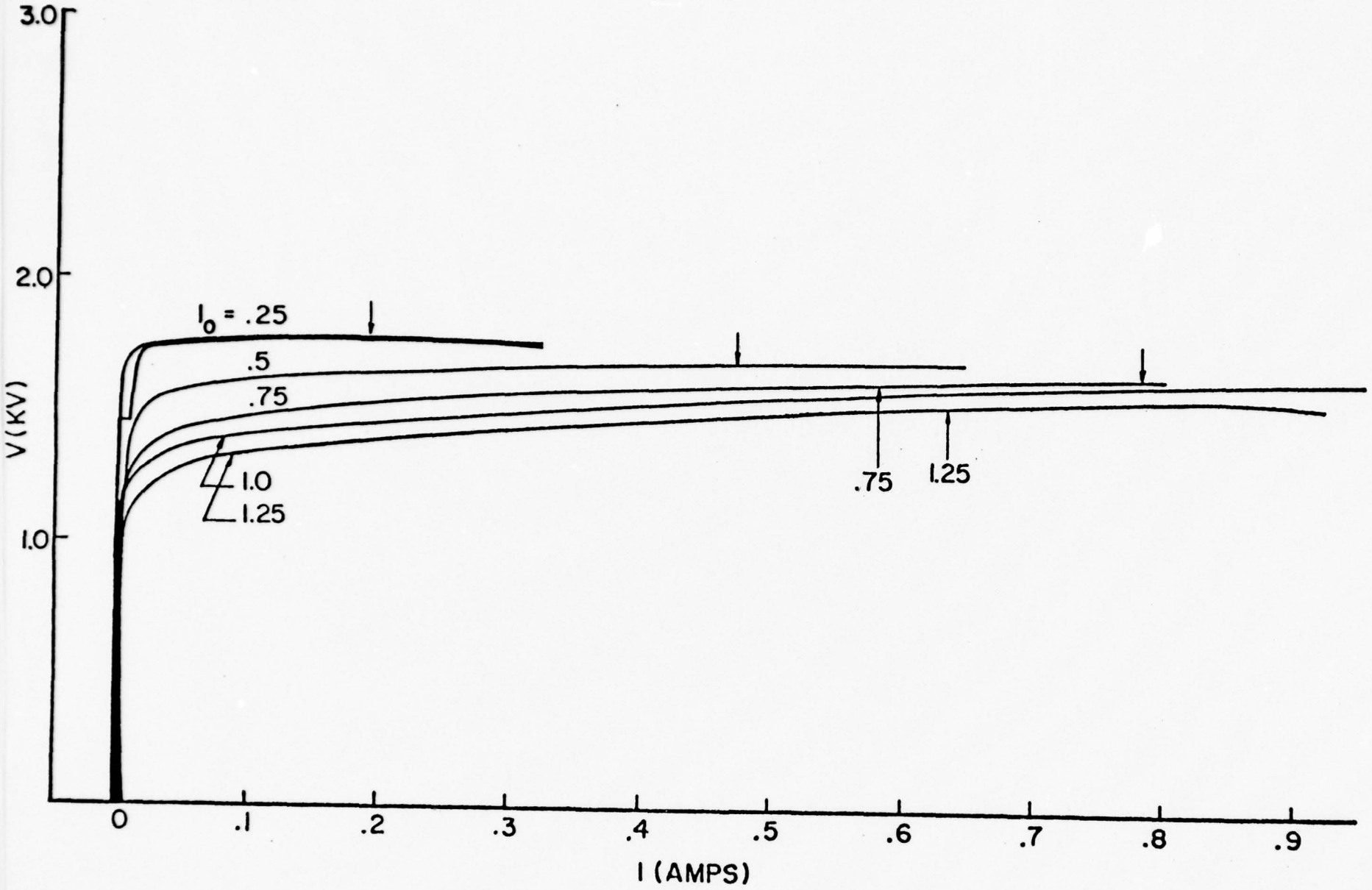

FIG. 8. Voltage-Current Characteristics for Several Pin Currents I_o (P_o = 30 psia).

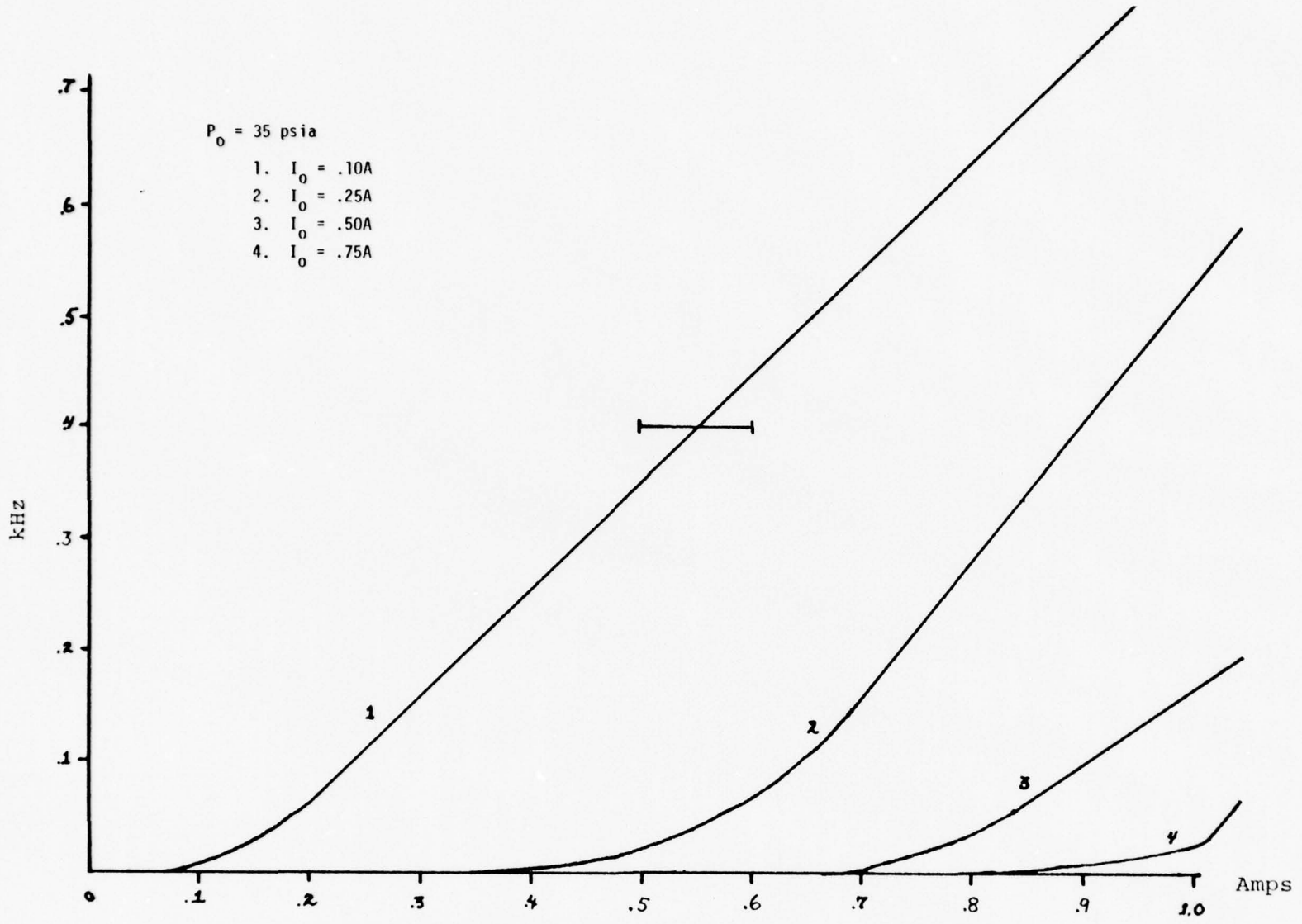

FIG. 9. ARCING RATE IN kHz VS. ANODE CURRENT IN AMPS.

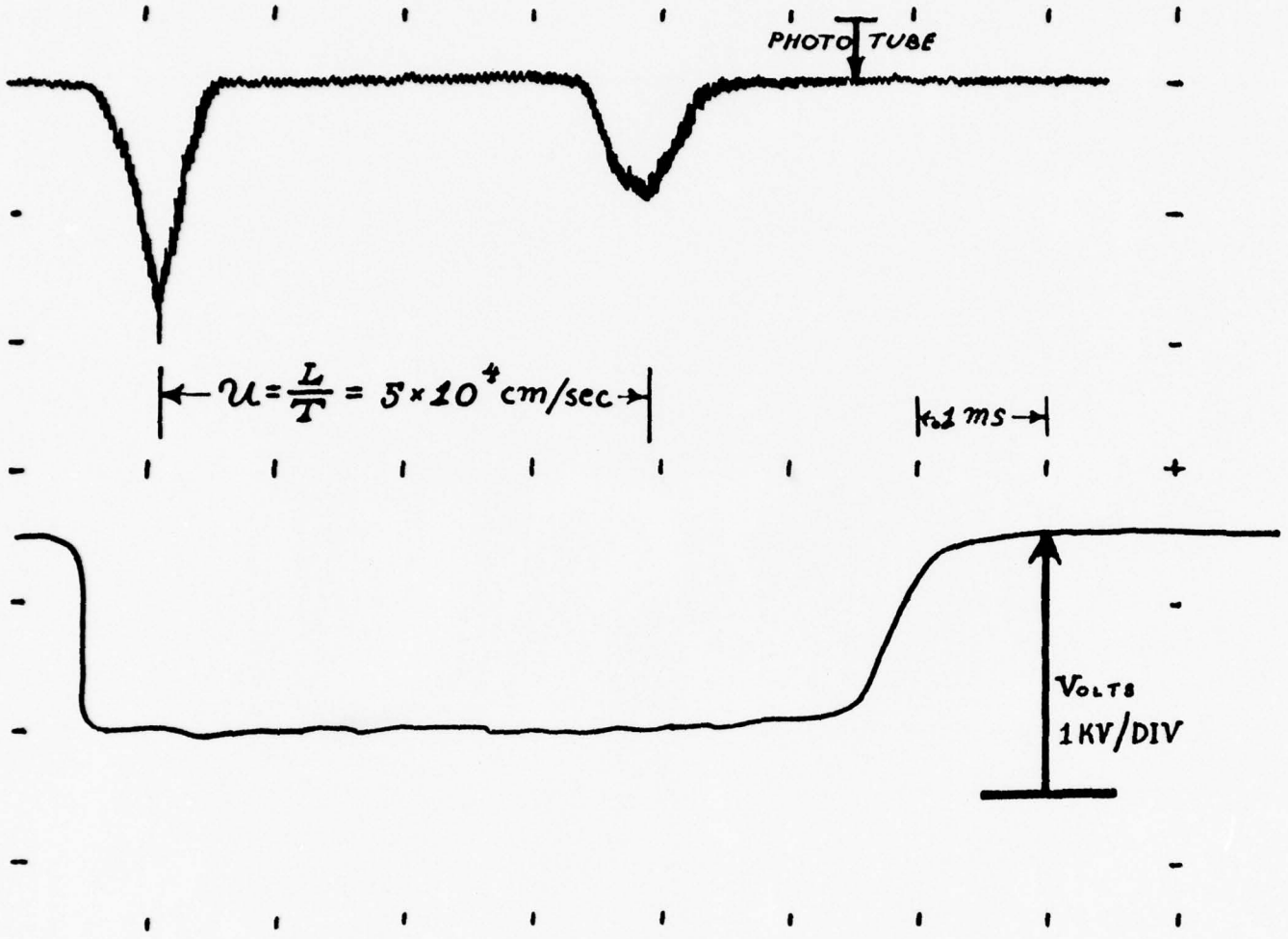

FIG. 10. OSCILLOGRAM SCHEMATIC; PHOTO-TUBE SIGNAL(INVERTED) VS. TIME, ALSO ANODE VOLTAGE VS. TIME; ONE ARC OBSERVED AT TWO TUNNEL LOCATIONS.

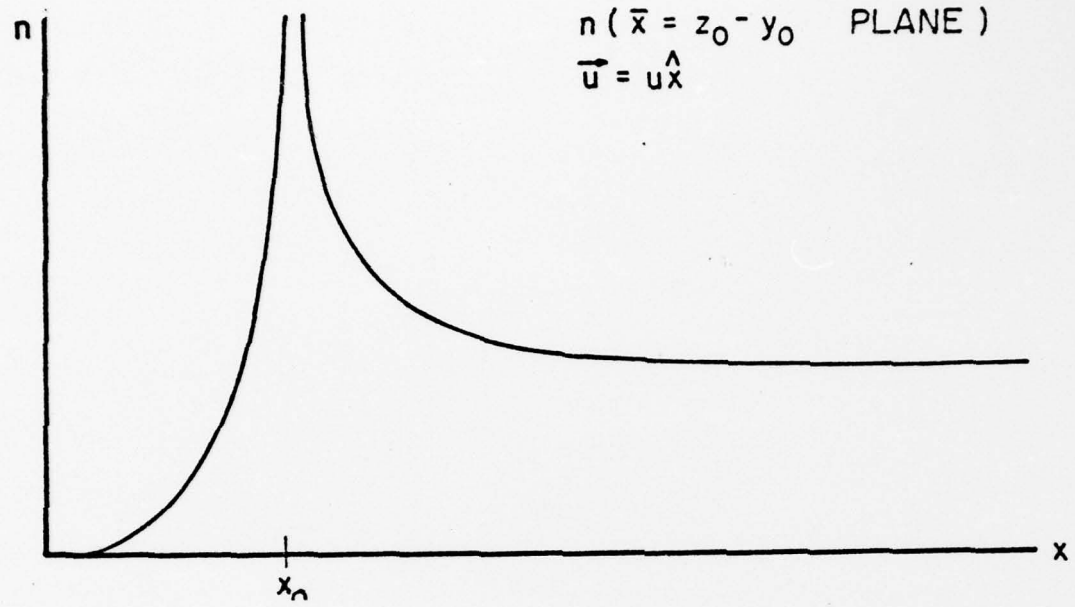

FIG. 11a. INFINITE SPACE SOLUTION: SCHEMATIC ALONG ONE STREAMLINE

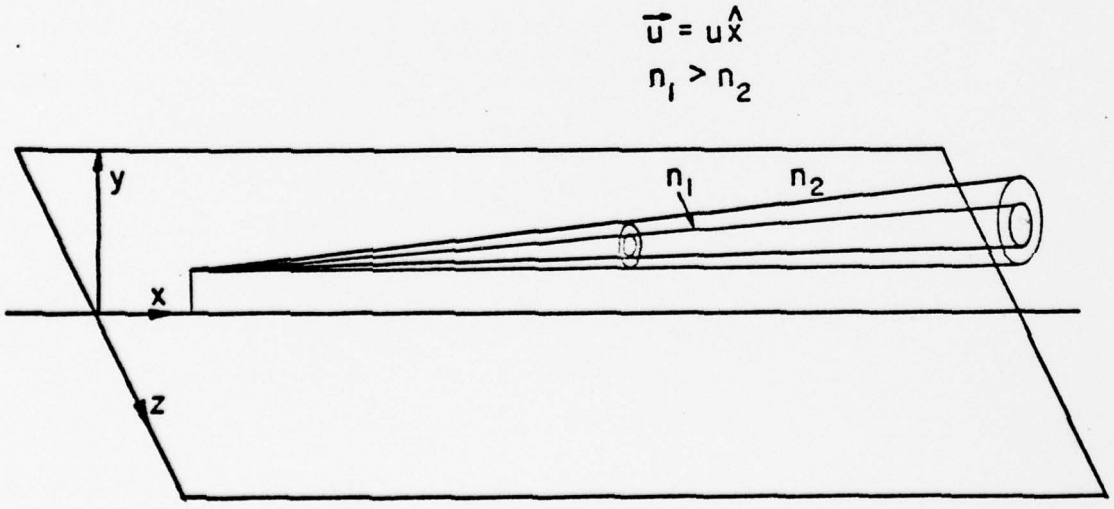

FIG. 11b. SEMI-INFINITE SPACE SOLUTION; CONSTANT DENSITY SURFACES; SCHEMATIC

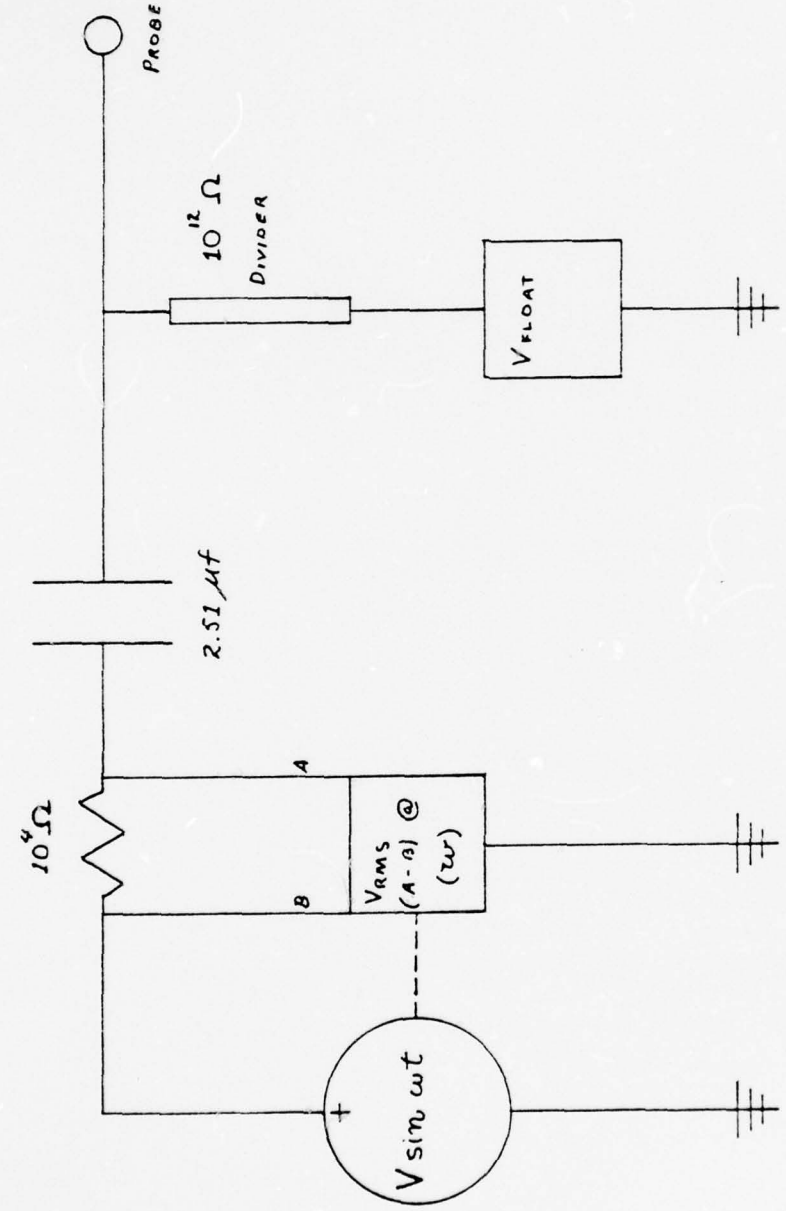

FIG. 12. CIRCUIT FOR PLASMA DENSITY AND FLOATING POTENTIAL PROBE.

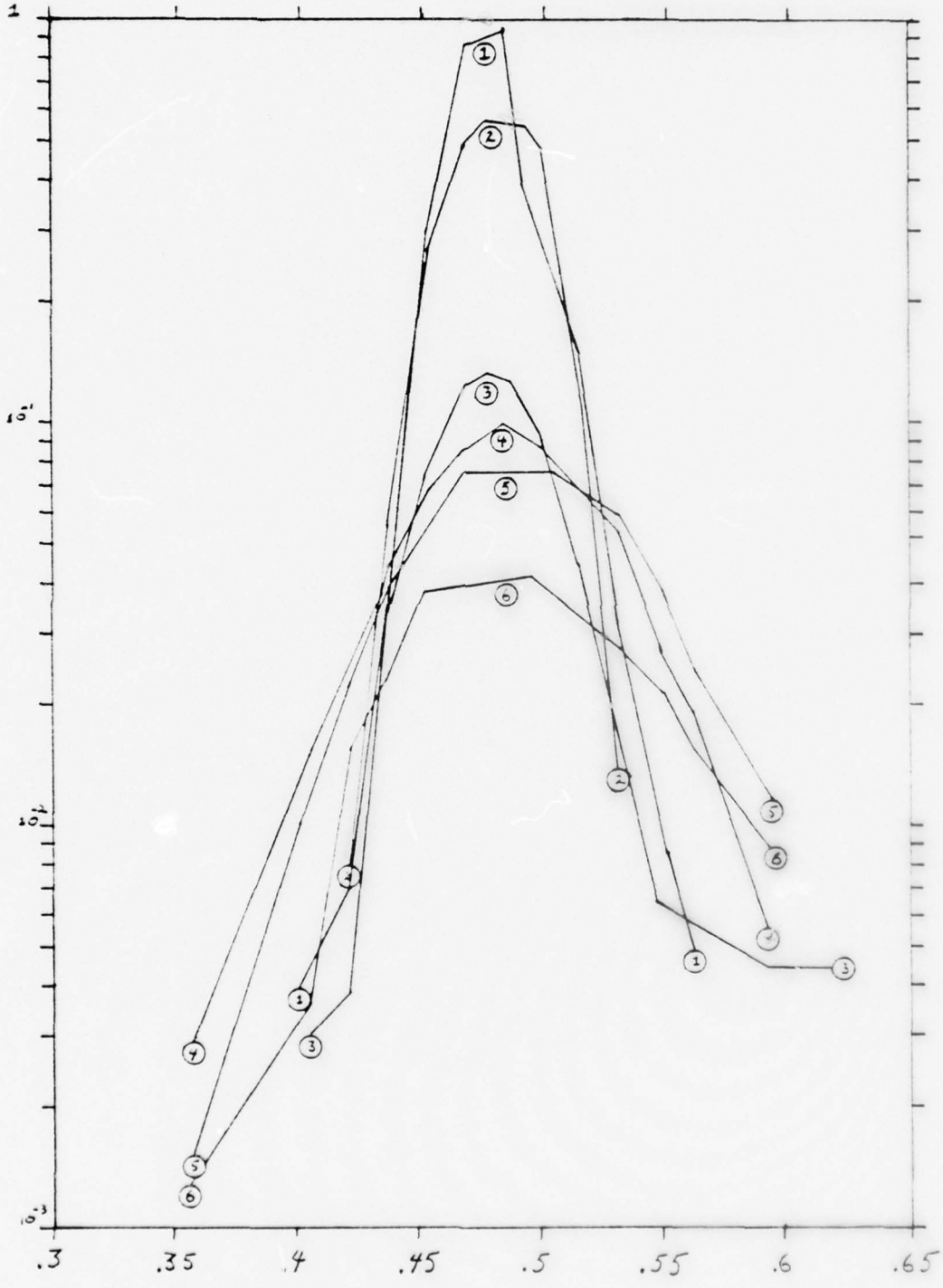

FIG. 13. NORMALIZED PROBE SIGNAL VS. HORIZONTAL POSITION (AS FRACTION OF TUNNEL WIDTH) AT SIX VERTICAL DISTANCES (1 THROUGH 6) FROM CATHODE.

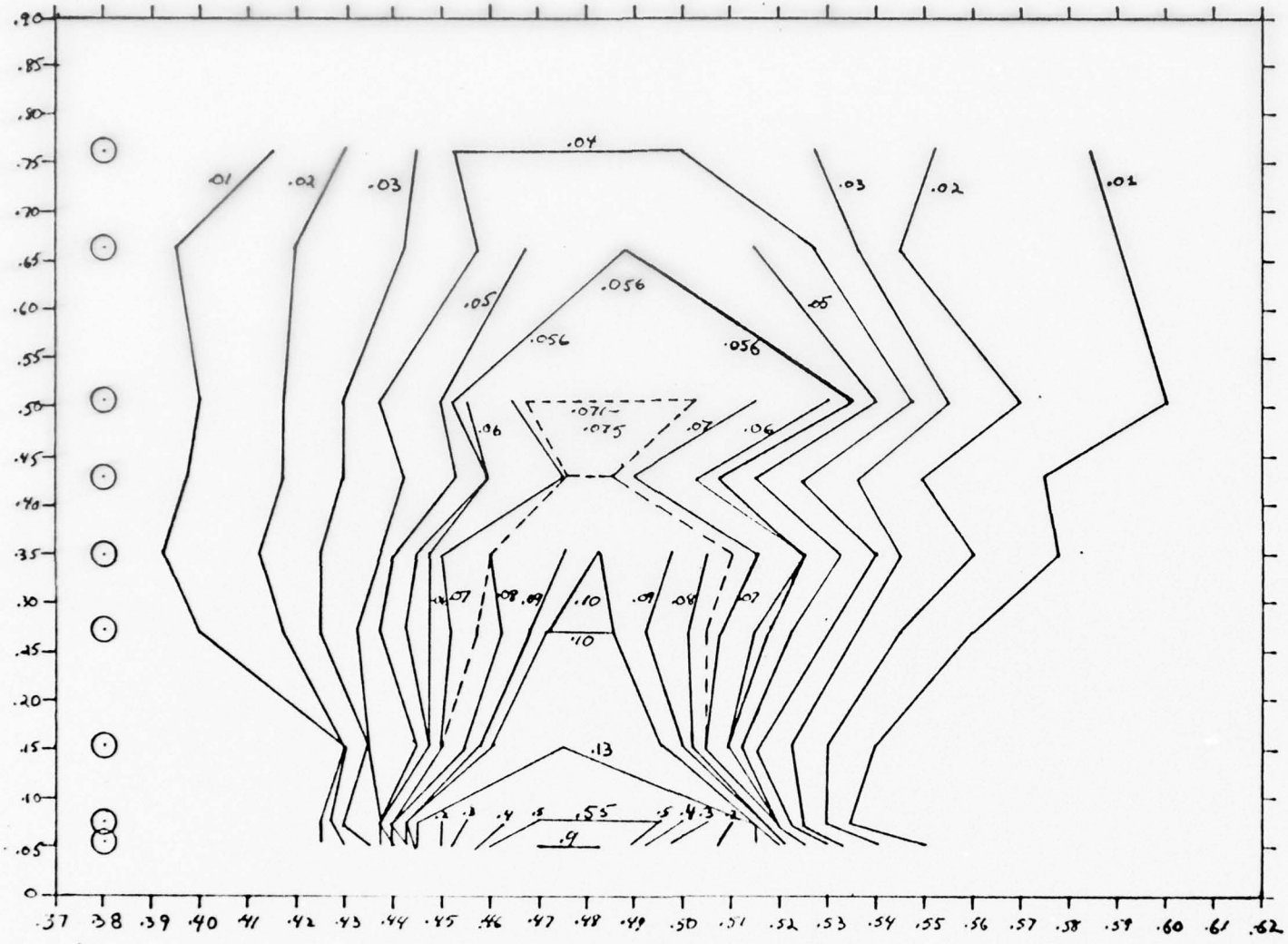

FIG. 14. CONSTANT PLASMA DENSITY (NORMALIZED PROBE SIGNAL) CONTOURS; AT CENTER PORT; ORDINATE IS HEIGHT FROM CATHODE AS FRACTION OF DISCHARGE GAP (2.54 cm.); ABSCISSA IS HORIZONTAL LOCATION AS FRACTION OF TOTAL WIDTH (6.4 cm.); CIRCLES AT HORIZONTAL SCAN LOCATIONS (FIG. 13); PROBE DIAMETER .064 cm.

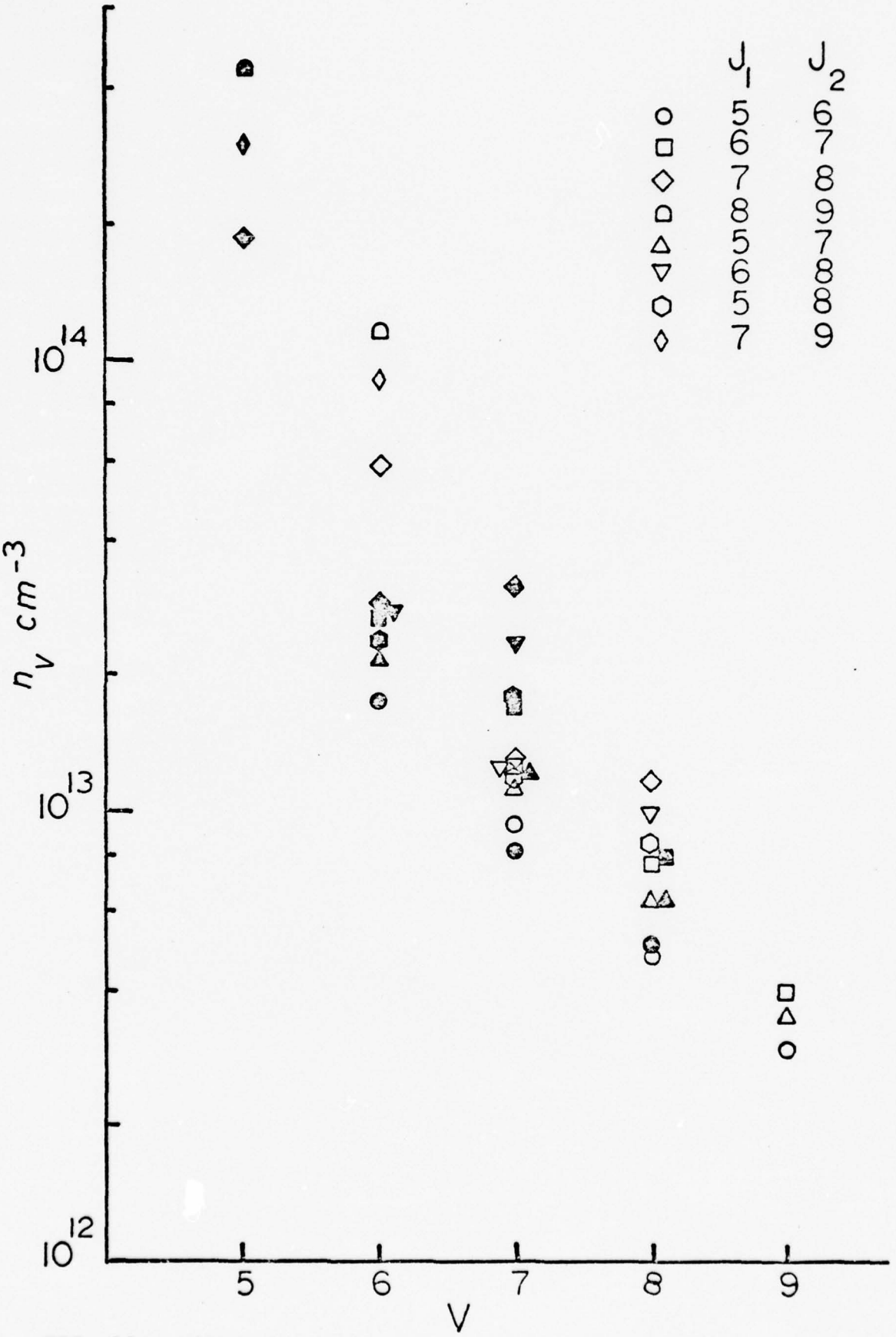

FIG. 15. Vibrational Populations Computed from Measured Gains Assuming Translational-Rotational Equilibrium T= 30.3°K.

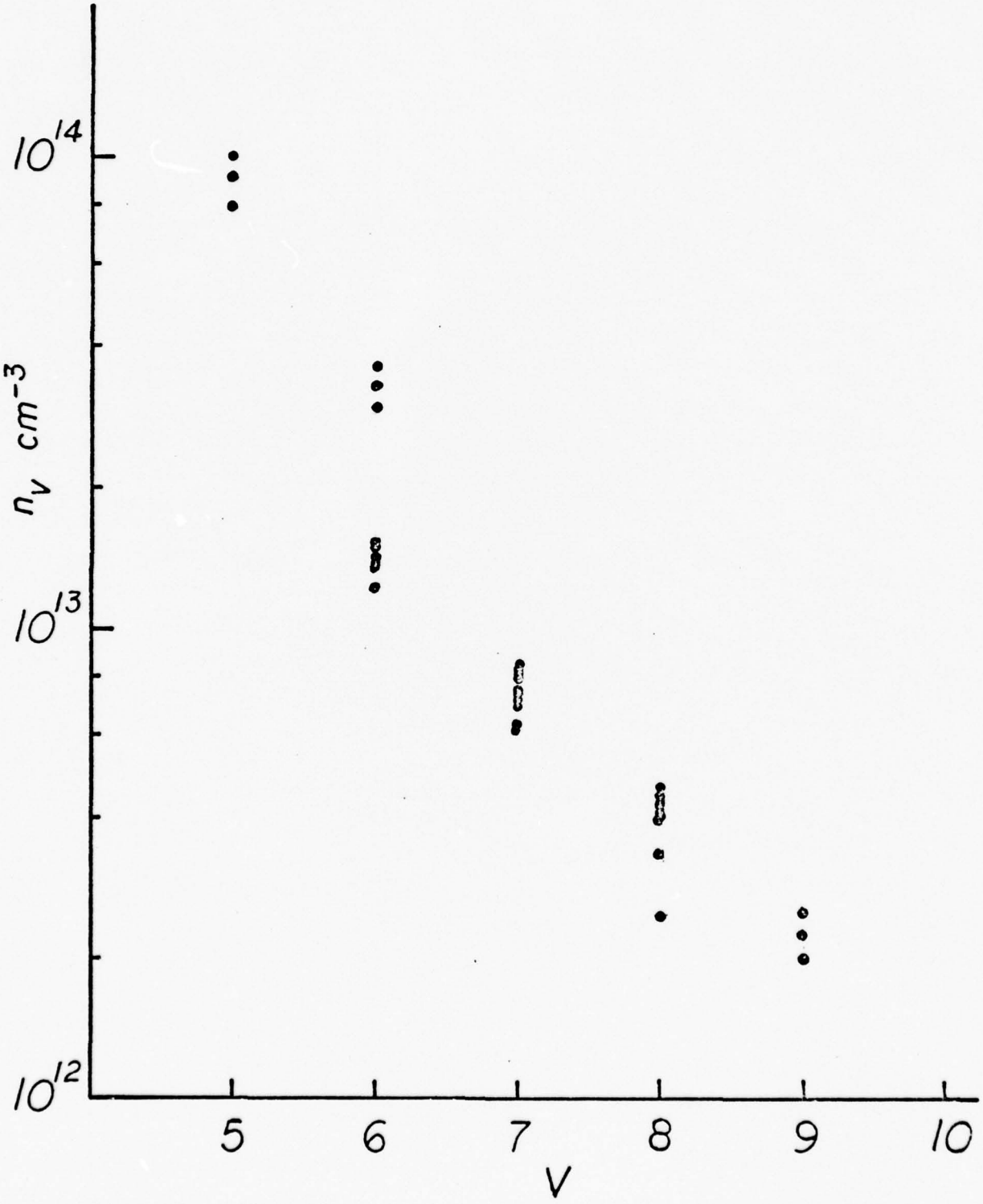

Fig. 16. Vibrational Poluations Computed from Measured Gains Assuming Rotational Temperature Distribution in Table III.B.1.

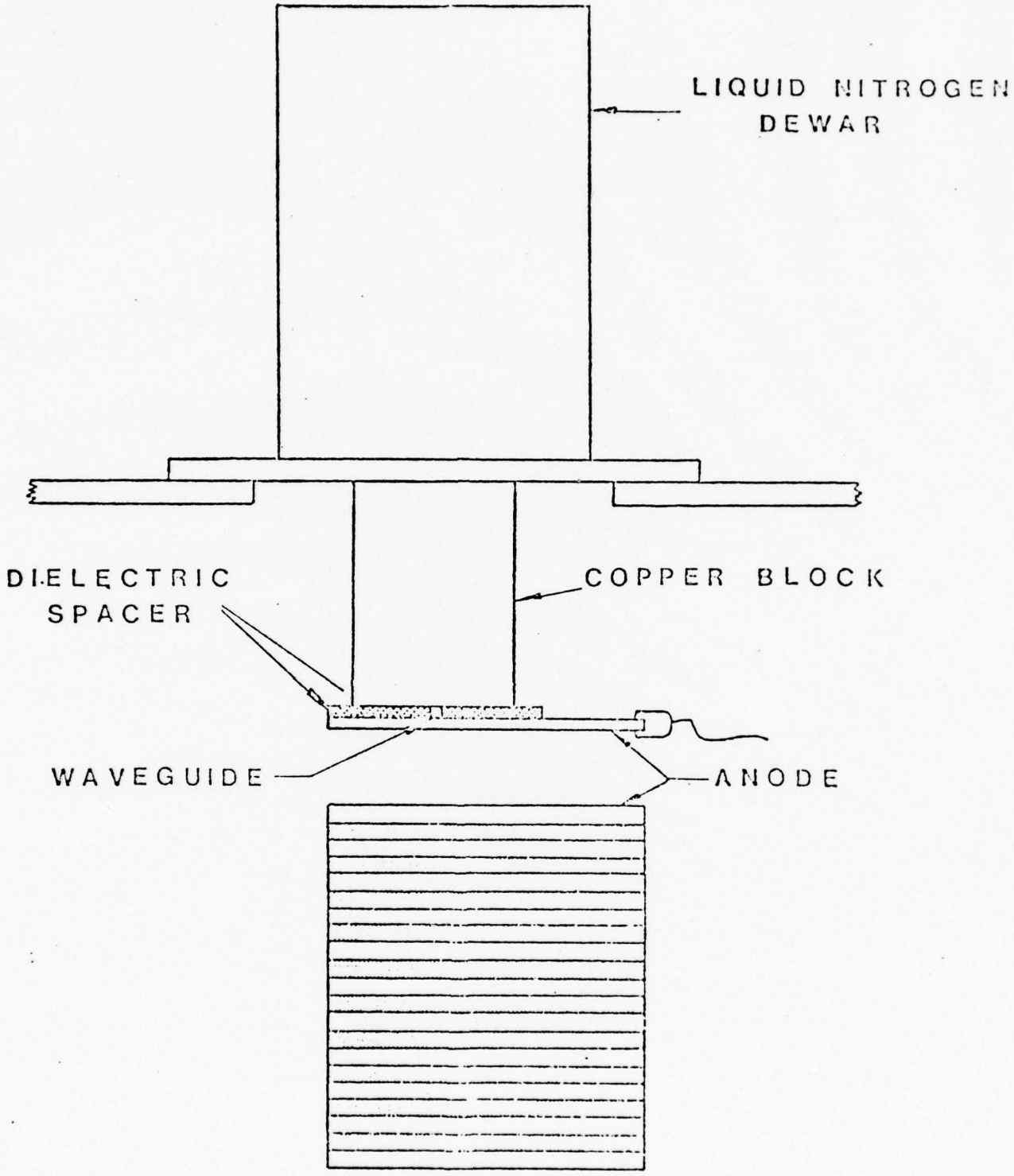

FIGURE 17: WAVEGUIDE SCHEMATIC

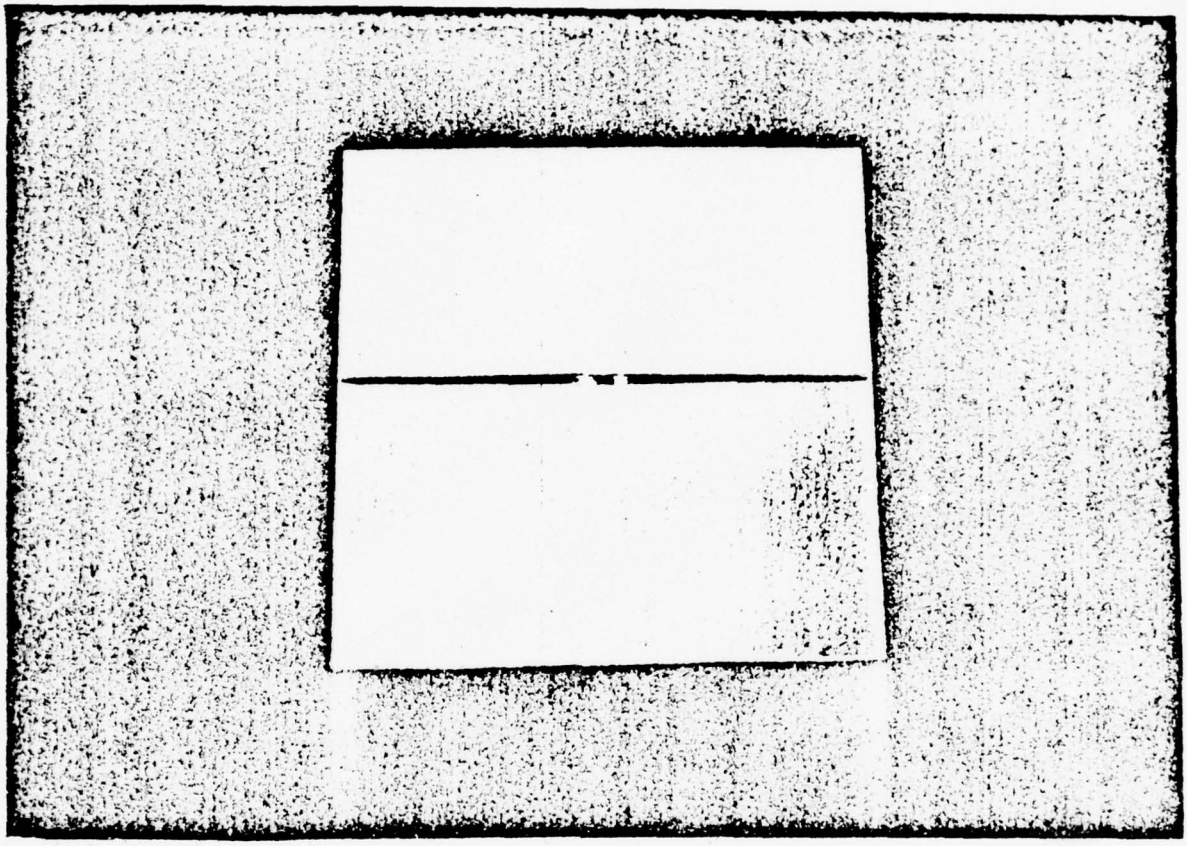

FIGURE 18: PLATE ANODE WITH DEPOSITED IMPURITY

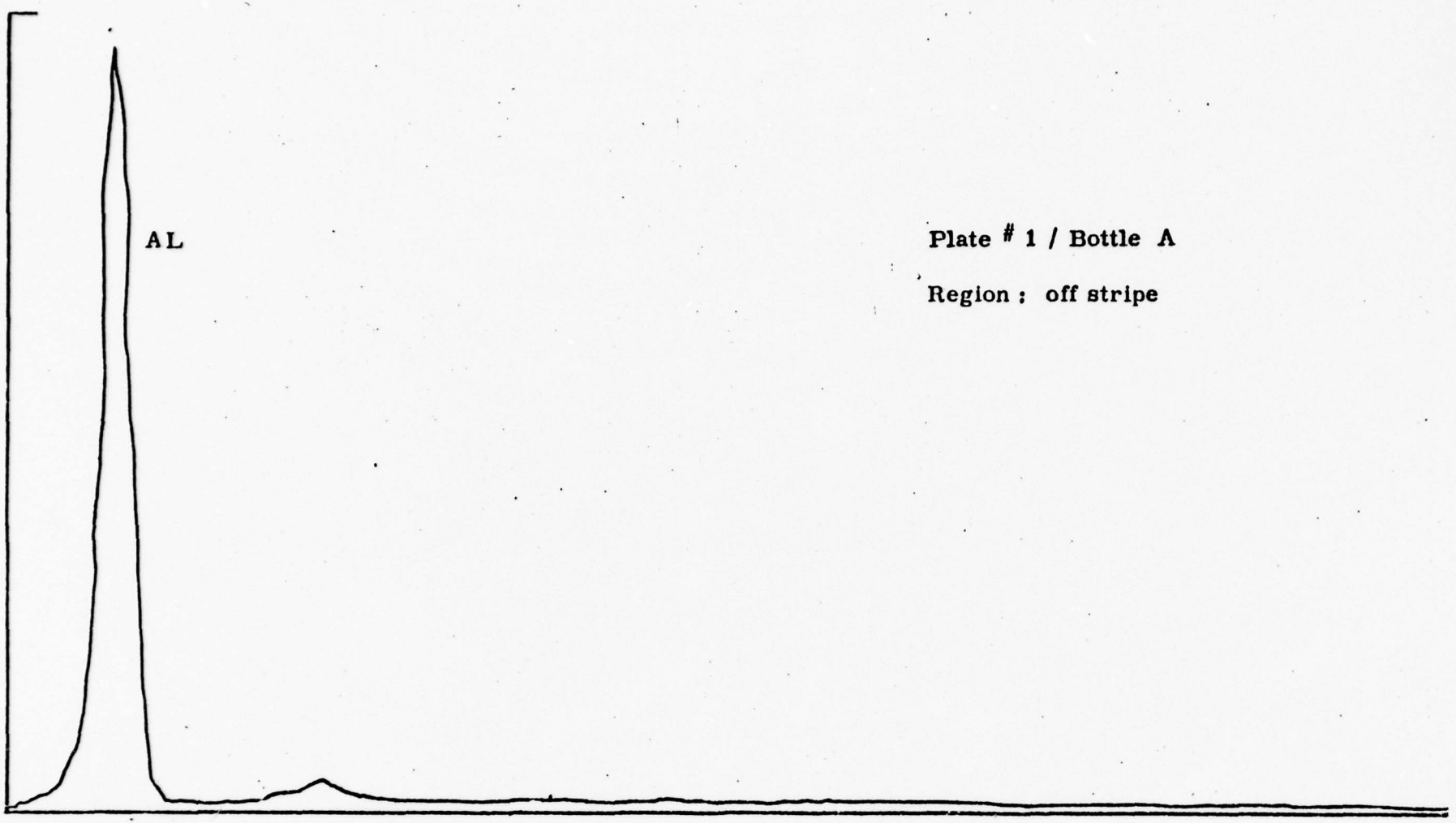

FIGURE 19: SEM SCAN

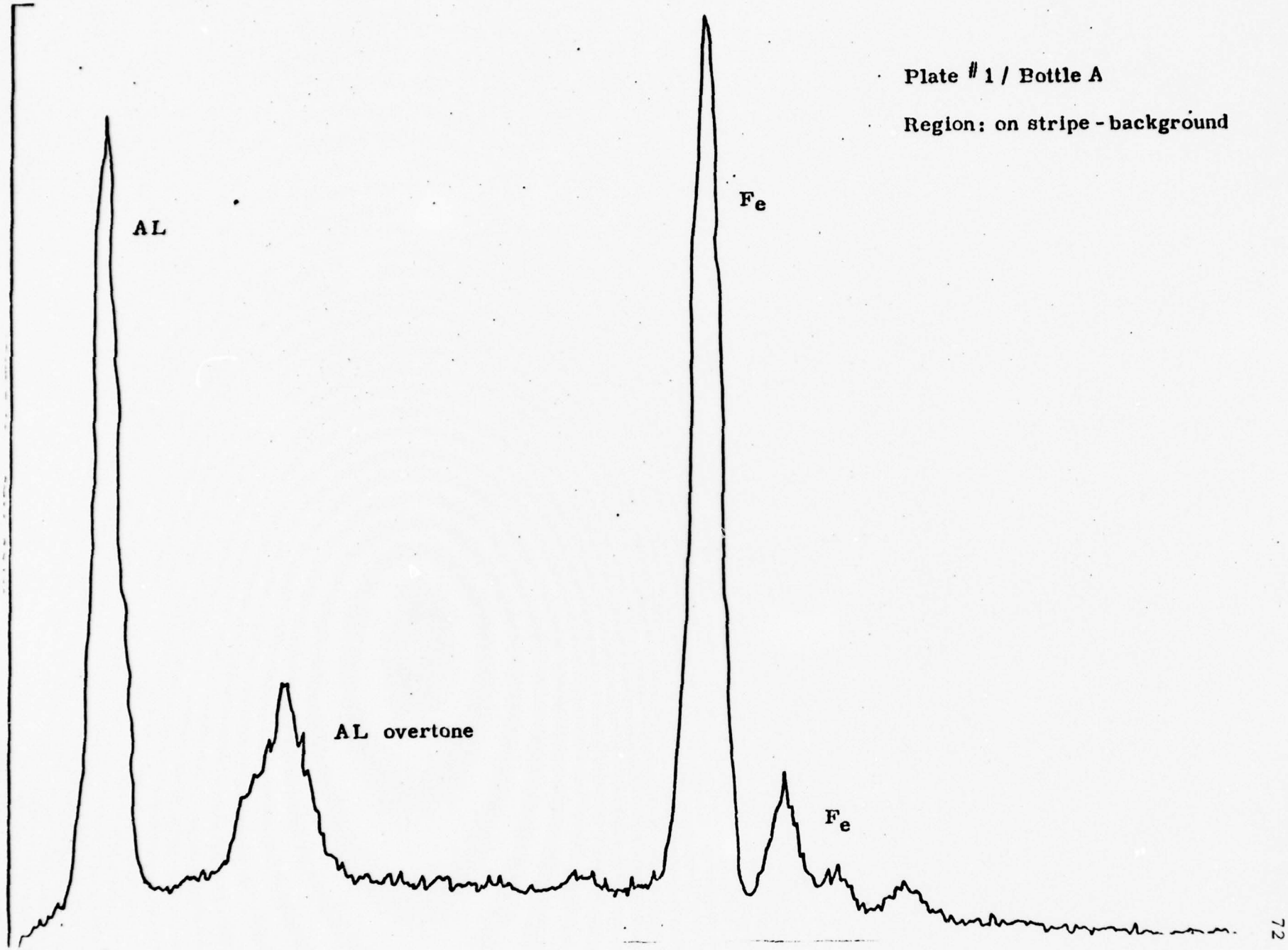

FIGURE 20: SEM SCAN

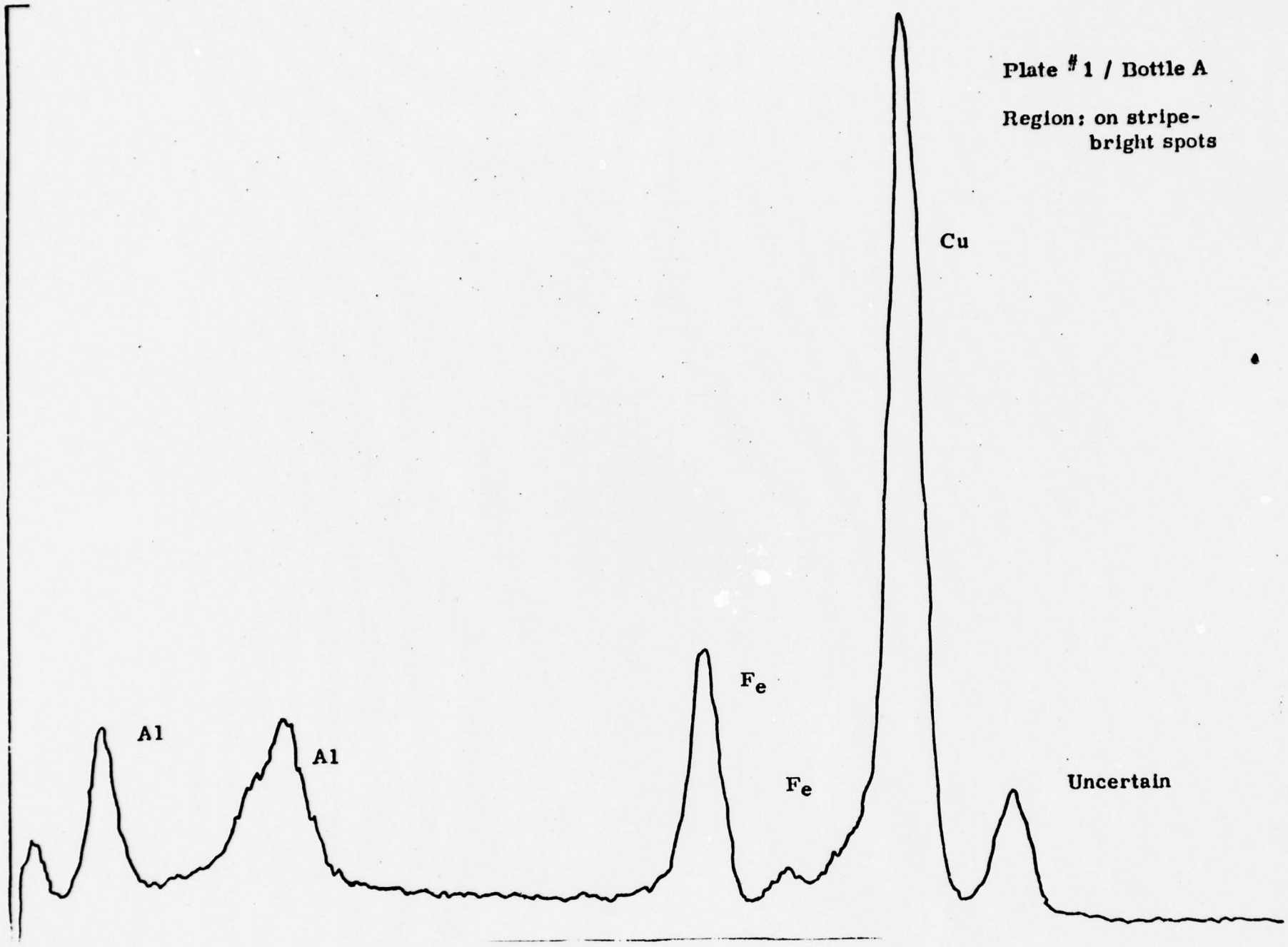

FIGURE 21: SEM SCAN

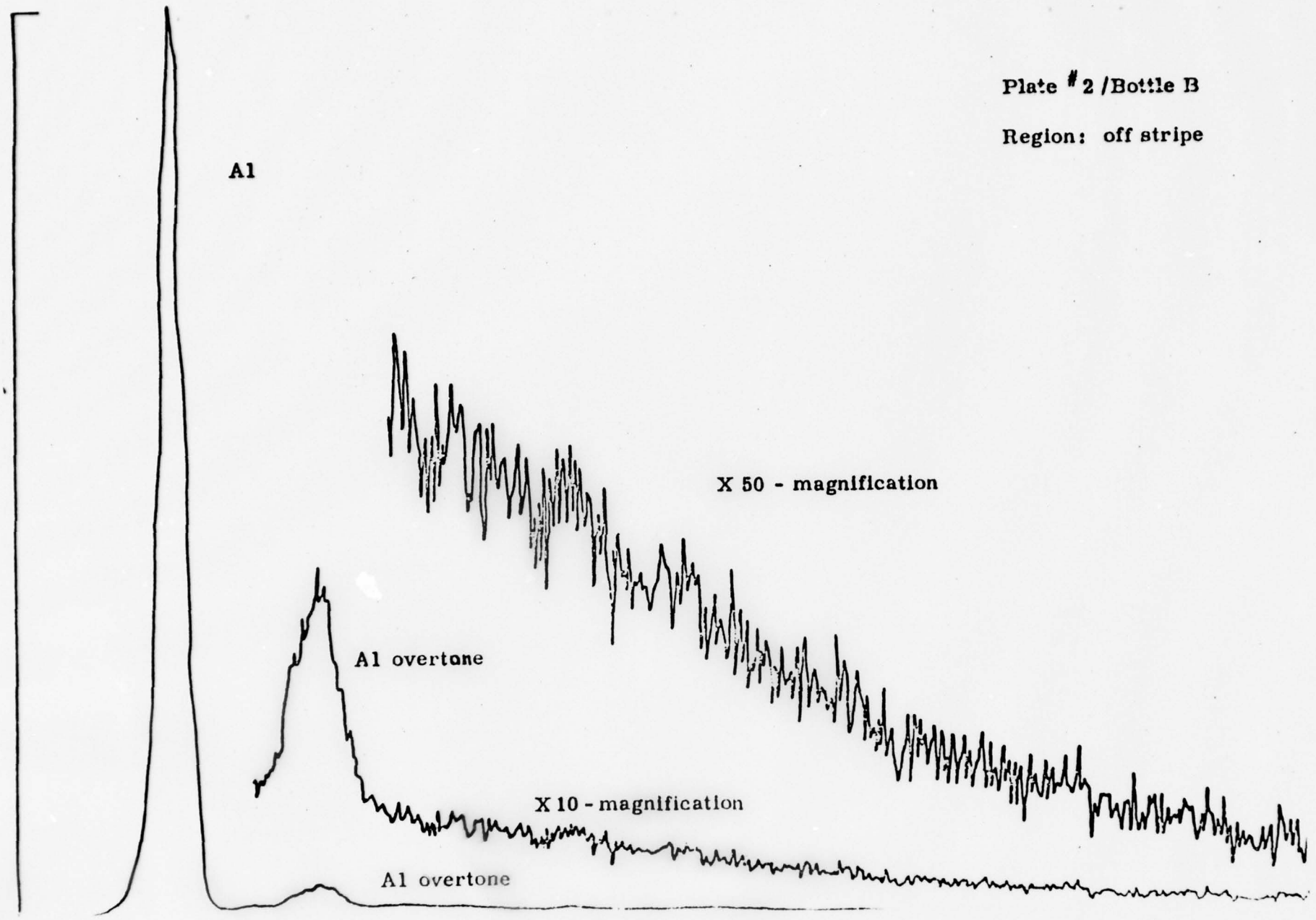

FIGURE 22: SEM SCAN

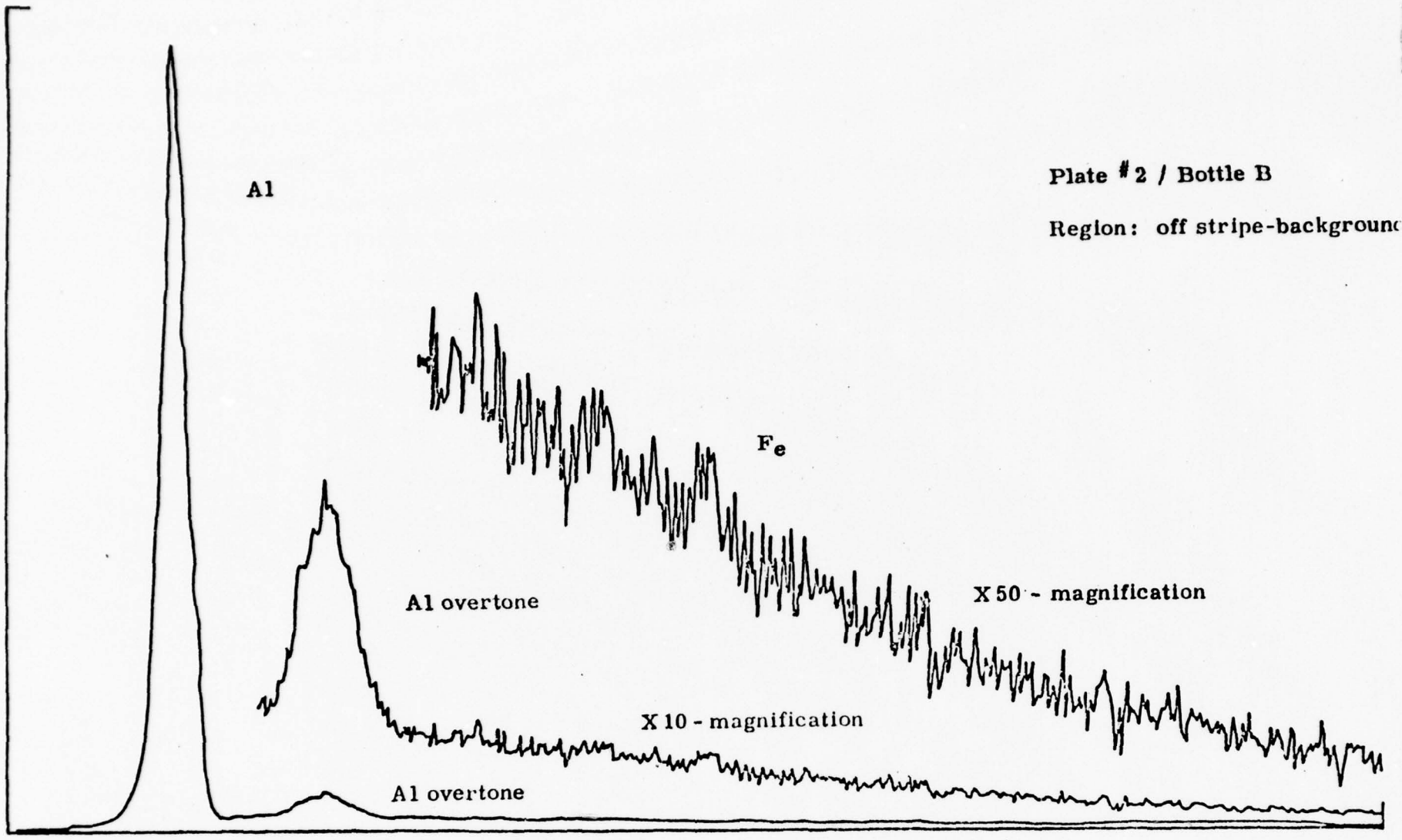

FIGURE 23: SEM SCAN

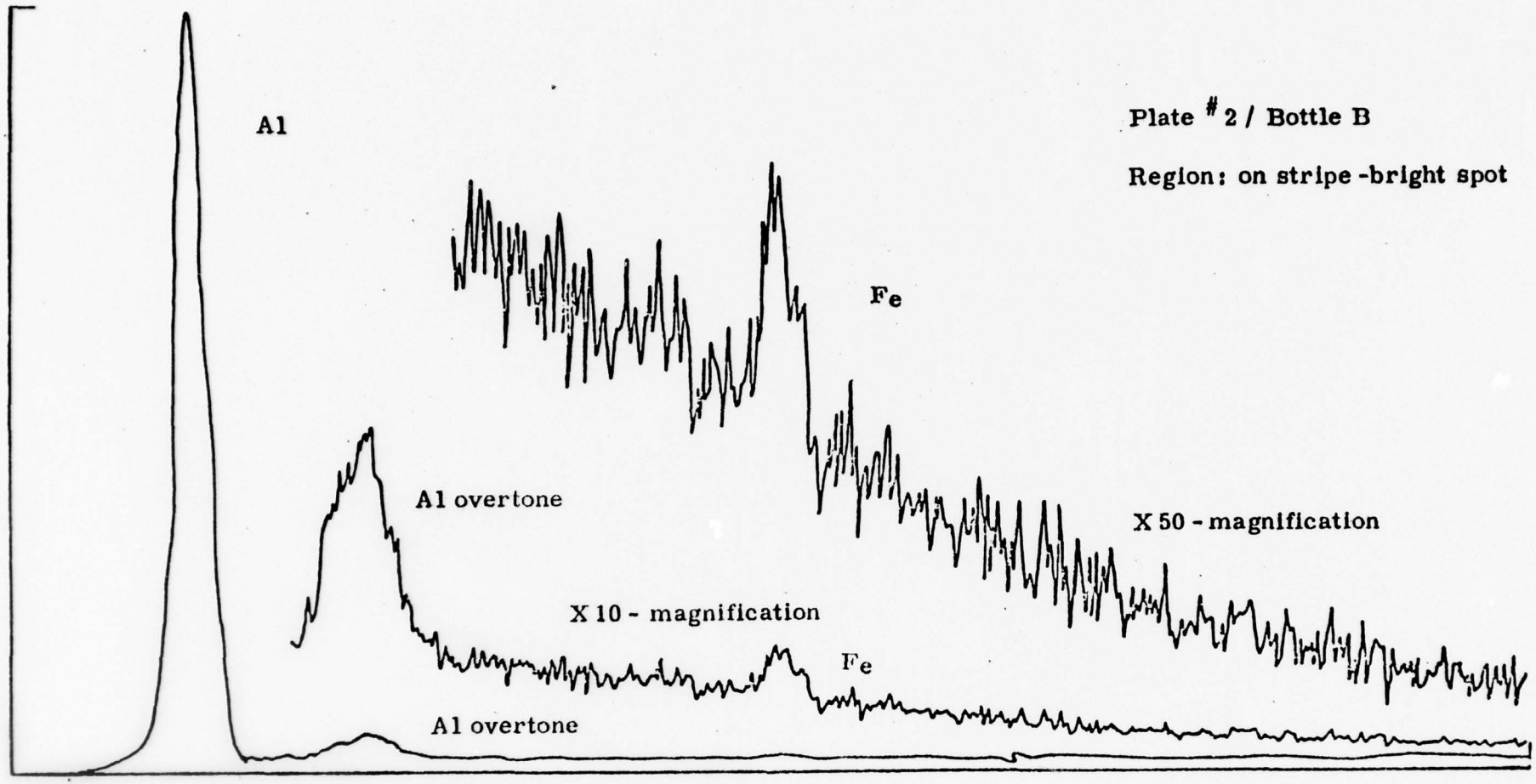

FIGURE 24: SEM SCAN

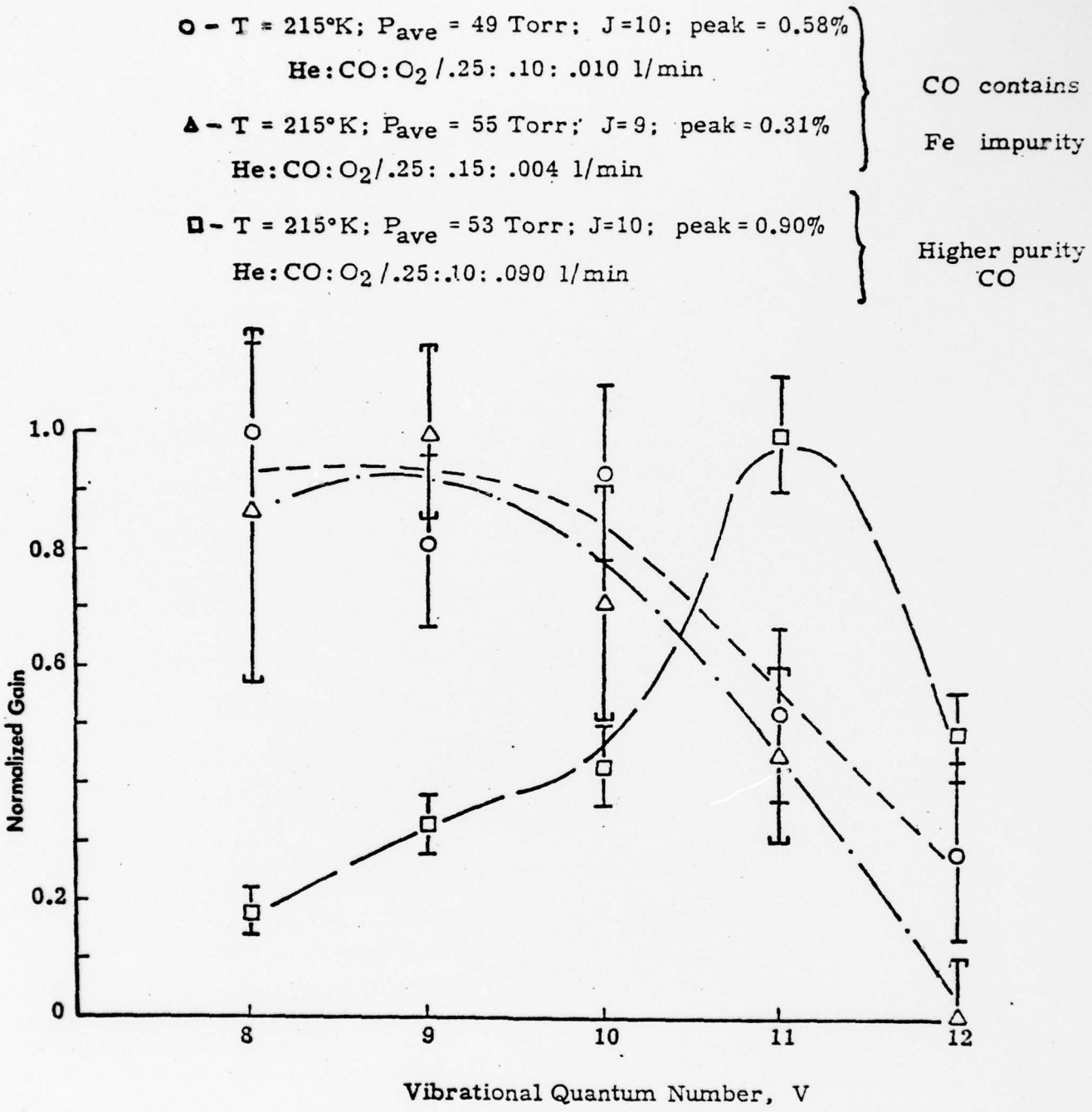

FIGURE 25:NORMALIZED GAIN VS. VIBRATIONAL QUANTUM NUMBER

$T = 215°K$; $P_{ave} = 55$ Torr; $V = 8$

$He:CO:O_2$ / .25: .15: .004 l/min

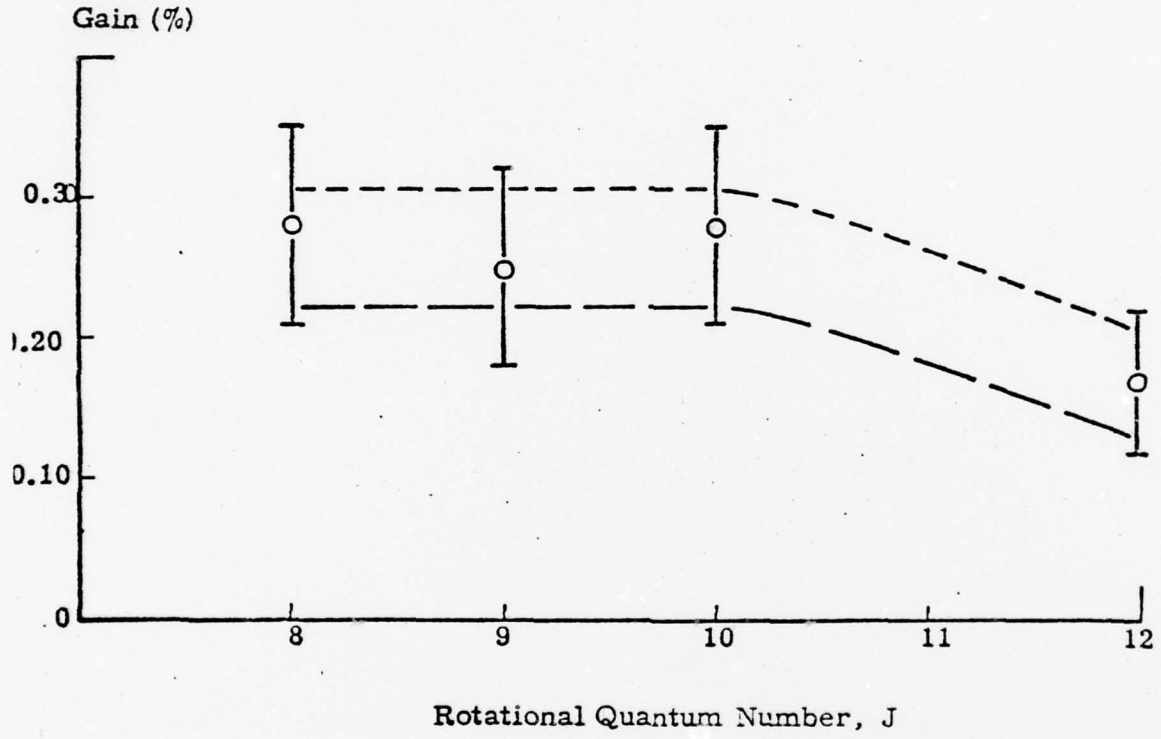

FIGURE 26: MEASURED GAIN VS. J-LEVEL

$T = 215°K$; $P_{ave} = 54$ Torr; Probe Line: 10 P (10)

$Q_{CO} = .10$ l/min; $Q_{He} = .25$ l/min

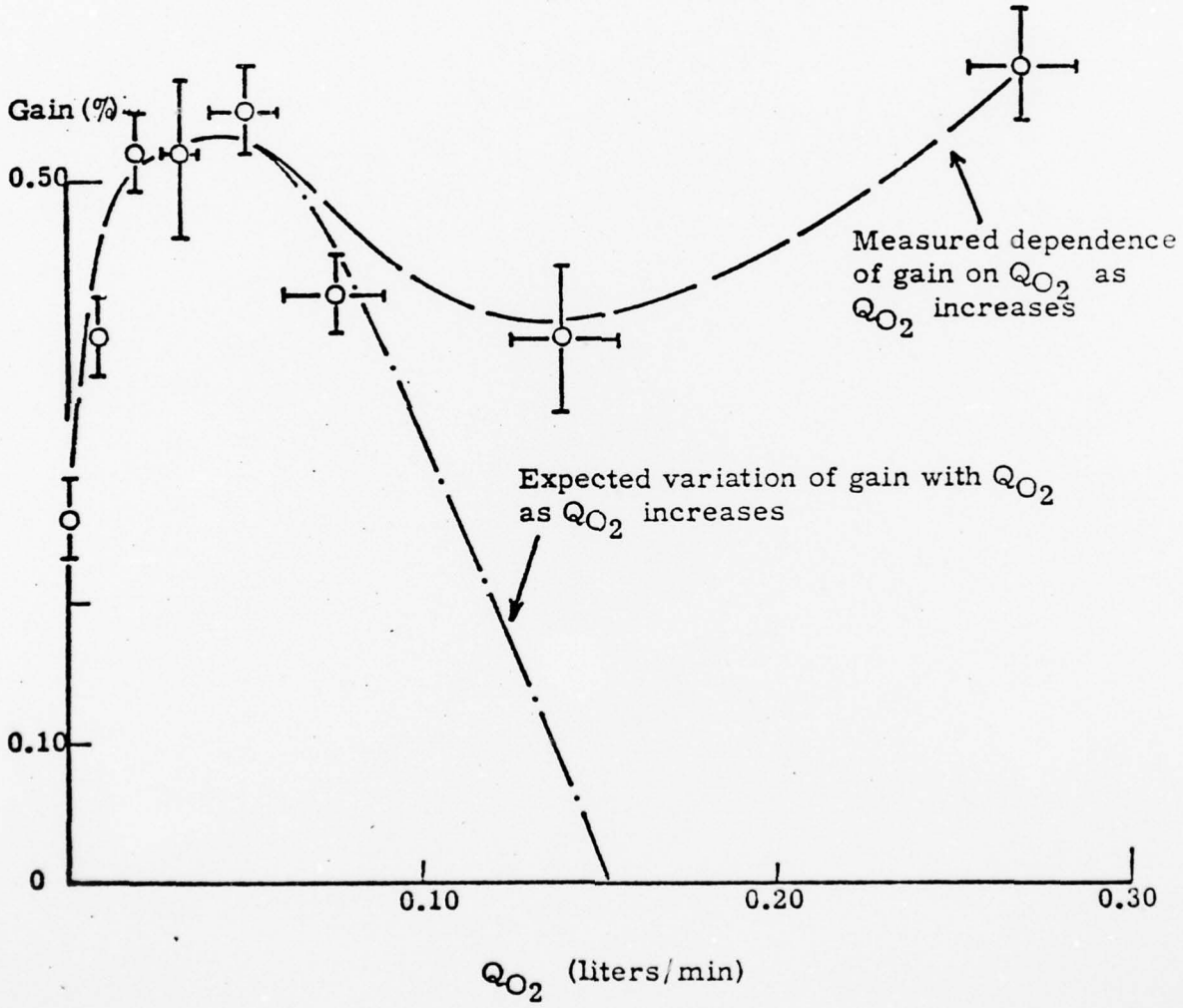

FIGURE 27: GAIN VS. O_2 FLOW RATE

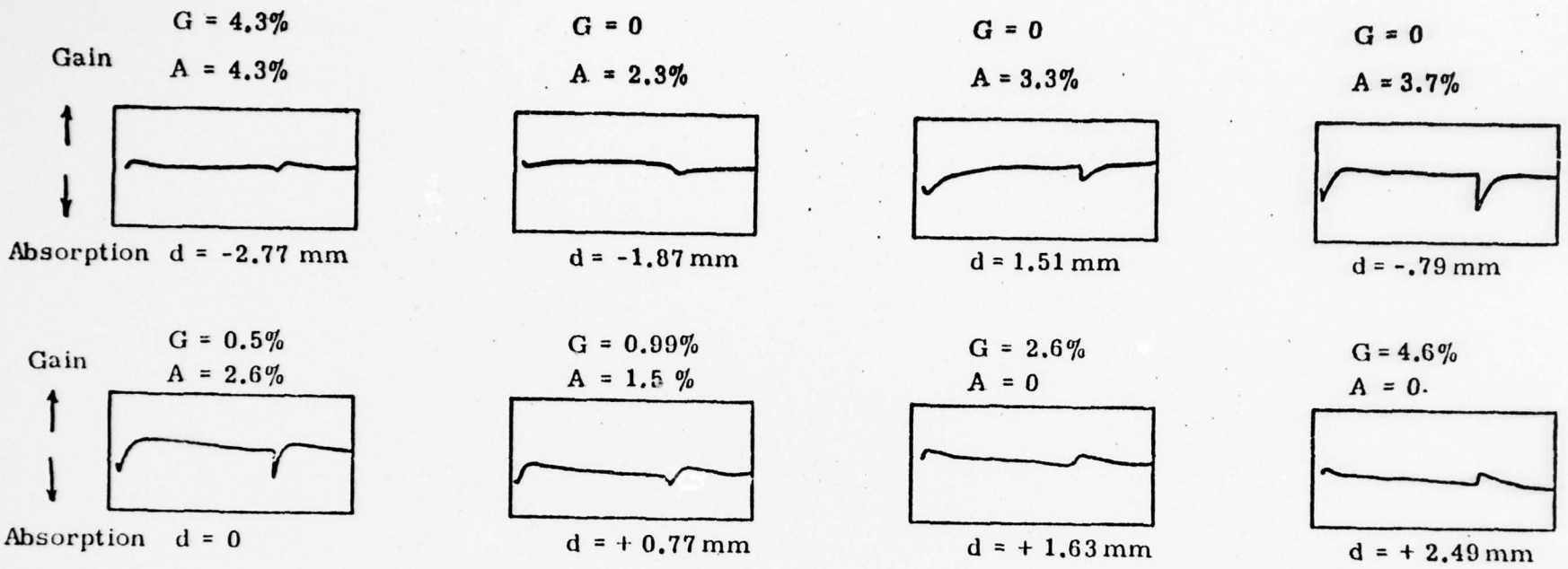

Time Scale : 200 μsec/div

d = separation of probe beam center from waveguide center
• toward cathode (+); toward anode (-)

FIGURE 28 : GAIN/ABSORPTION VS. PROBE BEAM POSITION

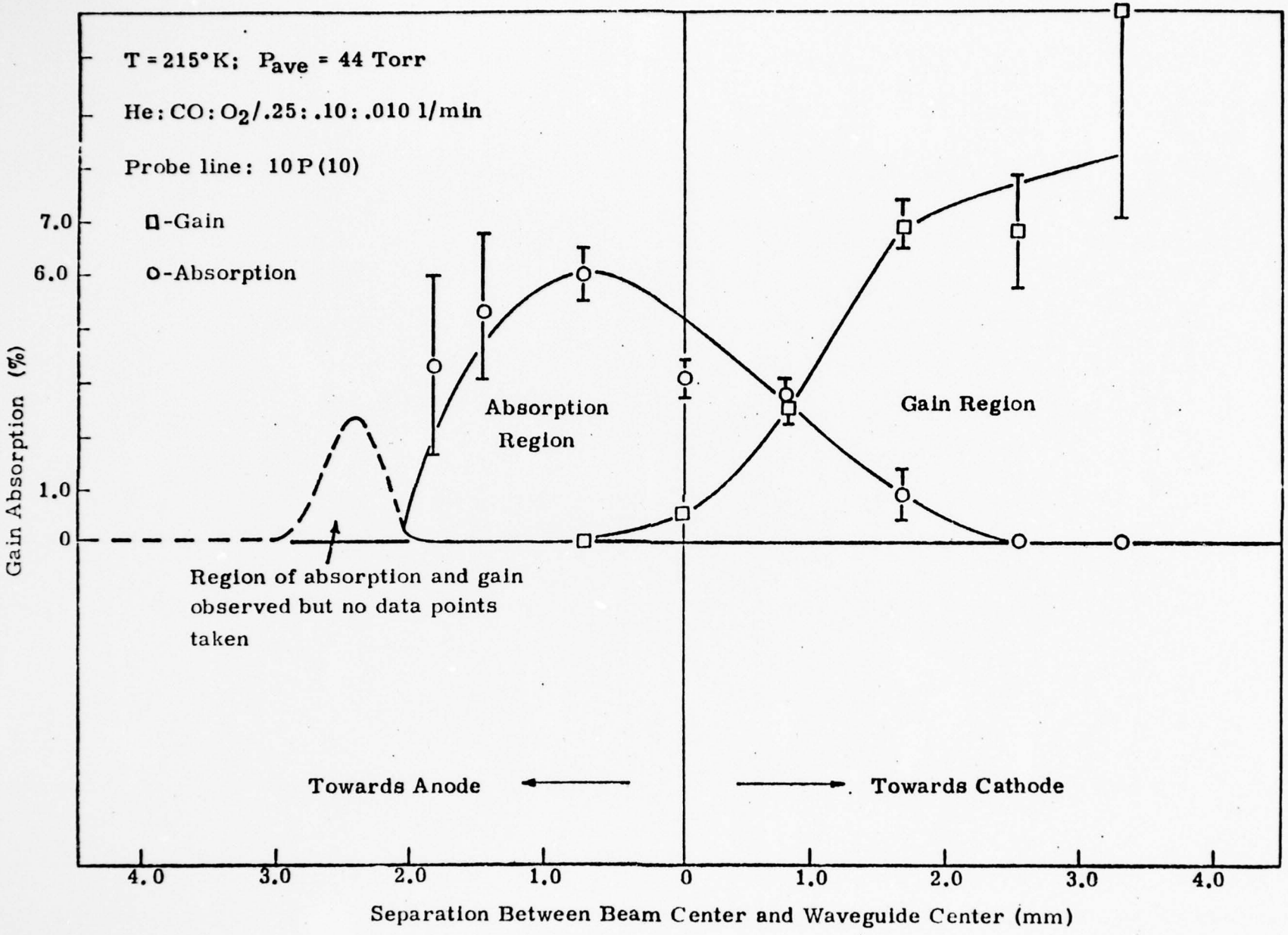

FIGURE 29: GAIN ABSORPTION VS. PROBE BEAM POSITION

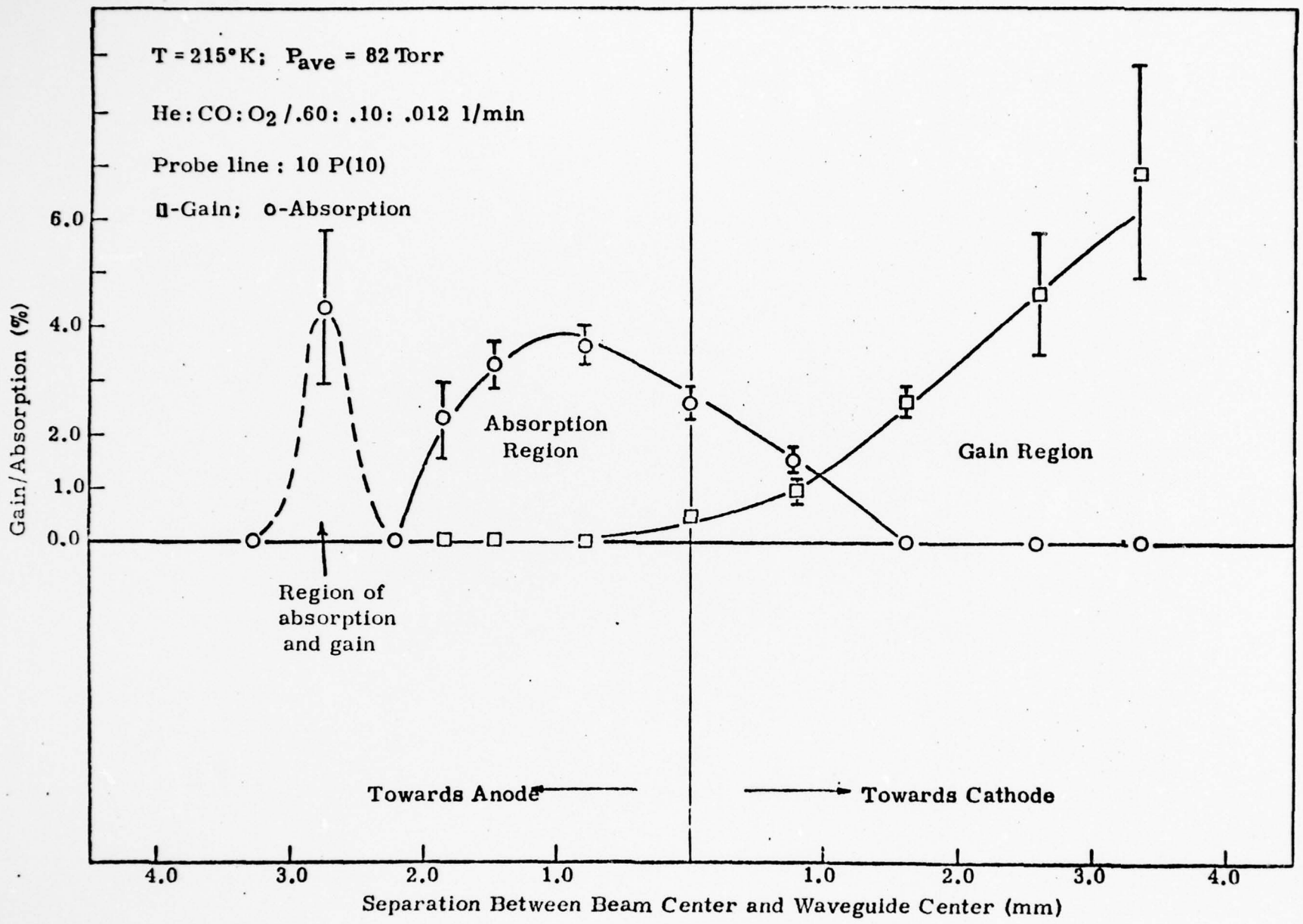

FIGURE 30: GAIN/ABSORPTION VS. PROBE BEAM POSITION

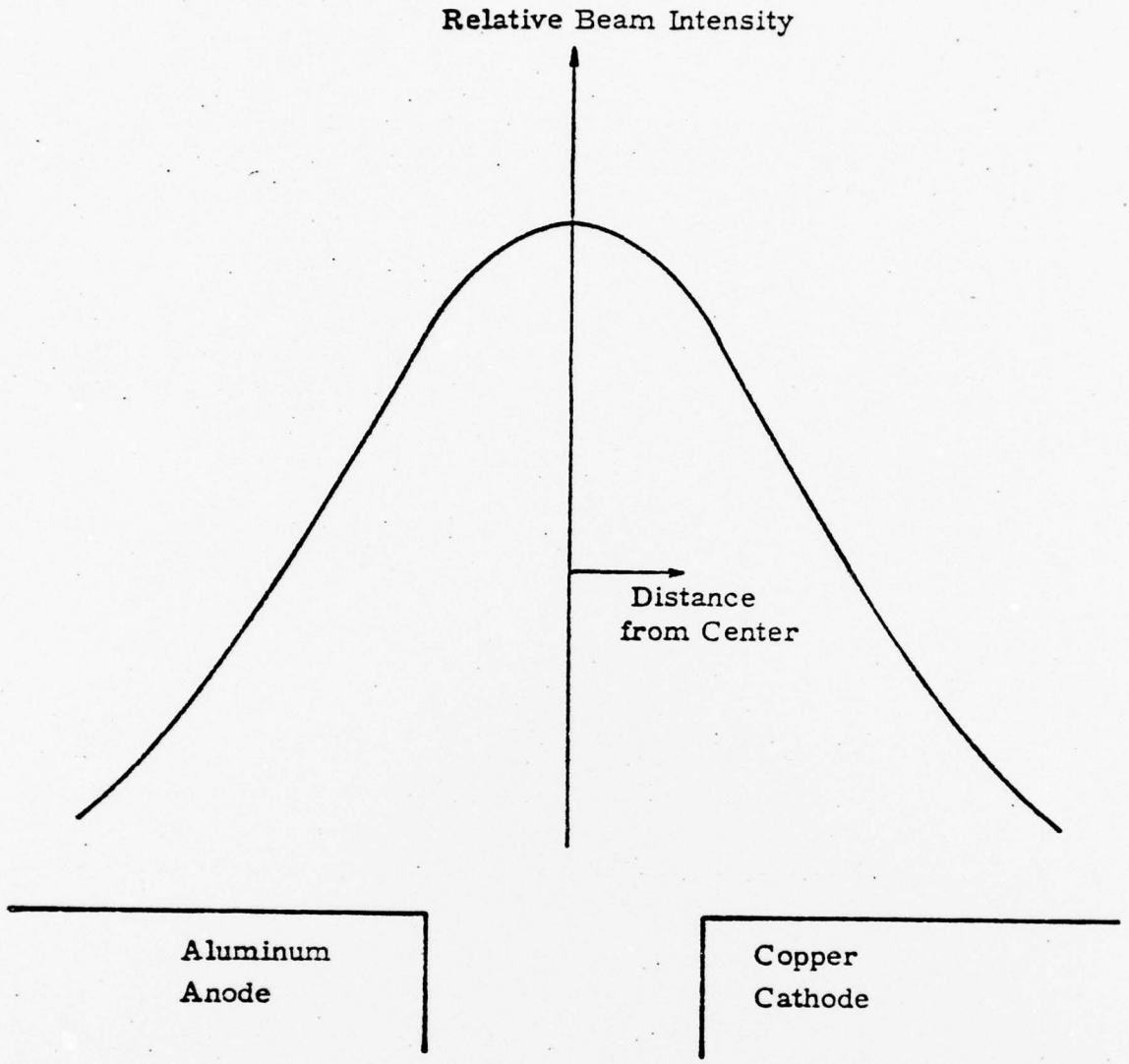

FIGURE 31: GAUSSIAN INTENSITY DISTRIBUTION

APPENDIX A

PUBLICATIONS, PRESENTATIONS AND THESES

1. M. Garcia and G. Bienkowski, "The Electron Energy Distribution Function in Electrically-Excited Molecular Gases" presented at 28th Annual Gaseous Electronics Conference, Rolla, Mo., in October 1975. (Abstract in APS Bulletin, Feb. 1976, p. 172).

2. G. Bienkowski, "A Scaling Law for Energy Transfer by Inelastic Electron-Molecule Collisions in Mixtures" presented at Princeton University in June 1976 and published by NASA in the Proceedings of the Princeton University Conference on Partially Ionized and Uranium Plasmas in September 1976.

3. M. Garcia, G. Bienkowski and J. Lawless, "Stabilization of a Supersonic Flow Gas Discharge by Auxiliary Pin Discharges" presented at the 29th Annual Gaseous Electronics Conference in Cleveland, Ohio, October 1976. (Abstract in APS Bulletin, February 1977, p. 194).

4. S. H. Lam, "An Analytical Theory of Vibrational Relaxation for Anharmonic Molecules Under Strongly Pumped Conditions", to appear in J. Chem. Phys., September 1977. Also presented at the 5th Conference of Chemical and Molecular Lasers, WAI4, St. Louis, Mo., April 1977. See Appendix C.

5. E. R. Fisher, H. Rabitz and S. H. Lam, "Comparison of Experimental and Theoretical Population Distributions in Electric Discharge CO-He Mixtures", presented at the 5th Conference of Chemical and Molecular Lasers, WAI7, St. Louis, Mo., April 1977. Manuscript in draft form. See Appendix B.

6. S. H. Lam and Papageorgis, N. "Quasi-Equilibrium Vibrational Population Distributions of Anharmonic Laser Systems" HR-7, 28th Annual Gaseous Electronic Conference, Rolla, Mo., October 1975. Summary appeared in JQE, QE-11, 715, 1975.

7. J. L. Boulnois, "CO Vibrational Kinetics in a Transverse Electric Discharge Waveguide Laser" Ph.D. Thesis, Aerospace and Mechanical Sciences Department, Princeton University, September 1975.

8. J. L. Boulnois and R. B. Miles, "Time Dependent Kinetics of CO Electric Discharge Lasers with Multi-Level Pumping", 4th Conference on Chemical and Molecular Lasers, St. Louis, Mo., October 1974.

9. P. J. Susko, "Small Signal Gain Measurements in a Low Temperature $CO-N_2$ Hypersonic Flow", MSE Thesis, Aerospace and Mechanical Sciences Department, Princeton University, 1977.

10. P. J. Susko and J. A. Smith, "Measured Small Signal Gains and Inferred *Rotational Nonequilibrium in Low Temperature* CO-N_2 *Flows*" *manuscript* in preparation for publication.

11. J. A. Smith, "Carbon Monoxide Electric Discharge Lasers" Invited talk for NASA Ames Research Center Technical Director and Staff, April 1976.

12. J. A. Smith, "Anharmonic Oscillator Laser Research at Princeton" Invited talk, Mechanical Engineering Department, Stanford University, November 1975.

APPENDIX B

CO-He VT RATES AT HIGH QUANTUM NUMBERS

E. R. FISHER

RIES, WAYNE STATE UNIVERSITY

H. RABITZ

DEPARTMENT OF CHEMISTRY, PRINCETON UNIVERSITY

S. H. LAM

DEPARTMENT OF AEROSPACE & MECHANICAL SCIENCES, PRINCETON UNIVERSITY

JUNE 1977

PRESENTED AT 5TH CONFERENCE ON CHEMICAL AND MOLECULAR LASERS,

WAI4, ST. LOUIS, MO. 1977

I. INTRODUCTION

In the present paper we shall report some quantitative information on CO-He VT rates at high vibrational quantum numbers ($i \gtrsim 25$) inferred from a collection of quasi-equilibrium CO vibrational population measurements recently obtained by Lightman and Fisher[1] at 150°K.

High quantum number rates are difficult to measure experimentally. Knowledge of such rates are important in kinetic calculations of CO laser systems. In the absence of reliable data, they are usually extrapolated from the relatively abundant low quantum number rates[2,3,4,5,6,7,8,9,10] using theoretically motivated scaling laws.[11,12,13] It is known that the location of the so-called Plateau-Boltzmann knee is strongly affected by the high quantum number rates assumed.[14,15] In the present paper, we shall take advantage of this sensitivity to infer some quantitative information on these rates from experimentally measured quasi-equilibrium CO population distributions. As shall be shown later, this indirect method can yield a certain ratio of VT to VV rates at high quantum numbers. However, because of the limited amount of experimental data available, we are able to infer information only near $i \gtrsim 25$ at T = 150°K. Nevertheless, the method of data reduction is interesting, and the results obtained, although limited, appear to be the only really high quantum number ($i > 20$) experimental CO-He VT data available at this time.

Recently, Brechignac[16] using a double resonance technique made measurements of CO-CO VV rates at high quantum numbers. One of his major conclusions was that the near-resonant VV rates extrapolated to high quantum numbers by the Sharma-

Brau[12] model appeared to be too high. For CO-He VT rates, the $9 \leq i \leq 13$ data by Hancock and Smith[3] appears to be the only moderately high quantum number data available in the literature at this time. A common VT rate extrapolation scheme suggested by Rich et al.[11] utilized the well-known SSH[17] theory. Recently, Verter and Rabitz[18] presented detailed theoretical (non-linear) calculations of CO-He rates, and their results at high quantum number and low temperatures ($T < 300°K$) disagreed substantially from the Rich extrapolation. In particular, the low temperature Verter-Rabitz VT rates increase with i much more rapidly at low quantum numbers and much more gradually at high quantum numbers than that predicted by the Rich extrapolation. The present work provides some limited evidence of the qualitative features of the Verter-Rabitz rates.

II. THE EXPERIMENTAL DATA

The Lightman and Fisher data[1] of CO vibrational population distributions mreasured in a CO-He electric discharge is reproduced in Figs. 1. The temperature of the system is 145-155°K. For details of the experimental procedures the readers are referred to the original paper.

The 7-torr and 4-torr He data are presented separately in Figs. 1a and 1b, respectively. It is seen that the "Plateau" begins at approximately $i \tilde{=} 10$, and the "Plateau-Boltzmann knee" occurs near or beyond $i \tilde{=} 30$, the upper limit of the data. The 7-torr data includes various combinations of CO pressures (.5, 10, 1.5-torr) and discharge power inputs.

Lightman and Fisher[1] also performed detailed computations of the CO population distributions using a computer code. The CO-CO VV rates assumed were based on the Sharma-Brau scaling, and various CO-He VT rates were used. They found that neither the extrapolation formula suggested by Rich et al. nor the theoretical rates by Verter and Rabitz could generate acceptable agreements with the

measured data; the former produced a Plateau-Boltzmann knee at too low values of i while the latter at too high values of i. When the Verter-Rabitz rates were augmented empirically by a multiplicative factor $(i+1)^{0.65}$, excellent agreements with the experimental data were obtained. (See Fig. 1b) Note that this augmentation factor is approximately 8 when $i \simeq 25$.

III. REPRESENTATION OF KINETIC RATES

Let $k^{VT}(i\downarrow)$ denote the single-quantum-jump VT rate of $i + 1 \rightarrow i$ collisions between a CO molecule and a He atom. Let $k^{VV}(i\uparrow,j\downarrow)$ denote the single-quantum-jump VV rate of $i \rightarrow i + 1$, $j + 1 \rightarrow j$ collisions between two CO molecules. Based on perturbation theories such as SSH,[17] the scaling laws can be expressed in the following forms[19]

$$k^{VT}(i\downarrow) = \omega^{VT}(T)\ell_i^{VT} A_i^{VT}(T) \tag{3.1}$$

$$k^{VV}(i\uparrow,j\downarrow) = \omega^{VV}(T)\ell_i^{VV} \ell_j^{VV} A_{ij}^{VV}(T) \tag{3.2}$$

where theoretically ℓ_i^{VT}, ℓ_i^{VV} are proportional to the square of the appropriate transition matrix elements and A_i^{VT} and A_{ij}^{VV} are called the adiabaticity factors.

Since for VT collisions the short range strongly repulsive part of the interaction potential dominates while for nearly-resonant VV collisions the long range dipole-dipole interaction dominates, ℓ_i^{VT} is expected to be different from ℓ_i^{VV}. We shall assume

$$\ell_i^{VT} = \frac{1 + i}{1 + \alpha C^{VT} i}, \quad \ell_i^{VV} = \frac{1 + i}{1 + \alpha C^{VV} i}, \tag{3.3}$$

where C^{VT} and C^{VV} are empirical constants and $\alpha = 5.98 \times 10^{-3}$ is the anharmonicity of CO. Usually, ℓ_i^{VT} is approximated[11] by taking $C^{VT} = -1$ while ℓ_i^{VV}

is obtained from the dipole-dipole transition matrix elements computed by Young and Eachus.[20] It can be shown that ℓ_i^{VV} so computed may adequately be represented by taking $C^{VV} = 1.5$.

The VT adiabaticity factor A_i^{VT} is generally expected to be an exponentially increasing function of i. Normalizing A_i^{VT} so that $A_o^{VT} = 1$, we can determine $\omega^{VT}(150°K) \simeq 1.5 \times 10^{-18}$ cm^3/sec-molecule from the available experimental data.[2] Although the Verter-Rabitz rates are computed from a fully non-linear theory, their rates can be correlated[19] by Eq. (3.1). At 150°K, the correlation yields

$$A_i^{VT}(150°K) = a_i \exp(0.09i), \text{ (Verter-Rabitz}^{18}\text{)}, \tag{3.5}$$

where $a_i(150°K)$ is a rapidly increasing function of i in the first few levels and tends to a constant value ($a_i(150°K) = 4.5$) for $i \gtrsim 10$. According to the Rich extrapolation, A_i^{VT} (150°K) is given by

$$A_i^{VT}(150°K) = \exp(0.24i), \text{ (Rich et al.}^{11}\text{)} \tag{3.6}$$

These two rates are seen to disagree strongly with each other at high quantum numbers.

Since the forward and the reverse rates are related by detailed balance, $A_{ij}^{VV}(T)$ is often rewritten as

$$A_{ij}^{VV}(T) = P_{ij}^{VV}(T) \exp\left[\left(\Delta E_j - \Delta E_i\right)/2kT\right], \tag{3.7}$$

where $P_{ij}^{VV}(T)$ is a symmetric matrix, E_i is the vibrational energy of the ith level ($E_i = i(1-\alpha(i-1))k\theta_{vib}$, $\theta_{vib} = 3084°K$), and $\Delta E_i = E_{i+1} - E_i = (1-2\alpha i)k\theta_{vib}$. Normalizing $P_{ij}^{VV}(T)$ so that $P_{ii}^{VV}(T) = 1$, we can determine $\omega^{VV}(150°K) \simeq 1.5 \times 10^{-12}$ cm^3/sec-molecule from the available low quantum number data. We shall define

the second moment of $P_{ij}^{VV}(T)$ by

$$b_i(T) = \frac{1}{2} \sum_{j=0}^{\infty} (i-j)^2 P_{ij}^{VV}(T) \tag{3.8}$$

Theoretically, P_{ij}^{VV} should depend primarily on $|i-j|$ and should decrease rapidly with $|i-j|$. Thus, $b_i(T)$ should be insensitive to i in the plateau region and shall be written hereafter simply as b(T). Using the experimental and theoretical data on $P_{0,j}^{VV}(150°K)$ collected by Brechignac, we obtain

$$b(T) \cong 6.6 \left(\frac{T}{150}\right)^{3/2} \tag{3.9}$$

IV. THE THEORETICAL PLATEAU DISTRIBUTION

Using a differential approximation first introduced by Brau[21] and later refined by Gordiets et al.[14] and Lam,[15] the Plateau distribution n_i of CO can be explicitly expressed in terms of the assumed kinetic rates:

$$n_i = \frac{1}{\ell_i^{VV}} \left\{ n_r \ell_r^{VV} - n_{He} \frac{T\omega^{VT}}{2bg\omega^{VV}} \sum_{j=r}^{i} \left(\frac{\ell_j^{VT}}{\ell_j^{VV}}\right) A_j^{VT} \right\} \tag{4.1}$$

where r is a reference quantum number, n_{He} is the number density of He which is assumed to dominate the VT processes, and $g = \Delta E_i - \Delta E_{i+1} = 2\alpha\theta_{vib} = 37°K$. Eq. (4.1) differs slightly from earlier works[14,15] by recognizing that ℓ_i^{VT} and ℓ_i^{VV} may be different as mentioned earlier.

We shall represent A_i^{VT} at high quantum numbers by

$$A_i^{VT}\ (150°K) = B_r \exp \beta(i-r) \tag{4.2}$$

where B_r and β are constants to be determined. Since ℓ_j^{VT}/ℓ_j^{VV} is only weakly dependent on j, we shall approximate it by ℓ_r^{VT}/ℓ_r^{VV}. Eq. (4.1) can now be re-written as

$$n_i = \frac{1}{\ell_i^{VV}} \left\{ n_r \ell_r^{VV} - n_{He}\, C\, \frac{e^{\beta(i-r)}-1}{1-e^{-\beta}} \right\} \tag{4.3}$$

AD-A043 184 PRINCETON UNIV N J DEPT OF AEROSPACE AND MECHANICAL--ETC F/G 20/5
ANHARMONIC OSCILLATOR LASERS.(U)
JUL 77 J A SMITH, S H LAM, G K BIENKOWSKI F44620-73-C-0059
UNCLASSIFIED AFOSR-TR-77-0956 NL

2 OF 2
ADA043184

END
DATE FILMED
9-77
DDC

where

$$C = \frac{B_r \; T \; \omega^{VT} \; \ell_r^{VT}}{2bg \; \omega^{VV} \; \ell_r^{VV}} \tag{4.4}$$

Eq. (4.3) contains only three kinetic rate related constants, C^{VV}, C, and β.

V. DATA REDUCTION

The data reduction procedure is as follows. From a given measured distribution, the value of n_r is first determined to fit the data at i = r, and then the values of C, C^{VV}, and β are determined by trial and error to obtain acceptable agreement over the range $10 \leq i \leq 30$. Choosing r = 25, it is found that so long as C is within 15% of 1.2×10^{-4}, acceptable fits can be generated with $C^{VV} \simeq -1$ to +1.5 and $\beta \simeq 0.001$ to 0.11. In other words, within the ranges indicated Eq. (4.3) is not sensitive to the values of C^{VV} and β, but is sensitive mainly to the value of C. The CO population distributions calculated by Eq. (4.3) using $C = 1.2 \times 10^{-4}$, $C^{VV} = 1.5$, and $\beta \approx 0.09$ are shown as dotted lines in Figs. 1. The solid line in Fig. 1b is the exact numerical solution obtain by Lightman and Fisher using the Verter-Rabitz rates augmented by $(i+1)^{0.65}$ as mentioned earlier.

V. RESULTS AND DISCUSSION

From Eqs. (3.1), (4.2), and (4.4) the CO-He VT rates at high quantum numbers can be written as

$$k^{VT}(i\downarrow) = \frac{2bg \; \omega^{VV} \; \ell_r^{VV}}{T \; \ell_r^{VT}} \; C \; \ell_i^{VT} \exp \beta(i-r) \; . \tag{5.1}$$

It is seen that for $i \sim r = 25$, the value of $k^{VT}(i\downarrow)$ is relatively insensitive to the uncertain values of C^{VV} and β in the indicated range. Using g = 37°K and the 150°K data for b, ω^{VV}, C quoted earlier, we have

$$k^{VT}(i\downarrow;150°K)\,cm^3/sec\text{-}molecule = 6.8 \times 10^{-16}\left(\frac{\ell_{25}^{VV}}{\ell_{25}^{VT}}\right)\ell_i^{VT} \exp \beta(i-25) \tag{5.2}$$

Using $C^{VV} = 1.5$, we have

$$k^{VT}(i\downarrow;150°K) = 1.3 \times 10^{-14}\,\frac{\ell_i^{VT}}{\ell_{25}^{VT}} \exp \beta(i-25) \tag{5.3}$$

which is the 150°K CO-He VT rates inferred from the Lightman and Fisher data.

The Verter-Rabitz and the Rich extrapolation rates can be written in similar forms:

Verter-Rabitz

$$k^{VT}(i\downarrow;150°K) = 1.9 \times 10^{-15}\left(\frac{\ell_i^{VT}}{\ell_{25}^{VT}}\right) \exp\left[0.09(i-25)\right] \tag{5.4}$$

Rich Extrapolation

$$k^{VT}(i\downarrow;150°K) = 1.8 \times 10^{-14}\left(\frac{\ell_i^{VT}}{\ell_{25}^{VT}}\right) \exp\left[0.24(i-25)\right] \tag{5.5}$$

Thus it is seen that near $i \tilde{=} 25$, the Verter-Rabitz rates are lower in magnitude than the present experimentally inferred rates by a factor of about 7, but their slow variation with i (β(Verter-Rabitz) = 0.09) is consistent with the Lightman and Fisher data. On the other hand, the Rich extrapolation rates intersect the experimentally inferred rates near i = 25, but deviates substantially from it for other values of i because of the relatively large value of β = 0.24 used. In the Rich extrapolation, β is estimated by the Keck and carrier[13] curve-fit representation of the VT adiabaticity factor:

$$\beta = \frac{4}{3}\,\alpha\theta_{vib}\sqrt{\theta^{VT}/8T} \tag{5.6}$$

where θ_{vib} = 3084°K is the characteristic vibrational temperature of CO and θ^{VT} is a constant proportional to the interaction length L of the short-range

epulsive potential. The value $\beta(150°K)$ is obtained[11] by using $\theta^{VT} = 0.114$ which corresponds to L = 0.2Å. It is of interest to observe that if a (normalized) detailed-balance factor is empirically included,[19] we would have

$$\beta = \frac{4}{3}\alpha\theta_{vib}\sqrt{\theta^{VT}/8T} - \frac{\alpha\theta_{vib}}{T} \quad , \tag{5.8}$$

yielding $\beta(150°K) = 0.114$ which is consistent with the present results.

Since experimental CO-He 1→0 VT rates are well-documented, the small value of β and the relatively large magnitudes of rates at high quantum numbers inferred from the Fisher-Lightman data suggest that A_i^{VT} must increase rapidly in the first few levels ($i \leq 10$). This observation is qualitatively consistent with the Verter-Rabitz results as correlated by Eq. (3.5). It was shown[19] that $a_i(T)$ is essentially unity for T > 300°K, but exhibits a rapid i dependence at the first few levels for 300°K > T ≥ 100°K. This interesting and unexpected behavior of the Verter-Rabitz results has so far not been satisfactorily interpreted theoretically. The present inferred rates provide the first experimental indications in support of this qualitative result.

It is important to note that the value of C inferred from the measured data is a ratio of VT and VV rates. Implicit in Eq. (5.3) is the assumption that the high quantum number nearly resonant VV rates are correctly scaled by the Young and Eachus transition matrix elements (since $C^{VV} = 1.5$ was used). Since recent measurements by Brechignac[16] indicates that such scaling appears to overestimate the high quantum number VV rates, our inferred rates will be similarly affected.

The data was originally reduced by choosing r = 10 as the reference quantum number. Although the combinations of C, C^{VV}, and β fitting the data appear disparate, the inferred CO-He VT rates from each set of parameters intersect

each other near $i \tilde{=} 25$, indicating that only the local VT rates are important for the given collection of data. The value of $r = 25$ was then chosen so that the curve-fitting became sensitive mainly to the value of C alone. Since the present inferred rates are obtained from a limited collection of data, additional experiments with a much wider range of external excitation strength and He pressures are clearly necessary to collaborate and refine the present findings.

REFERENCES

1. A. J. Lightman and E. R. Fisher, "Measurements of CO Vibrational Distributions in Mixtures with N_2, O_2, Ar and He", presented at 5th Conference on Chemical and Molecular Lasers, WAI6, St. Louis, Mo. (1977).

2. W. S. Drozdoski, R. M. Young, R. D. Bates, Jr., and J. K. Hancock, J. Chem. Phys. 65 1542 (1976).

3. G. Hancock and I.W.M. Smith, Appl. Opt. 10 1827 (1971).

4. R. C. Millikan and D. R. White, J. Chem. Phys. 39 98 (1963).

5. D. J. Miller and R. C. Millikan, J. Chem. Phys. 53 3384 (1963).

6. J. C. Stephenson and E. R. Mosburg, J. Chem. Phys. 60 3562 (1970).

7. H. T. Powell, J. Chem. Phys. 63 2635 (1975).

8. P. B. Sackett, A. Hordvik, and H. Schlossberg, Appl. Phys. Lett. 22, 367 (1973).

9. C. Wittig and I.W.M. Smith, Chem. Phys. Lett. 16 292 (1972).

10. M. C. Gower, G. Srinivasan, and K. B. Billman, J. Chem. Phys. 63 4206 (1975).

11. J. W. Rich, J. A. Lordi, R. A. Gibson, and S. K. King, CAlspan Corp. Rept. WG-5164-A-3 (1974).

12. R. D. Sharma and C. A. Brau, J. Chem. Phys. 50 924 (1969).

13. J. Keck and G. Carrier, J. Chem. Phys. 43 2284 (1974).

14. B. F. Gordiets and Sh. S. Mamedov, Prik. Mat. Teor. Fiz. 3 13 (1974).

15. S. H. Lam, "An Analytical Theory of Vibrational Relaxation for Anharmonic Molecules under Strongly Pumped Conditions, submitted to J. Chem. Phys. (1977).

16. Ph. Brechignac, "Near Resonant VV Transfer Rates for High-lying States of Diatomic Gases", private communication, submitted to J. Chem. Phys. (1977).

17. R. N. Schwartz, Z. I. Slawsky, and K. F. Herzfeld, J. Chem. Phys. 20 1591 (1952). Also see R. N. Schwartz and K. F. Herzfeld, J. Chem. Phys. 22 767 (1954).

18. M. Verter and H. Rabitz, J. Chem. Phys. 64 2939 (1976).

19. S. H. Lam and H. Rabitz, "Correlation of Vibration Translation Rates for CO-He", in preparation (1977).

20. L. A. Young and W. J. Eachus, J. Chem. Phys. 44 4195 (1966).

21. C. A. Brau, Physica 58 533 (1972).

FIGURE CAPTIONS

Fig. 1a CO vibrational population distributions measured by Lightman and Fisher[1] with 7-torr He. Dotted lines are Plateau distributions computed from Eq. (4.3) using $C = 1.2 \times 10^{-4}$, $C^{VV} = 1.5$, and $\beta = 0.09$.

Fig. 1b CO vibrational population distributions measured by Lightman and Fisher[1] with 4-torr He. Solid line is exact solution computed by using tne CO-He VT rates by Verter and Rabitz augmented by $(i+1)^{0.65}$. Dotted line is Plateau distribution computed from Eq. (4.3) using $C = 1.2 \times 10^{-4}$, $C^{VV} = 1.5$, and $\beta = 0.09$.

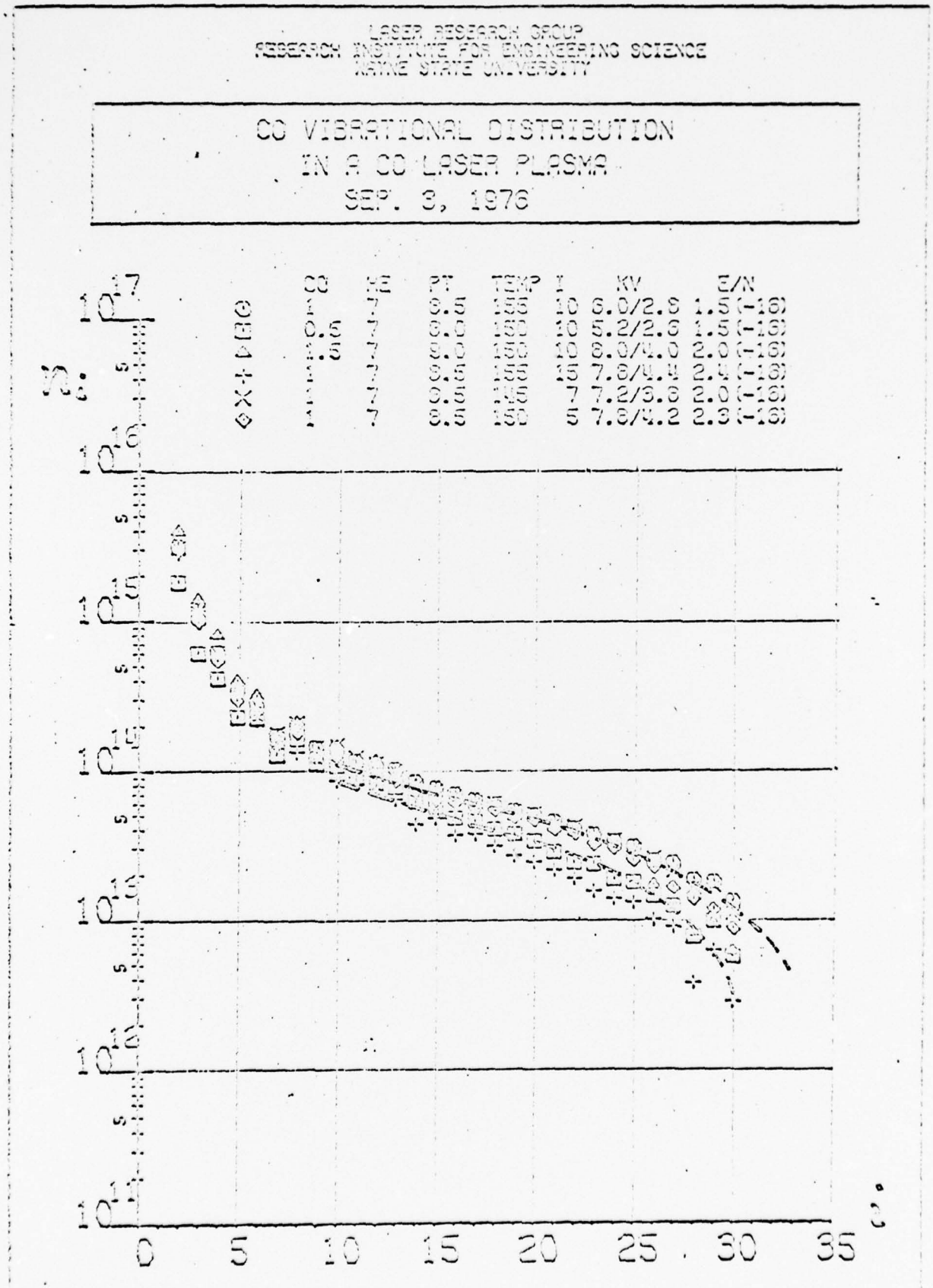
LASER RESEARCH GROUP
RESEARCH INSTITUTE FOR ENGINEERING SCIENCE
WAYNE STATE UNIVERSITY
CO VIBRATIONAL DISTRIBUTION
IN A CO LASER PLASMA
SEP. 3, 1976
CO
0.5
.5%
PT
TEMP
I
KV
E/N
3.5 155 10 6.0/2.8 1.5(-16)
3.0 150 10 5.2/2.6 1.5(-16)
3.0 150 10 6.0/4.0 2.0(-16)
3.5 155 15 7.8/4.4 2.4(-16)
3.5 155 7 7.2/3.6 2.0(-16)
3.5 150 5 7.8/4.2 2.3(-16)
V
0
5
10
15
20
25
30
35

LASER RESEARCH GROUP
RESEARCH INSTITUTE FOR ENGINEERING SCIENCE
WAYNE STATE UNIVERSITY

CO VIBRATIONAL DISTRIBUTION IN A CO LASER PLASMA

SEP. 1, 1976

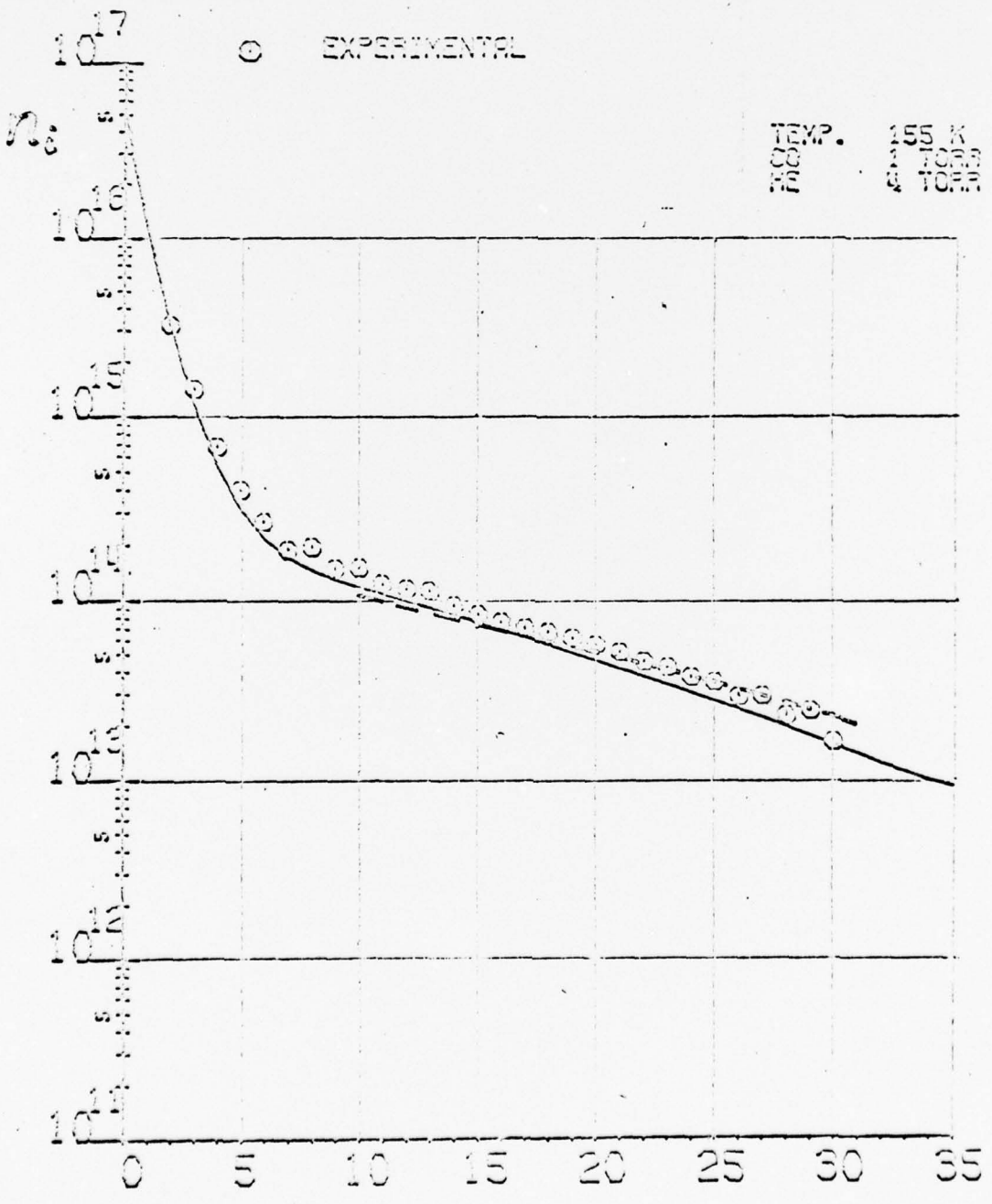

APPENDIX C

AN ANALYTICAL THEORY OF VIBRATIONAL RELAXATION FOR ANHARMONIC MOLECULES UNDER STRONGLY-PUMPED CONDITIONS

S. H. LAM

DEPARTMENT OF AEROSPACE AND MECHANICAL SCIENCES

PRINCETON UNIVERSITY

PRINCETON, NEW JERSEY

MARCH 1977

A B S T R A C T

An analytical theory of vibrational relaxation is presented showing explicitly the effects of the strength of the pumping, the anharmonicity of the energy level spacings, and the VV and VT kinetic rate models. The quasi-equilibrium population distribution, the loci of the Treanor-Plateau boundary and the Plateau-Boltzmann knee, the nominal magnitude of the plateau, the ground-level vibrational temperature, and the rates of vibrational quanta and energy dissipations are obtained. A method for deducing quantitative information on kinetic rates at high quantum numbers from measured population distributions is suggested.

AN ANALYTICAL THEORY OF VIBRATIONAL RELAXATION FOR ANHARMONIC MOLECULES UNDER STRONGLY-PUMPED CONDITIONS

S. H. Lam†

I. INTRODUCTION

When a diatomic gas at temperature T is subjected to external vibrational excitation (such as an electric discharge), its vibrational population distribution N_i will deviate from the equilibrium Botlzmann distribution given by

$$N_i^B(T) \equiv N_o \exp(-E_i/kT) \tag{1.1}$$

where E_i is the energy of the i^{th} vibrational level. The non-equilibrium N_i is governed by a system of master kinetic equations and depends in general on the strength of the external excitation, the anharmonicity of the energy levels, and the relevant kinetic rates. The vibrational relaxation process is dominated by the fact that, in some average sense, VV collision rates are much more rapid than VT collision rates. Vibrational quanta externally pumped into the gas can be redistributed by numerous quanta-conserving VV collisions before being deactivated by the much slower VT collisions. We shall be interested in the quasi-equilibrium distributions of N_i under strongly pumped conditions.

By assuming that VT rates are uniformly negligible in comparison to VV rates, Osipov[1] showed that for harmonic oscillators N_i would remain Boltzmann and could be characterized by a single vibrational temperature T_v:

†Department of Aerospace and Mechanical Sciences, Princeton University, Princeton, New Jersey

$$N_i \tilde{=} N_i^B(T_v), \quad \text{harmonic oscillators.} \tag{1.2}$$

The more general result, valid for arbitrary energy level spacings, was obtained by Treanor, Rich, and Rehm[2]:

$$N_i \tilde{=} N_i^{TRR}(T;\gamma) \equiv N_i^B(T) \exp(i\gamma) \tag{1.3}$$

where the constant γ replaced T_v as the single parameter. In either case, a relatively simple relaxation equation could be derived for T_v or γ.

These simple and elegant theories serve adequately only when the strength of the external excitation is weak. Motivated by its applications to molecular infrared lasers, the complete master kinetic equations have recently been extensively studied numerically.[3,4,5,6] The computed N_i under strongly pumped conditions exhibits the following general features. (a) In the lower levels, $0 \leq i < i^*$, N_i indeed can be approximated by $N_i^{TRR}(T;\gamma)$ for some $\gamma > 0$. (b) In the intermediate levels, $i^* < i < i^{**}$, N_i is relatively flat and decreases slowly with i. (c) For $i \tilde{=} i^{**}$, N_i drops sharply and tends toward $N_i^B(T)$. These three regions shall be called the Treanor, the Plateau, and the Boltzmann regions, respectively. These qualitative features appear to be relatively insensitive to the kinetic rate models used.

The physical interpretations of the above observations are clear.[3] Normally, vibrational quanta are pumped into the gas mostly at low levels. When the pumping is weak and the input quanta can be deactivated by local VT collisions, the Treanor distribution results. When the pumping is sufficiently strong, local VT deactivations become inadequate. The rapid, quanta-conserving VV collisions aided by the small anharmonicity of the energy levels then preferentially transport the excess quanta up the vibrational ladder to be deactivated

by the much faster VT collisions there. The Plateau region which appears only under strongly pumped conditions serves primarily as a conveyer belt between the source and the sink of vibrational quanta.

In the present paper, we present a simple theory of vibrational relaxation for anharmonic oscillators under strongly pumped conditions. In contrast to numerical studies where kinetic rates and other input data must be explicitly specified, our analytical results are expressed in terms of the input data, showing clearly the effects of kinetic rate models. The analytical techniques used follow closely the works of Brau[7] and Gordiets et al.[8,9] The quasi-equilibrium distribution N_i, the loci of the Treanor-Plateau boundary and the Plateau-Boltzmann knee $N^*(i)$ and $N^{**}(i)$, the ground-level vibration temperature T_{vo}, the nominal magnitude of the plateau $\bar{N}_o$, and the rates of vibrational quanta and energy dissipation D^{VT} and D_{vib} are obtained. It is shown that only a few parameters suitably extracted from the large collection of VV and VT rates are important. A method for quantitative determination of kinetic rate information at large quantum numbers from experimental N_i measurements is suggested.

II. KINETIC RATE MODELS

We shall assume that E_i can be adequately represented by

$$E_i = i\left[1-\alpha(i-1)\right] k\theta_{vib} \tag{2.1}$$

where α is the anharmonicity and θ_{vib} is the characteristic vibrational temperature of the diatomic molecule in question. We shall use Δ to denote the forward difference operator. The energy level spacing is thus given by

$$\Delta E_i \equiv E_{i+1} - E_i = (1-2\alpha i)k\theta_{vib}. \tag{2.2}$$

Applying Δ to Eq. (2.2), we have

$$\Delta^2 E_i \equiv \Delta(\Delta E_i) = -2\alpha k\theta_{vib}. \tag{2.3}$$

For CO, $\alpha = 5.98 \times 10^{-3}$ and $\theta_{vib} = 3084°K$. We shall see that, inspite of its smallness, the anharmonicity α plays an important role in the later developments.

The major kinetic rates of interest are the so-called VV and VT single-quantum-jump rates. Let $k^{VV}(i\uparrow,j\downarrow)$ denote the vibration-vibration (VV) rate of a $i \to i+1$, $j+1 \to j$ collision between two molecules of interest. Let $k_a^{VT}(i+1 \rightleftarrows i)$ denote the vibration-translation (VT) rate of a $i+1 \rightleftarrows i$ collision between a molecule of interest and a partner atom or molecule identified by the subscript a. Guided by the well-known SSH theory,[10,11,12] we shall formally express k^{VV} and k_a^{VT} as follows:

$$k^{VV}(i\uparrow,j\downarrow) \equiv \omega^{VV}(T)\ell_i\ell_j A_{ij}^{VV} \exp\left[(\Delta E_j - \Delta E_i)/2kT\right] \tag{2.4}$$

$$k_a^{VT}(i+1 \rightleftarrows i) \equiv \omega_a^{VT}(T)\ell_i A_{i,a}^{VT} \exp\left[(\pm\Delta E_i - \Delta E_i)/2kT\right], \tag{2.5}$$

where ℓ_i, A_{ij}^{VV}, and $A_{i,a}^{VT}$ are dimensionless and are normalized as follows:

$$\ell_o = 1, \quad A_{ii}^{VV} = 1, \quad A_{o,a}^{VT} = 1 . \tag{2.6}$$

In addition, detailed-balance requires $A_{ij}^{VV} = A_{ji}^{VV}$. The dimension of k^{VV} and k_a^{VT}(cm^3/molecule-sec) is carried by ω^{VV} and ω_a^{VT} representing $k^{VV}(1\uparrow, 1\downarrow)$, $k_a^{VT}(1 \to 0)$ respectively.

Theoretically, ℓ_i is proportional to the square of the oscillator matrix element and A_{ij}^{VV} and $A_{i,a}^{VT}$ are the adiabaticity factors. Physically, ℓ_i^2 gives the quantum number scaling of the resonant-exchange VV rates:

$$k^{VV}(i\uparrow, i\downarrow) = \omega^{VV}\ell_i^2. \tag{2.7}$$

For harmonic oscillators, ℓ_i can be shown to be simply $i + 1$. We shall assume here simply that ℓ_i is known and that $\Delta^2\ell_i$ is small.

The VV adiabaticity factor A_{ij}^{VV} depends in principle on both i and j. Guided by the theories of Landau and Teller[13] and SSH, we shall assume that

$$A_{ij}^{VV} = A^{VV}(\xi;T) \tag{2.8}$$

where ξ is the so-called adiabasy parameter[14] defined by

$$\xi = \alpha\theta_{vib} \, |i-j| \sqrt{\theta^{VV}/T} \tag{2.9}$$

and θ^{VV} is a constant which depends on the reduced mass and the interaction potential of the collision. For CO, θ^{VV} is $O(10^{-1})°K^{-1}$. In addition, we shall assume that $A^{VV}(\xi;T)$ decreases exponentially with increasing ξ to reflect the fact that nearly-resonant collisions are much more rapid than non-resonant collisions. Note that in general A_{ij}^{VV} may also depend on $i + j$ but this dependence has been neglected.

The VT adiabaticity factor $A_{i,a}^{VT}$ is also expected to depend on an analogous adiabasy parameter. We shall merely require that $A_{i,a}^{VT}$ increases exponentially with i.

III. THE MASTER KINETIC EQUATIONS

We consider a diatomic gas with number density n_m in the presence of an atomic diluent with number density n_a. The master kinetic equations can readily be written in the following form:

$$\frac{d}{dt} \sum_{k=i+1}^{\infty} N_k = F_i^{VV} + F_i^{VT} + F_i^{e}, \quad i = 0,1,2,\ldots, \tag{3.1}$$

where N_i is the normalized vibrational population distribution of the molecules

$$\sum_{i=0}^{\infty} N_i = 1, \tag{3.2}$$

and the dissociation level is represented by $i = \infty$. The terms F_i^{VV}, F_i^{VT}, F_i^{e} represent the net fluxes of molecules (per molecule per second) going from <u>any</u> level at or below level i to <u>any</u> level at or above i + 1 by VV, VT and any other processes, respectively. The VV and VT fluxes can be written as follows:

$$F_i^{VV} = n_m \sum_{j=0}^{\infty} \left[k^{VV}(i\uparrow,j\downarrow) N_i N_{j+1} - k^{VV}(j\uparrow,i\downarrow) N_j N_{i+1} \right], \tag{3.3}$$

$$F_i^{VT} = n_a \left[k_a^{VT}(i \rightarrow i+1) N_i - k_a^{VT}(i+1 \rightarrow i) N_{i+1} \right], \tag{3.4}$$

where we have assumed, for the sake of simplicity, that F_i^{VT} is dominated by collisions with the diluent atoms. In general, F_i^{VT} should be the sum of all VT contributions including self-collisions.

Using the VV and VT rate formulas discussed earlier, we can rewrite Eqs. (3.3) and (3.4) as follows:

$$F_i^{VV} = n_m \omega^{VV} \sum_{j=0}^{\infty} S_{ij}(M_j - M_i), \tag{3.5}$$

$$F_i^{VT} = n_a \omega_a^{VT} f_i(1 - M_i), \tag{3.6}$$

where S_{ij} is a symmetric matrix

$$S_{ij} = S_{ji} \equiv s_i A^{VV}(\xi;T) s_j, \tag{3.7}$$

and s_i and f_i are given by

$$s_i = \ell_i N_i \exp(-\Delta E_i/2kT), \tag{3.8}$$

$$f_i = s_i A_{i,a}^{VT} \exp(-\Delta E_i/2kT) . \tag{3.9}$$

The auxiliary dependent variable M_i is defined by

$$M_i \equiv \frac{N_{i+1}}{N_i} \frac{N_i^B(T)}{N_{i+1}^B(T)}$$

$$= \exp \Delta\left(\frac{E_i}{kT} + \ell n\, N_i\right). \tag{3.10}$$

Note that $M_i = 1$ and $M_i = \exp \gamma$ correspond to $N_i = N_i^B(T)$ and $N_i = N_i^{TRR}(T;\gamma)$, respectively.

The master kinetic equations can now be written in the following compact form:

$$\sum_{j=0}^{\infty} S_{ij}(M_j - M_i) = \varepsilon^{VT}(M_i - 1) f_i - Q_i, \tag{3.11}$$

where

$$\varepsilon^{VT} \equiv \frac{n_a}{n_m} \frac{\omega_a^{VT}}{\omega^{VV}}, \tag{3.12}$$

$$Q_i = \frac{1}{n_m \omega^{VV}} \left[F_i^e - \frac{d}{dt} \sum_{k=i+1}^{\infty} N_k\right]. \tag{3.13}$$

The term F_i^e represents mainly external excitation (such as electric discharge, radiative transitions, etc.) but may include multi-quanta-jump and other processes. The dimensionless Q_i combines these external excitations and the unsteady term and is to be considerd as a forcing term in Eq. (3.11). The conventional master kinetic equations can be recovered from Eq. (3.11) by applying the forward difference operator Δ.

Summing Eq. (3.11) over all i, we obtain the so-called quanta conservation equation

$$\frac{d\sigma}{dt} = \sum_{i=0}^{\infty} F_i^e - D^{VT}, \tag{3.14}$$

where σ is the specific quanta (average number of quanta per molecule) defined by

$$\sigma \equiv \sum_{i=0}^{\infty} iN_i = \sum_{i=0}^{\infty} \sum_{k=i+1}^{\infty} N_k \ , \tag{3.15}$$

and D^{VT} is the rate of quanta deactivation by VT collisions

$$D^{VT} \equiv - \sum_{i=0}^{\infty} F_i^{VT} = n_a \omega_a^{VT} \sum_{i=0}^{\infty} (M_i - 1) f_i \ . \tag{3.16}$$

The contribution from quanta-conserving VV collisions vanishes identically.

Multiplying Eq. (3.11) by ΔE_i and then summing over all i, we obtain the vibrational energy equation:

$$\frac{d}{dt} e_{vib} = \sum_{i=0}^{\infty} F_i^e \Delta E_i - D_{vib} \ , \tag{3.17}$$

where e_{vib} is the specific vibrational energy:

$$e_{vib} \equiv \sum_{i=0}^{\infty} E_i N_i = \sum_{i=0}^{\infty} \sum_{k=i+1}^{\infty} N_k \Delta E_i \ , \tag{3.18}$$

and D_{vib} is the rate of dissipation of vibrational energy by both VV and VT collisions:

$$D_{vib} \equiv - \sum_{i=0}^{\infty} F_i^{VV} \Delta E_i - \sum_{i=0}^{\infty} F_i^{VT} \Delta E_i \ . \tag{3.19}$$

IV. PRELIMINARY DISCUSSION

We may consider $n_m \omega^{VV}$ and $n_a \omega_a^{VT}$ to be representative frequencies of VV and VT collisions, respectively. The dimensionless parameter ε^{VT} can thus be interpreted as the number of VT collisions per VV collision and is in general a small number. We shall define Q_{total} by

$$Q_{total} \equiv \sum_{i=0}^{\infty} Q_i = \frac{1}{n_m \omega^{VV}} \left\{ \sum_{i=0}^{\infty} F_i^e - \frac{d\sigma}{dt} \right\} \tag{4.1}$$

which may be loosely interpreted as being the number of quanta externally pumped into a molecule of interest per VV collision. Under most practical situations of interest, Q_{total} is also a small number. We shall confine our attention to strongly-pumped conditions defined by

$$1 >> Q_{total} >> \varepsilon^{VT} . \tag{4.2}$$

In addition, since the bulk of the vibrational population resides in the first few levels, we shall assume that Q_i occurs mainly at low levels. Consequently, Q_{total} can be approximated by summing over only the first few levels.

If we formally invoke Eq. (4.2) and completely neglected the right-hand side of Eq. (3.11), we would obtain

$$\sum_{j=0}^{\infty} S_{ij}(M_j - M_i) \cong 0 \tag{4.3}$$

from which the Treanor solution M_i = constant can immediately be recovered by inspection. While this simple and elegant solution can be justified for weakly-pumped ($1 >> \varepsilon^{VT} >> Q_{total}$) conditions, it is known to be incorrect for strongly-pumped ($1 >> Q_{total} >> \varepsilon^{VT}$) conditions. In fact, Brau[7] has shown that this Treanor solution is not unique but is merely a member of a family of solutions for Eq. (4.3).

The major physical simplification underlying the present development is the dominance of the rapid nearly-resonant VV collisions over the slower non-resonant VV collisions. The VV adiabaticity factor $A^{VV}(\xi;T)$ is generally expected to be some exponentially decreasing function of ξ. Consequently, the elements of the non-linear symmetric matrix operator S_{ij} as defined by Eq. (3.7) are expected to be largest in the vicinity of the diagonal. Under the assumption that $A^{VV}(\xi;T)$ decreases sufficiently rapidly with ξ (see Eqs. (7.7) later), the matrix operator

S_{ij} can be converted into a differential operator. The original discrete system of master kinetic equations, Eq. (3.11), thus becomes a single ordinary differential equation which can be studied in details by standard techniques.[7]

V. THE DIFFERENTIAL APPROXIMATION

For $A^{VV}(\xi;T)$ decreasing sufficiently rapidly with ξ, the main contributions to F_i^{VV} as given by Eq. (3.5) will come from nearly-resonant ($j \cong i$) collisions. Accordingly, we formally expand M_j and s_j about $j = i$ as follows

$$M_j = M_i + (j-i)\Delta M_i + \frac{1}{2}(j-i)^2\Delta^2 M_i + \ldots , \tag{5.1}$$

$$s_j = s_i + (j-i)\Delta s_i + \ldots , \tag{5.2}$$

Substituting the above in Eqs. (3.5) and (3.7), we obtain formally:

$$F_i^{VV} = n_m \omega^{VV} \left\{ a_i s_i^2 \Delta M_i + b_i \Delta(s_i^2 \Delta M_i) + \ldots \right\} \tag{5.3}$$

where

$$a_i(T) \equiv \sum_{j=0}^{\infty} (j-i) A^{VV}(\xi;T)$$

$$b_i(T) \equiv \sum_{j=0}^{\infty} \frac{1}{2}(j-i)^2 A^{VV}(\xi;T) .$$

For values of i sufficiently large such that the lower limits of the summation are unimportant,

$$i >> \hat{i}(T) \equiv (T/\theta^{VV})^{\frac{1}{2}}/\alpha\theta_{vib} , \tag{5.4}$$

$a_i(T)$ and $b_i(T)$ become independent of i. We obtain

$$a_i(T) \cong \sum_{n=-\infty}^{\infty} n A^{VV}(n/\hat{i};T) = 0 ,$$

$$b(T) \equiv b_i(T) \cong \sum_{n=0}^{\infty} n^2 A^{VV}(n/\hat{i};T) . \tag{5.5}$$

Thus the leading approximation to F_i^{VV} can be written as follows:

$$F_i^{VV} \cong bn_m\omega^{VV}\Delta(s_i^2\Delta M_i), \quad i >> \hat{i} . \tag{5.6}$$

Note that non-resonant VV contributions ($|j-i| >> \hat{i}$), even those with partners from the highly populated lower levels, have been neglected. We shall re-examine this approximation later in Section VII.

Under strongly pumped conditions, the number of levels with significant populations can be relatively large. We shall take advantage of this observation and represent the discrete variables N_i, M_i, ℓ_i, E_i, etc. by continuous functions $N(i)$, $M(i)$, $\ell(i)$, $E(i)$, etc. We further assume that

$$1 >> |\Delta \ell n\, N_i|, \; 1 >> \delta \equiv -\frac{\Delta^2 E_i}{kT} > 0 , \tag{5.7}$$

so that Δ can be approximated by the differential operator d/di. For example, M_i as defined by Eq. (3.10) can be represented by

$$M_i = M(i) \cong \exp\left[\frac{d}{di}\left(\frac{E}{kT} + \ell n\, N\right)\right] , \tag{5.8}$$

and ΔM_i by

$$\Delta M_i \cong \frac{dM}{di} = M\frac{d^2}{di^2}\left(\frac{E}{kT} + \ell n\, N\right). \tag{5.9}$$

Using this differential approximation, Eq. (5.6) can be written as

$$F_i^{VV} \cong bn_m\omega^{VV}\frac{d}{di}\left\{(N\ell)^2\left(\frac{d^2}{di^2}\ell n\, N - \delta\right)\right\}. \tag{5.10}$$

Note that the VV adiabaticity factor $A^{VV}(\xi;T)$ is represented only by its second moment $b(T)$ which can be written alternatively as:

$$b(T) \cong \hat{i}^3\int_0^\infty \xi^2 A^{VV}(\xi;T)d\xi . \tag{5.11}$$

The detailed shape of $A^{VV}(\xi;T)$ is seen to be unimportant so long as it decreases sufficiently rapidly with ξ.

The term F_i^{VT} can similarly be approximated by a continuous function. For strongly pumped conditions, the magnitude of M_i is generally very large except in the Boltzmann region where it is approximately 1.0. We shall denote i^{**} to be the Plateau-Boltzmann boundary defined tentatively by $M(i<i^{**}) >> 1$ and $M(i \gtrsim i^{**}) \cong 1$. Eq. (3.6) can thus be written as

$$\begin{aligned} F_i^{VT} &\cong n_a \omega_a^{VT} \; N\ell A_a^{VT}(i), \quad 0 < i < i^{**} , \\ &\cong 0 . \qquad\qquad , \quad i \gtrsim i^{**} . \end{aligned} \tag{5.12}$$

Using Eqs. (5.10) and (5.12), the originally discrete master kinetic equations can be represented by the following differential equation:[7]

$$\begin{aligned} b \frac{d}{di}\left\{(N\ell)^2\left[\frac{d^2}{di^2}\ell nN - \delta\right]\right\} &= \varepsilon^{VT} N\ell A_a^{VT} - Q, \; \hat{i}(T)<<i<i^{**}, \\ &= 0 , \qquad\qquad i \geq i^{**} , \end{aligned} \tag{5.13}$$

where $Q(i)$ is the continuous representation of Q_i.

VI. THE NOMINAL PLATEAU DISTRIBUTION

If the right-hand side of Eq. (5.13) is formally neglected, we obtain upon integration[7]

$$b(N\ell)^2\left[\frac{d^2}{di^2}\ell nN - \delta\right] = - C \tag{6.1}$$

where C is an integration constant. In spite of the approximations invoked, we can readily verify that $N(i;C=0)$ is precisely the Treanor solution:

$$N(i;C=0) = N^{TRR}(i;i_{min}) \equiv N_o \exp\left\{i\delta\left(\frac{i}{2} - i_{min}\right)\right\} \tag{6.2}$$

where the integration constant i_{min} is the location of the so-called Treanor minimum. It is clear that for $C \neq 0$ a family of non-Treanor solutions can be generated. The approximate Plateau distribution $N\ell$ = constant first pointed out by Caledonia and Center[3] is seen to be an approximate solution of Eq. (6.1) with $C > 0$.

Because $A_a^{VT}(i)$ increases rapidly with i, the right-hand side of Eq. (5.13) is not uniformly negligible, and the integration constant C is in fact not a constant. Before attacking Eq. (5.13) directly, we shall first introduce the nominal plateau distribution $\bar{N}(i)$ defined as follows:

$$-b\delta \frac{d}{di}(\bar{N}\ell)^2 = \varepsilon^{VT}\,\bar{N}\ell A_a^{VT}\,, \qquad \bar{N}(0) = \bar{N}_o\,, \tag{6.3}$$

where $\bar{N}_o$ is a constant to be determined later. Integrating, we obtain[8,9]

$$\ell\bar{N}(i) = \bar{N}_o - \ell N^{**}(i) \tag{6.4}$$

where

$$N^{**}(i) \equiv \frac{\varepsilon^{VT}}{2b\delta\ell}\int_o^i A_a^{VT}di \tag{6.5}$$

and is seen to be solely a function of the VV and VT rate models. For $\bar{N}_o >> \varepsilon^{VT}$, $\bar{N}(i)$ is approximately $\bar{N}_o/\ell$ until the exponentially increasing $A_a^{VT}(i)$ intervenes, bending it sharply downward. The knee of the bend occurs approximately at the intersection of $\bar{N}(i)$ and $N^{**}(i)$. The location i^{**} where $\bar{N}(i)$ vanishes is related implicitly to $\bar{N}_o$ by

$$\bar{N}_o = \frac{\varepsilon^{VT}}{2b\delta}\int_o^{i^{**}} A_a^{VT}di\,. \tag{6.6}$$

For $i \gtrsim i^{**}$, $\bar{N}(i)$ is identically zero.

We shall presently show that $\bar{N}(i)$ is an approximation to $N(i)$ in the Plateau region. Subtracting Eq. (6.3) from Eq. (5.13) we obtain

$$b\frac{d}{di}\left\{(N\ell)^2\left[\frac{d^2}{di^2}\ell nN-\delta\right]\right\} = -b\delta\frac{d}{di}(\bar{N}\ell)^2 - Q + \varepsilon^{VT}g, \qquad \hat{i} << i < i^{**}, \tag{6.7}$$

where

$$g(i) \equiv (N\ell - \bar{N}\ell)A_a^{VT} . \tag{6.8}$$

Integrating Eq. (6.7) from 0 to i^{**} and noting that the net VV contribution must vanish identically, we obtain

$$b\delta\bar{N}_o^2 = Q_{total} - \varepsilon^{VT}\int_0^{i^{**}} g\,di \tag{6.9}$$

which is simply the quanta conservation equation (3.14) expressed in an alternative form. Integrating Eq. (6.7) from i to i^{**}, we obtain

$$b(N\ell)^2\left[\frac{d^2}{di^2}\ell nN-\delta\right] = -b\delta(\bar{\bar{N}}\ell)^2, \quad \hat{i} << i < i^{**}, \tag{6.10}$$

where

$$(\bar{\bar{N}}\ell)^2 = (\bar{N}\ell)^2 - \frac{1}{b\delta}\int_i^{i^{**}}(Q-\varepsilon^{VT}g)di . \tag{6.11}$$

Eq. (6.10) is simply Eq. (6.1) with a variable $C = b\delta(\bar{\bar{N}}\ell)^2$.

We shall choose $\bar{N}(i)$ *by the requirement that the integrals of* $\varepsilon^{VT}g(i)$ in Eqs. (6.9) and (6.11) be uniformly small. Under strongly-pumped conditions, Eq. (6.9) yields $\bar{N}_o \tilde{=} (Q_{total}/b\delta)^{\frac{1}{2}}$ and Eq. (6.11) yields $\bar{\bar{N}}(i)$ in terms of $\bar{N}(i)$ and $Q(i)$. Since $g(i)$ contains $A_a^{VT}(i)$ which generally increases exponentially with i, we conclude further that $N(i)$ must approach $\bar{N}(i)$ rapidly as i increases. Only in the vicinity of i^{**} where the local values are both small can $N(i)$ begin to deviate from $\bar{N}(i)$ and to approach a local equilibrium Boltzmann there. In

other words, $\bar{N}(i)$ is the leading approximation to $N(i)$ in the Plateau region, $N^{**}(i)$ is the locus of the Plateau-Boltzmann knee of the solutions, and i^{**} is the location of the Plateau-Boltzmann boundary.

Using Eq. (4.1) for Q_{total} in Eq. (6.9) and comparing with Eq. (3.14), we obtain

$$D^{VT} = n_m \omega^{VV} b \delta \bar{N}_o^2 + n_a \omega_a^{VT} \int_o^{i^{**}} g di \ . \tag{6.12}$$

The first term represents the rate of upward transport of quanta by nearly-resonant VV collisions and is seen to be independent of VT rates even though these quanta are eventually deactivated at high levels by VT collisions. The second term is a small correction representing the rate of local low-level VT deactivations and can be computed after $N(i)$ has been found.

VII. THE TREANOR-PLATEAU TRANSITION

In the vicinity of the Treanor-Plateau boundary i^*, the solution is expected to approach $N^{TRR}(i;i_{min})$ on one side and to approach $\bar{N}(i;\bar{N}_o)$ on the other. The value of i^* or i_{min} can be related to $\bar{N}_o$ by a local transition analysis as follows.

We shall tentatively assume that $i^* >> \hat{i}$ so that Eq. (6.10) remains valid in this transition region. Since the dominant external excitation is assumed to occur mainly in the first few levels, the $Q(i)$ contribution in Eq. (6.11) can be neglected, yielding $\bar{\bar{N}}(i) \cong \bar{N}(i)$ for $i \gtrsim i^*$. For $i < i^*$, accurate representation of $\bar{\bar{N}}(i)$ is not required provided that $(\bar{\bar{N}}/N)^2$ becomes locally small. Thus, in the transition region, $\bar{\bar{N}}(i)$ may be approximated by a constant, $\bar{N}_* \equiv \bar{N}(i^*)$. The equation governing the Treanor-Plateau transition is then[7]

$$\frac{1}{\delta} \frac{d^2}{di^2} \ell n N = 1 - \left(\frac{\bar{N}_*}{N} \right)^2 \ . \tag{7.1}$$

The magnitude of $\bar{N}_*$ is assumed to be small in comparison to the ground level population N_0:

$$(\bar{N}_*/N_0)^2 << 1 \ . \tag{7.2}$$

Even though both $\bar{\bar{N}} \overset{\sim}{=} \bar{N}_*$ and the differential approximation underlying Eq. (7.1) cannot be formally justified for $0 \leq i \overset{\sim}{=} \hat{i}$, it is nevertheless clear that the transition solution will automatically approach $N^{TRR}(i;i_{min})$ as $i \to 0$ so long as Eq. (7.2) is satisfied. Consequently, we shall use Eq. (7.1) in the extended region $0 \leq i \overset{\sim}{=} i^*$ to describe the Treanor-Plateau transition. The values of $\bar{N}_*$ and i_{min} are yet unknown but will be determined presently.

Eq. (7.1) can be integrated once to yield

$$\frac{d}{di} \ell nN = - \left\{ \delta \left[2 \ \ell n \frac{N}{\bar{N}_*} - \left(\frac{\bar{N}_*}{N} \right)^2 + 1 \right] \right\}^{1/2}$$

where $N(i >> i^*) = \bar{N}_*$ has been imposed. Integrating again, we obtain an implicit representation of the Treanor-Plateau transition solution:[7]

$$i\sqrt{\delta} = \int_{\ell n \frac{N}{\bar{N}_*}}^{\ell n \frac{N_0}{\bar{N}_*}} \frac{dx}{\left[2x - e^{-2x} + 1 \right]^{1/2}} \ . \tag{7.4}$$

Note that $N/\bar{N}_*$ is a universal function of $i\sqrt{\delta}$ and $\bar{N}_*/N_0$ and is independent of kinetic rate models.

As mentioned previously, this transition solution automatically approaches $N^{TRR}(i)$ as $i \to 0$ provided $(\bar{N}_*/N_0)^2 << 1$. The value of i_{min} appearing in Eq. (6.2) can now be determined by matching the derivative of ℓnN and ℓnN^{TRR} at $i = 0$, yielding

$$i_{min} \overset{\sim}{=} \left\{ 2 \left(\ell n \frac{N_0}{\bar{N}_*} - 1 \right) / \delta \right\}^{1/2} . \tag{7.5}$$

Since i_{min} is the location of the Treanor minimum of the particular $N^{TRR}(i,i_{min})$ which osculates N(i) at i = 0, we may conveniently identify it to be the Treanor-Plateau boundary i^*. Hence, the locus of the Treanor-Plateau boundary $N^*(i)$ can be obtained by inverting Eq. (7.5) and setting $i_{min} = i^*$. We obtain

$$N^*(i) \cong 0.61\, N_0 \exp\left(-\delta i^2/2\right). \tag{7.6}$$

For given value of $\overline{N}_0$, the intersection of $N^*(i)$ and $\overline{N}(i;N_0)$ immediately yields the values of $\overline{N}_*(\overline{N}_0)$ and $i^*(\overline{N}_0)$.

The above analysis may be refined by using a more accurate representation of $\overline{\overline{N}}(i)$. In addition, in the vicinity of i^{**} a separate Plateau-Boltzmann transition analysis is required. Since these refinements are not of major practical interest, they will not be presented here.

The assumption $\hat{i} >> i^*$ invoked earlier can now be examined. Using Eq. (7.5) for i^*, we obtain a lower bound for the value of θ^{VV}:

$$\theta^{VV} >> \frac{1}{\alpha\theta_{vib}\left(\ell n \frac{N_0}{\overline{N}_*} - \frac{1}{2}\right)}. \tag{7.7a}$$

Furthermore, in the derivation of Eq. (5.6) which eventually led to the differential approximation, contributions to F_i^{VV} by non-resonant VV collisions, including those with partners from the highly populated lower levels, have been neglected. A rough estimate yields the following condition on $A^{VV}(\xi;T)$:

$$A^{VV}\,(\xi = i/\hat{i};T) << \frac{b\ell N^*(i)}{N_0}, \quad i \cong i^*, \tag{7.7b}$$

which must be satisfied in addition to Eq. (7.7a). If Eqs. (7.7) are not satisfied, the Treanor-Plateau transition will depend on detailed information on $A^{VV}(\xi;T)$ and must be studied using the original discrete form of the master kinetic equations. For CO, Eqs. (7.7) are comfortably satisfied by most VV rate

models assumed in theoretical calculations.

VIII. SUMMARY OF RESULTS

By taking advantage of the dominance of the nearly-resonant VV collisions, we have derived using the differential approximation[7] the loci of the Treanor-Plateau boundary $N^{*}(i)$ and the Plateau-Boltzmann knee $N^{**}(i)$. $N^{*}(i)$ is shown to be independent of kinetic rate information provided that Eqs. (7.7) is satisfied. $N^{**}(i)$, on the other hand, is found to depend on both VV and VT rates.[8,9] At any given temperature, these loci can readily be computed and plotted as illustrated in Fig. 1. The family of nominal plateau distribution $\bar{N}(i;\bar{N}_o)$ can also be plotted and its intersection with $N^{*}(i)$ yields immediately the values of $i^{*}(\bar{N}_o)$ and $\bar{N}_{*}(\bar{N}_o)$. In the first few levels, $N(i)$ is osculated by a Treanor distribution $N^{TRR}(i,i_{min})$ with $i_{min} = i^{*}(\bar{N}_o)$. As i increases, $N(i)$ crosses $N^{*}(i)$ via the Treanor-Plateau transition solution to approach $\bar{N}(i;\bar{N}_o)$ in the Plateau region, bending sharply downward as it crosses $N^{**}(i)$ and tending toward a local Boltzmann distribution near $i^{**}(\bar{N}_o)$. The strongly-pumped condition is satisfied whenever the solution passes substantially above the intersection of $N^{*}(i)$ and $N^{**}(i)$ so that a distinct Plateau region exists. Fig. 1 also shows a comparison of the present results with exact numerical solutions of the original discrete equations for a CO-He 1:9 mixture at 100°K using a computer code developed by Boulnois.[15] The agreement is surprisingly good in view of the approximations invoked. Note that these discrete solutions were computed using 39 levels which appeared to be inadequate for the two more strongly-pumped cases.

The equivalent ground level vibrational temperature T_{v_o} defined by fitting the first few levels by $N^{B}(T_{v_o})$ can readily be computed:

$$T_{v_o} \cong \left\{ \frac{T\theta_{vib}}{2\alpha\left[2\ \ell n \frac{N_o}{\bar{N}_{*}} - 1\right]} \right\}^{\frac{1}{2}} . \tag{8.1}$$

Other gross quantities of interest, such as $\sigma(\bar{N}_o,T)$ and $e_{vib}(\bar{N}_o,T)$, can also be computed. The value of $\bar{N}_o$ or its time evolution is governed by the quanta conservation equation (3.14) with D^{VT} given by Eq. (6.12):

$$\frac{d}{dt}\sigma(\bar{N}_o,T) = \sum_{i=0}^{\infty} F_e^i - n_m\omega^{VV}\left[b\delta\bar{N}_o^2 + \varepsilon^{VT}\int_o^{i^{**}} g\,di\right]. \tag{8.2}$$

The small correction term $\varepsilon^{VT}g$ representing low-level local deactivations may be included with no difficulty. Once $\bar{N}_o(t)$ has been found, the vibrational state of the molecule of interest is completely determined. Hence under quasi-equilibrium conditions $\bar{N}_o$ can be considered simply as a state variable which together with T completely specifies $N_i(\bar{N}_o,T)$, $\sigma(\bar{N}_o,T)$, and $T_{v_o}(\bar{N}_o,T)$. The rate of dissipation of vibrational energy D_{vib}, however, is not a state function and must be computed from Eq. (3.17) instead of Eq. (3.19):

$$D_{vib} = \sum_{i=0}^{\infty} F_i^e\,\Delta E_i - \frac{d}{dt}e_{vib}(\bar{N}_o,T)\ . \tag{8.3}$$

IX. DISCUSSION

The kinetic rates have been expressed in Section II in terms of ω^{VV}, ω_a^{VT}, ℓ_i, $A^{VV}(\xi;T)$, and $A_{i,a}^{VT}(T)$. The same ℓ_i is used for both VV and VT rates because of its theoretical significance. For anharmonic oscillators, ℓ_i is often represented by

$$\ell = \frac{i+1}{1-C_1\alpha i} \tag{9.1}$$

where C_1 is a positive constant of order unity. The VV adiabaticity factor $A^{VV}(\xi;T)$ is often assumed to be the sum of two exponentials representing contributions from long-range and short-range forces. As pointed out by Brau,[7] so long as Eqs. (7.7) are satisfied the detailed shape of $A^{VV}(\xi;T)$ is unimportant. Only

b(T), its second moment, appears in the theory. On the other hand, the present theory shows that accurate information[17] on $A^{VT}_{i,a}(T)$, particularly at high levels, is required. Since $A^{VT}_{i,a}(T)$ is expected to depend on i exponentially, we may assume (see Eq. (2.9))

$$A^{VT}_{i,a}(T) = \exp\left(i\alpha\theta_{vib}\sqrt{\frac{\theta^{VT}}{T}}\right), \tag{9.2}$$

where θ^{VT} may be temperature dependent. Consequently, all the kinetic rate information can be represented by only five parameters, $\omega_a^{VT}(T)$, $\omega^{VV}(T)$, C_1, b(T), and $\theta^{VT}(T)$.

Using Eqs. (9.1) and (9.2), $\bar{N}(i)$ can be rewritten as

$$\bar{N}(i) = \frac{1-C_1\alpha i}{i+1}\left\{\bar{N}_o - C_o\sum_{j=0}^{i}\exp\left(jC_2\right)\right\} \tag{9.3}$$

where

$$C_o(T) \equiv \frac{n_a\omega_a^{VT}}{n_m\omega^{VV}}\,\frac{T}{4b\alpha\theta_{vib}}\,,\quad C_2(T) = \alpha\theta_{vib}\sqrt{\frac{\theta^{VT}}{T}}\,. \tag{9.4}$$

It is seen that all kinetic rate as well as energy level spacing information are represented here by only three parameters, C_o, C_1, and C_2. The simplicity of Eq. (9.3) suggests the possibility of deducing the values of $C_o(T)$, C_1, and $C_2(T)$ from a family of experimentally measured N_i distributions. At the present time, experimental rate information at high levels is rather limited; most reported data[18,19,20] are concerned primarily at the lower levels. The values of $C_o(T)$, C_1, and $C_2(T)$ deduced as suggested will be welcome complements to conventional measurements.

Brau[7] was first to use the differential approximation, deriving Eq. (5.13) and obtaining a family of approximate solutions N(i;C) from Eq. (6.1), including the Treanor-Plateau transition solutions. The cumulative effects of VT

deactivations was neglected and the relationship between C and the strength of external excitation Q_{total} was not given. Gordiets et al.[8,9] first recognized the importance of VT (and radiative) deactivations in the Plateau region, and obtained approximate Plateau distributions from Eq. (5.13) by replacing $d^2\ell nN/di^2$ with -2δ, an empirical factor suggested by curve-fitting of direct numerical solutions. In the present work, this empirical adjustment which is difficult to justify mathematically is avoided by the artifice of introducing $\bar{N}(i)$ by definition. In their effort to relate $\bar{N}_o$ (or C) with Q_{total}, Gordiets et al. evaluated D^{VT} from Eq. (3.16) by omitting $N^{**}(i)$ from $\bar{N}(i)$ in the Plateau region. By noting that

$$\sum_{j=0}^{i^{**}} \varepsilon^{VT} A_a^{VT}(i) \sum_{j=0}^{i} \varepsilon^{VT} A_a^{VT}(j) = \frac{1}{2}\left[\varepsilon^{VT} \sum_{j=0}^{i^{**}} A_a^{VT}(i)\right]^2 = 2(b\delta\bar{N}_o)^2$$

it is relatively straightforward to show that D^{VT} (see Eq. (10) of Ref. 8) is approximately twice the correct result given here. An added advantage of the present procedure is the simplicity of the expression, Eq. (6.12), obtained for D^{VT}, showing clearly the contributions of high-level and low-level deactivation contributions. Together with the explicit identification of $N^{*}(i)$ and $N^{**}(i)$ as the appropriate loci, the present theory yields a complete and quantitative picture of vibrational relaxation problems under strongly pumped conditions.

ACKNOWLEDGMENT

This research was supported by AFOSR (F44620-73-0059).

REFERENCES

1. A. I. Osipov, Soviet Phys. Doklady 5, 102 (1960).

2. C. F. Treanor, J. W. Rich, and R. G. Rehm, J. Chem. Phys. 48, 1798 (1968).

3. G. E. Calendonia and R. Center, J. Chem. Phys. 55 552 (1971).

4. B. Abraham and E. R. Risher, J. Appl. Phys. 43 4621 (1972).

5. J. W. Rich, J. Appl. Phys. 42, 2719 (1971).

6. W. R. Lacina, Northrop Corp. Report 71-32R, pt. II, (1971).

7. C. A. Brau, Physica, 58 , 533 (1972).

8. B. F. Gordiets,Sh. S. Mamedov, and L. A. Shelepin, Ah. Eksp. Teor. Fiz. 67, 1287 (1974).

9. B. F. Gordiets and Sh. S. Mamedov, Prik. Mat. Teor. Fiz. 3, 13 (1974).

10. R. N. Schwartz, Z. I. Slawsky, and K. F. Herzfeld, J. Chem. Phys. 20, 1591 (1952).

11. R. N. Schwartz and K. F. Herzfeld, J. Chem. Phys. 22, 767 (1954).

12. J. Keck and G. Carrier, J. Chem. Phys. 43 2284 (1965).

13. L. D. Landau and E. Teller, Physick. Z. Sowjetunion 10, 34 (1936).

14. K. F. Herzfeld and T. A. Litovitz, *Absorption and Disperson of Ultrasonic Waves*, Academic Press, N. Y. (1959).

15. J. L. Boulnois, "Carbon Monoxide Vibrational Kinetics in a Transverse Electric Discharge Wave Guide Laser", Ph.D. Thesis, Department of Aerospace and Mechanical Sciences, Princeton University, Princeton, N. J. (1975).

16. M. Verter and H. Rabitz, J. Chem. Phys. 64, 2939 (1976).

17. W. S. Drozdoski, R. M. Young, R. D. Bates, Jr., and J. K. Hannock, J. Chem. Phys. 65, 1542 (1976).

18. R. C. Millikan and D. R. White, J. Chem. Phys. 39, 98 (1963).

19. D. J. Miller and R. C. Millikan, J. Chem. Phys. 53, 3384 (1970).

FIGURE CAPTION

Fig. 1 Comparison with numerical solutions. The solid dots are numerical solutions for a 1:9 CO-He mixture at 100°K with various pumpings at the ground level. The VV rates are taken from Rich[5] and the VT rates are recent theoretical data by Verter and Rabitz.[16] Thirty-nine levels are used which appear insufficient for the two more strongly-pumped cases. The analytical solutions are shown as solid lines.

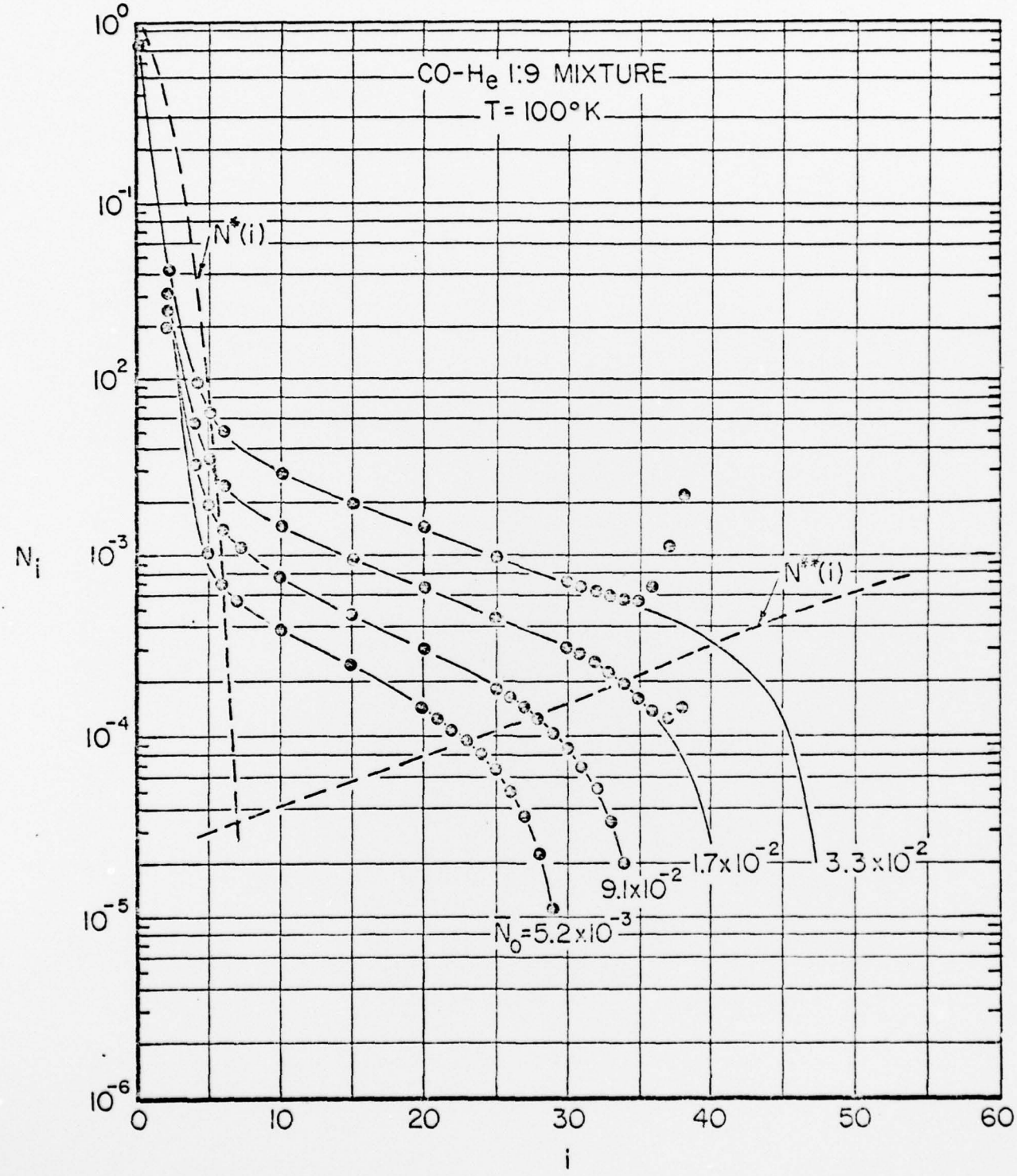
CO-He 1:9 MIXTURE
T= 100°K
N*(i)
N**(i)
9.1x10^-2
1.7x10^-2
3.3x10^-2
N0=5.2x10^-3
Ni
i
10^0
10^-1
10^-2
10^-3
10^-4
10^-5
10^-6
0
10
20
30
40
50
60